POLITECNICO DI TORINO

DIMEAS - DEPARTMENT OF MECHANICAL AND AEROSPACE ENGINEERING

MASTER OF SCIENCE DEGREE
IN
AUTOMOTIVE ENGINEERING

Master's degree thesis

NVH analysis of electric motors for hybrid and electric powertrains

Supervisors:
Prof. Andrea Tonoli
Prof. Renato Galluzzi
Dr. Irfan Khan

Candidate:
Roberto Sannino
s266837

Academic Year 2021-2022

Abstract

Electrification in the automotive market has grown rapidly over the last decade as a result of new government regulations imposed to reduce emissions. This has resulted in an increase in the market share of electric vehicles. With the advancement of this technology, engineers have faced new challenges in the design of new vehicles, one of which is related to NVH and occupant comfort. As a result, considerable effort is being expended to reduce noise and vibration while increasing efficiency in order to achieve better ranges.

The main goal of this thesis work is to investigate and comprehend the primary causes of noise and vibration generation in electric machines, as well as the impact of design choices on electric machine losses and noise generation. The first section investigates the effect of two different winding configurations, concentrated and distributed windings with the same rotor geometry, on Sound Power Level (SPL) and electric machine losses. The second section of the study focuses on the sensitivity analysis of the NVH, and electric machine losses caused by the stator slot opening. Furthermore, the effects of different tooth shapes (flat and with fillet) are investigated. The key performance indicators used to evaluate the best trade-off solution are cogging torque, ripple torque, electric machine losses, and SPL.

The analysis is carried out with an Interior Permanent Magnet (IPM) motor, but the proposed methodology is easily adaptable to other topologies. The FEMM code was used to design the electric machines.

Acknowledgements

First and foremost, I want to thank Prof. Andrea Tonoli and Prof. Renato Galluzzi for providing me the opportunity to work on this exciting topic and for their assistance during the thesis work. Then, I want to express my heartfelt gratitude to Dr. Irfan Khan for his assistance, professionalism, and availability over these months.

An enormous thank you goes to my family for supporting me on this journey, which has been both difficult and challenging; without them, none of the progress I've achieved during my studies would have been possible.

Thank you also to all of my friends who encouraged me, especially at the start of this project, and never made me feel the distance between us.

Thank you to everyone I met at LIM. You helped me feel less lonely, and I will be eternally thankful for making me feel like part of a family. I hope to meet all of you again along my professional journey.

Then, I want to thank everyone I met in Turin throughout these months for introducing me to the city and for the good times.

Table of Contents

List of Figures

List of Tables

CHAPTER I
Introduction

Due to increased customer awareness of global warming, the demand for electric vehicles has increased quickly in recent years. In fact the sales of electrified vehicles (electric and hybrid) has increased from less than 5% of the global passengers cars sales in 2017 to 12% of 2020 [1] [2]. According to the projections, this trend is meant to increase more, with electric cars predicted to account for more than half of the worldwide market share in 2026, and zero-emissions vehicles expected to replace combustion engines as the main powertrain for new light-duty vehicles by 2035.

Furthermore, governments has also implemented regulation which aims to boost the demand of electric vehicles; the European Union in fact has imposed the ban of new gasoline engines by the 2035, as part of its "fit for 55" plan, which aims to reduce the union's net greenhouse gas emission by 55 percent by 2030 compared to 1990 levels and to achieve climate neutrality by 2050 [3]. Other countries, including the United States, China, and the United Kingdom, are pursuing the same phase-out of internal combustion engine goals, with new gasoline and diesel engine automobile sales prohibited from 2035.

1.1 Thesis motivation

The increased demand for electric vehicles has resulted in various issues related to the powertrains. One of them is the NVH issue, which occurs when the vibration generated inside the motors can cause noise to enter inside the vehicle cabin, creating discomfort to the occupants. This problem has immediately attracted the attention of researchers and manufacturers. Indeed, the analysis of the main parameters causing this noise has become of main relevance for the engineers to better understand the phenomena and guide them during the design stage of a new product.

As it will be clear during this dissertation, there are many potential solutions during the preliminary phase of a project, and each of them have an impact on the final behaviour of the motor. For this reason, is crucial for the OEMs to have a set of simulation in which a comparison between alternative design solution is made, in order to save money and time.

This allows them to estimate the final behaviour of the motors and identify the best trade-off between noise attenuation and performance before beginning manufacturing.

1.2 Theoretical background

There are several eletric motors technologyies available on the market. The first way to classify the various technologies for the electric motors is based on the supply type. So as showed in figure 1.1, there are two main categories of motor: DC motors and AC

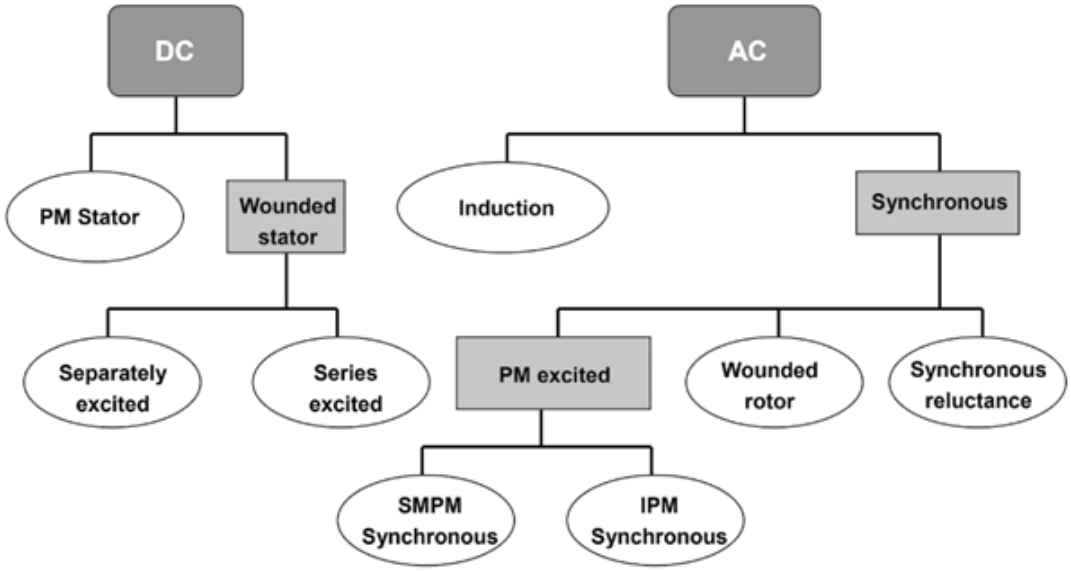

Figure 1.1 – DC motor and AC motors classification

motors.

In any case, they must all provide torque. To do so these technologies rely on two mechanism:

- Lorentz force
- Reluctunce forces

The first mechanism, as the name suggests, is based on the Lorentz law:

$$|F| = Bil\ sin\alpha \tag{1. 1}$$

In which:

- F is the Lorentz force [N]
- B is the magnetic induction [T]
- i is the current

- l is the active length of the winding [m]
- α is the angle between the induction and current direction vectors

The magnetic induction can be produced by permanent magnets or current-carrying windings, whereas the current flowing in the induction circuit can be supplied by an external circuit, as in DC and AC synchrounous machines, or induced by electromagnetic induction as happens in AC induction machines.

Instead in the machines which exploit the reluctance, a coil is installed on the stator. When the curret starts to flow throught the windings, it generates a flux that attracts the rotor pole in order to put it in a minimum co-energy posistion. The reluctance forces depends on the interacting surfaces, the square of the magnetic induction and the difference of the inverse of the permeability of the materal constituing the parts of the system and the one and the airgap.

Looking at the automotive market AC motors are the most widely used technology among the OEMs. In fact, the advantages of this family of motors are:

- Lower maintenance needs. In fact in DC motors the wear of the brushes requires a higher need of maintenance.
- Higher maximum speed. AC machines can have a maximum speed at least two times higher than a DC machine.
- Higher torque for the same power level
- Lower rotor complex manufacturability due to the presence in DC motors of commutators and windings
- Lower Joule losses. In fact DC motors have distributed windings on the rotor which produce higher Joule losses and making harder the heat dissipation
- Higher efficiency
- Higher transient power

As showed in figure 1.1, there are many different possible architectures in the AC motors field. The most widely adopted for traction purposes are:

a) *Induction or asynchronous motors*. In these machines the stator is made up of poles that carry the supply current to induce a magnetic field that penetrates the rotor. To optimize the distribution of the magnetic field, the windings of the stators are placed in slots around the stator, with the magnetic field having the same

number of north and south pole. Some motors, like the one showed in figure 1.1(*a)*, will features a squirrel cage rotor, in which the windings may have the rotor bars skewed to smooth out the torque for each revolution. This technology is the simplest one possible and can may operate in any environment; then due to the absence of brushes and commutators, they have also low costs and low requirements in terms of maintenance. Anyway, for this technology the control of the speed is difficult, and the starting torque is extremely poor; for these reasons, it is not extensively used for traction.

b) *Permanent Magnet (PM) Synchronous motors*. This machine presents the inductor circuit formed by the PM on the rotor side, while the induced circuit is mounted on the rotor side. In AC application, as above mentioned, it operates without brushes, nevertheless, this requires more precise mechanical sensors to prevent ripple torque. There are diverse types of PM machines:

   b.1) *Surface Mounted Permanent Magnet (SMPM) Synchronous motors.* In this kind of machines the magnet are mounted at the periphery of the rotor. Between the AC machines this is the technology which guarantees the highest specific torque and peak efficiency. Anyway, due to the higher iron losses, the efficiency at part load is quite poor. Nonetheless, this technology is currently one of the most widely adopted in the automotive industry.

   b.2) *Internal Permanent Magnet (IPM) Synchronous motors*. This technology is similar to the previous one. In this case, the magnets are installed inside the rotor core. With respect to the PM motor, the IPM machines have lower specific torque and peak efficiency, but they perform better at part load. This technology also offers an easier flux weakening capability and lower limitation at high speed.

   b.3) *Permanent Magnet Assisted Synchronous Reluctance Motor (PMASynRM).* In this kind of motors there is a hare of reluctance torque is significant compared to the PM electrical torque. The benefits of this kind of motor is that, adding PMs to a reluctance motor, there will be an increase of the motor power factor. Furthermore, low PM material is required,

reducing so the final cost of the motor. Anyway there should be enough material to prevent demagnetization by deep flux weakening [4].

c) *Switched Reluctance motors*. Also in this technology the stator has winding mounted around the stator teeth. The peculiarity of this technology, anyway, is that there are not magnets or coils on the rotor. In fact for this machine, the rotor for this machine is a solid salient-pole rotor made of soft magnetic material, usually laminated steel. These machines have an extremely high robustness, and they are relatively easy to manufacture in large quantities due to their low cost. In terms of performances, this machine has higher torque at low speeds and higher efficiency. Anyway, since only one pole pair is active, there is an extremely low magnetic utilisation. In addition, this technology exhibits excessive ripple torque and noise.

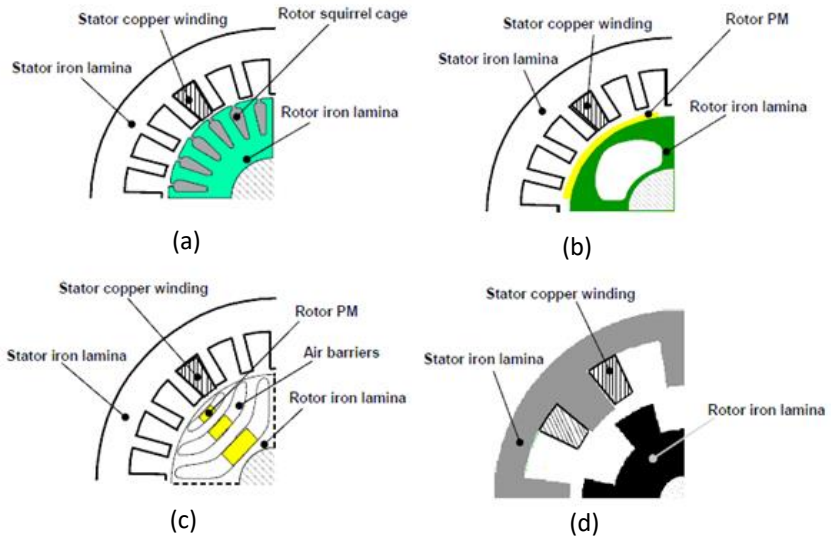

Figure 1.3 – AC motor technologies example. (a) Induction motor (b) PM synchronous motor (c) IPM Synchronous Reluctance (d) Switched Reluctance motor

For what concerns this analysis, the technology chosen is the IPM synchronous motor. Anyway the methodology adopted for this work can be further extended to all the electric motors above mentioned.

1.3 Thesis objectives

The aim of this work is to be beneficial not just for academic objectives, but also for industrial applications.

Hence, the first step of this analysis, which will be covered in the next chapter, is first to conduct an extensive literature review, focusing on the actual state of the art IPM synchronous motors and the parts of which it is composed. Since the analysis wants to address the NVH issue, all the parts will be analysed from this prospective, also trying to find the reasons behind the noise and vibration generation in all these parts. On this aspect in literature there are different research on this aspect developed by the international community during the past years.

Then, since the major goal of this dissertation is to determine the main variables that impact on noise and vibration generation while taking performance and design restrictions into account. To do this, the simulation will be carried out using to the Altair™ software Flux and Flux Motors. These simulations are of main relevance since they usually are time-expensive and data-expensive. As a result, it is extremely crucial for companies to have a general idea of what the optimum design solutions are before beginning manufacture of a new motor. The parameters under consideration for this study will be:

- Influence of the type of winding, i.e., concentrated and distributed
- Influence of the slot opening
- Influence of a flat tooth design
- Influence of the height of the shoe on the flat tooth

1.4 Thesis outline

After this brief introduction, the work will be organised in the following way:

- **Chapter 2:** In this chapter a deeper analysis of the Internal Permanent Magnet (IPM) is conducted based on the literature review. There will be first a broad examination of the IPM motors first, followed by a dissertation of the main parts composing these electric motors considered, attempting to give an idea about their contribution to noise and vibration generation.
- **Chapter 3:** Here the way the procedure to model the motor is showed. Then, considering distinctive design solutions, a testing phase is carried out. The different motor will be compared considering the same output performance in

terms of torque and rotational speed. Anyway, not only the NVH behaviour is addressed in these tests, but also the engine losses and the engine map.

- **Chapter 4:** In this chapter the results will be showed and a there will be a discussion on them.
- **Chapter 5:** This is the last chapter which concludes the analysis and gives some suggestion for potential future works.

CHAPTER II

Literature review

In this chapter contains a summary of what has been found in literature revie. The aim of this part of the work was to learn about the awareness of the community about two distinct aspects.

The first one to be highlighted is the analysis of the various sources from which noise and vibrations are generated.

Then, the second aspect to be highlighted is the analysis of the different parts of which is made up a IPM motor. In particular, the attention is given to the impact on the NVH issue of each part.

2.1 Source of noise in IPM motors

To classify the different sources of noise and vibration is not an easy task. Anyway an efficient work is made by the authors of [5], in which the various sources are categorised according to the nature of their origin, as shown in Figure 2.1.

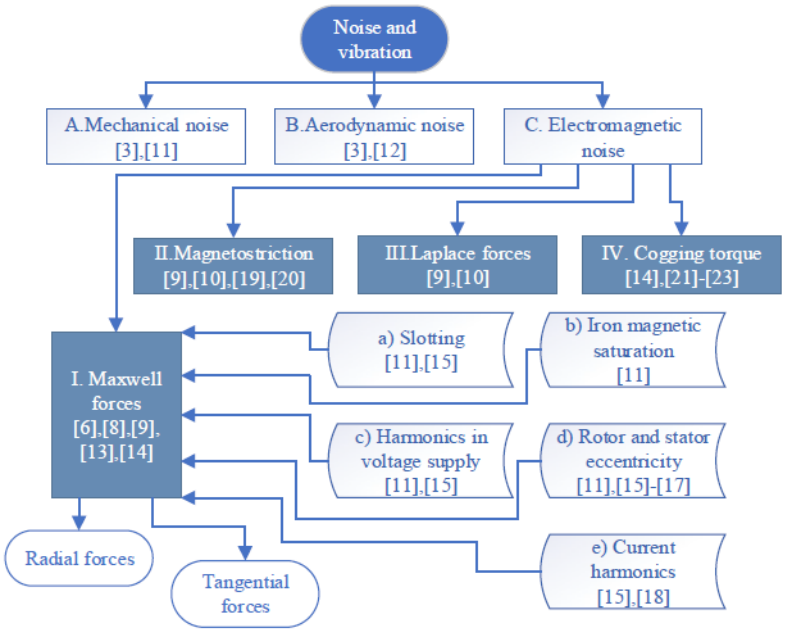

Figure 2.1 - Noise and vibration sources classification

As can be seen from the picture, the three main sources of noise are:

- Mechanical noise

- Aerodynamic noise
- Electromagnetic noise

The first source of noise is generated by the mechanical components of the motors such as fasteners and bearings; however, also errors during the design, production and assembly stages that can cause some eccentricity between the stator and the rotor which can produce noise. However, for the purposes of our investigation, this kind of source is irrelevant; mechanical noise is usually characterised by a low frequency range, and hence, even when perceived by the human ear, it does not generate the same amount of discomfort as a higher frequencies noise. Furthermore, this source can be easily identified, and the attenuation methods are well known.

For what concerns the aerodynamic noise instead, it is caused by the fans and the ventilation ducts that many electric machines have; however, most of the PM cars are water-cooled or air-cooled, so this source is not of interest for this analysis.

Coming at the electromagnetic noise, it is the most prominent and complex kind of noise generated by electrical machines; for this reason, this work concentrates on this kind of noise. The electromagnetic noise refers to the vibration produced within the motor due to the electromagnetic forces; the main component of this forces is the radial force acting on the stator tooth surface.

2.1.1 Electromagnetic noise generation mechanism

There are several mechanisms which generates noise due to the variation of electromagnetic forces. These mechanisms can be further classified as:

- Maxwell forces
- Magneto-strictive forces
- Laplace forces
- Cogging torque

Maxwell forces are the principal sources of electromagnetic noise and refers to the forces acting on the rotor and stator teeth. They are always normal to the tooth surface and can be decomposed into radial and tangential component. The latter produces the electromagnetic torque, but it is also responsible for the vibration of rotor teeth and torque ripple. The radial one instead, is the main cause of noise generation in PM motors, as it

acts on the inner surface bore of the stator and its teeth and causing the deformation of the housing.

One important issue related to the force calculation is the accuracy. Various approaches are presented in literature; however, two methods are the most widely adopted for the Maxwell force calculation: the Virtual Work Principle (VWP) and the Maxwell Tensor (MT) [6].

The VWP allows to obtain an integrated force which acts on the stator's tooth directly from the resultant of the nodal force calculated inside the tooth. Considering H as the magnetic field and B the magnetic flux density, H_i and B_i will be the respective components in Cartesian frame reference. So the nodal force expression is based on an equivalence between the magnetic co-energy variation and the force applied on a domain Ω, such that the force amplitude is each direction is:

$$F_s = \frac{\partial}{\partial s}\int_\Omega \int_0^H B \cdot dH d\Omega \tag{2.1}$$

Where $s \in \{x, y, z\}$. Then, discretizing the domain Ω the equation (2.1) can be applied to the single element e such that:

$$F_s = \int_e \left(-B^T \cdot \mathbb{J}^{-1} \cdot \frac{\partial \mathbb{J}}{\partial s} \cdot H + \int_0^H B \cdot dH |\mathbb{J}^{-1}| \frac{\partial |\mathbb{J}|}{\partial s}\right) dV \tag{2.2}$$

With $\mathbb{J}$ the Jacobian of the matrix of the element e.

Considering the case in which the B-H curve is linear the integrand of B can be simplified as:

$$\int_0^H B \cdot dH = \int_0^H \mu H \cdot dH = \frac{\mu}{2}|H|^2 \tag{2.3}$$

With H equal to the amplitude of each element. To implement the VWP algorithm a loop around each element is considered; hence, once computed the previous formula the contribution of each element is added. So the local force F_s^i applied on each node i is:

$$F_s^i = \sum_{\forall e | i \in e} \int_e \left(-B^T \cdot \mathbb{J}^{-1} \cdot \frac{\partial \mathbb{J}}{\partial s} \cdot H + \frac{\mu}{2} |H|^2 |\mathbb{J}^{-1}| \frac{\partial |\mathbb{J}|}{\partial s} \right) dV \tag{2.4}$$

Instead for what concerns the MT, the integrated force per stator's tooth is obtained by integrating the magnetic pressure in the air gap over a path that embraces the tooth. The calculation starts from the definition of the Maxwell stress tensor T:

$$T_{i,j} = B_i H_j - \frac{\mu}{2} \delta_{i,j} \sum_{k=1}^{n} |H_k|^2 \tag{2.5}$$

Then, defining a surface S around a volume V to apply the divergence theorem, with n the normal to S. So the global force F which applies on the volume V is equal to:

$$F = \iiint_V \nabla \cdot T dV = \oint_S \left((B \cdot n) H - \frac{\mu}{2} |H|^2 n \right) ds \tag{2.6}$$

This force can be applied to the ferromagnetic tooth surrounded by a dotted circular path as showed in fig 2.2; In this way the force can be rewritten as:

$$\begin{cases} F_n \approx \frac{1}{2} \int_S \frac{|B_n|^2}{\mu_0} - \mu_0 |H_t|^2 ds + \Gamma_n^{S \cap S'} - \frac{1}{2} \int_{S'} \frac{|B_n|^2}{\mu} - \mu |H_t|^2 ds' \\ F_t \approx \int_S B_n H_t ds - \int_{S'} B_n H_t ds' + \Gamma_t^{S \cap S'} \end{cases} \tag{2.7}$$

Where:

- μ is the magnetic permeability
- μ_0 the void permeability
- X_n and X_t are components of a vector field projected respectively on the normal n and tangential t direction
- $\Gamma^{S \cap S'}$ is the gap term corresponding to the integration over the interface between the stator and the air

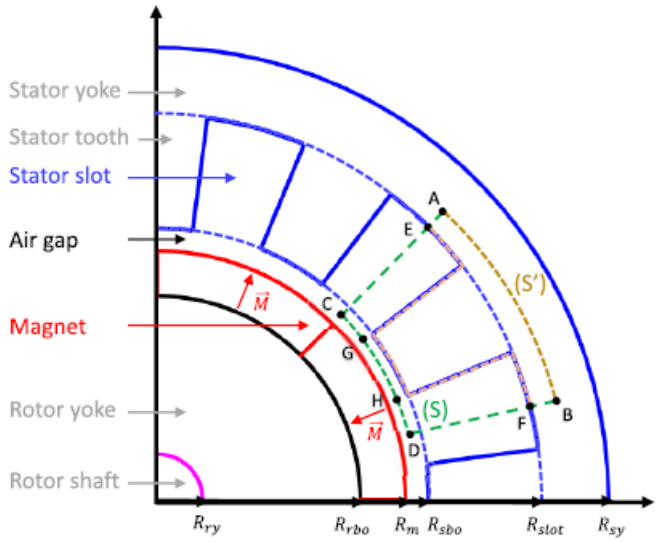

Figure 2.3 – Circular path S definition

This form assumes that the divergence theorem is still valid even if there is a discontinuity in the permeability as in the stator-air interference.

Other than that, neglecting $\Gamma^{S\cap S'}$ null since the integration surface between E and F in fig 2.2 has a low magnetic field. Also adding the hypothesis $\mu \gg \mu_0$, the force expression reduces to:

$$\begin{cases} F_n \approx \frac{1}{2}\int_S \frac{1}{\mu_0}|B_n|^2 ds \\ F_t \approx \int_S B_n H_t ds \end{cases} \tag{2.8}$$

In vibro-acoustic application is often neglected the term H_t which leads to:

$$\begin{cases} F_n \approx \frac{1}{2}\int_S \frac{1}{\mu_0}|B_n|^2 ds \\ F_t \approx 0 \end{cases} \tag{2. 9}$$

Coming at the factor that influence the Maxwell forces, the following can be listed:

- Slotting effect: in the stator structure, the slot opening causes the break of the uniformity of the ideally cylindrical airgap. This changes the reluctance of the airgap periodically. Hence the magnetomotive force will be distributed around the airgap in a harmonic way.
- Saturation: the iron magnetic saturation can cause a distortion of the magnetic flux distribution; this results in more harmonics in the total electromagnetic force

- Voltage supply: it is induced by the Pulse Width Modulation (PWM) of the input signal. Therefore, the harmonics are then reflected in the electromagnetic force around the airgap
- Also the rotor and stator eccentricity can cause vibration since this can again modify the cylindrical shape of the airgap causing a significant variation of the permeance in the airgap.
- Current harmonics: this also affects the vibration generation. In fact, current harmonics generated by the PMW can generate extra vibrations and noise frequencies also increasing the noise sharpness due to their high frequency content.

Then, considering the magneto-strictive forces, since the stator core is made of conductive steel, when it is immersed into an external magnetic field it is subjected to a magneto-restrictive force. Anyway this magnetic field is not constant due to the presence of the airgap. As a result, it rapidly changes in time, causing a vibration of the stator core and, consequently, the entire machine.

Laplace forces instead, act on the stator coils causing it to vibrate. This can also lead to some risks for the insulation of the coils and, in some cases, leading to short circuits and failures.

Cogging torque (CT) finally, is the parasitic torque created by the attraction forces generated by the stator teeth and the PM of the rotor. Most of the researchers address this as the main contributor to the total noise spectrum. Anyway it has been demonstrated that a motor with low cogging torque is not always less loud.

In fact in [7] the authors have examined five distinct slot/pole layouts considering the same output performance in terms of torque/speed. At first the cogging torque performances are evaluated. Then the displacement at the stator tooth periphery is evaluated considering the equation for a fixed-fixed supported beam showed in (2.10):

$$\varepsilon_{max} \propto \frac{\omega\left(\frac{L}{4m}\right)^2}{E\rho L\left(R_o^4 - R_i^2\right)}\left(\frac{L}{2m} - \frac{L}{4m}\right)^2 \qquad (2.10)$$

Where:

- ω = force distribution

- R_0= outer radius
- R_i= inner radius
- m =mode number
- E= Young modulus
- ρ = material density
- L= length

Since the displacement is inversely proportional to the vibration mode number is preferable to have a machine with higher mode number.

This radial pressure leads to vibration and, therefore, acoustic noise, following the scheme showed in fig 2.2.

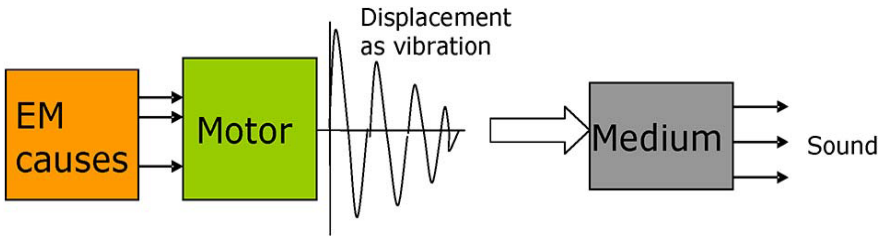

Figure 2.5 - Noise propagation scheme for electromagnetic forces

This noise is once again proportional to the vibration mode number and in fact, the motors that initially showed the best performances in terms of cogging and ripple torque performance have worse noise Sound Power Level (SPL) behaviour since their mode vibration number was between 2 and 3, whereas motors showing poor cogging torque and ripple torque results have a lower SPL.

2.2 IPM motors structure and its influence on noise generation mechanism

Once showed the primary sources of noise and vibration generation, the attention may shift to the various machine components. They will be detailed first in terms of their function inside the motor, followed by the factors that impact the motor's NVH behaviour.

2.2.1 Stator

The stator is the fixed part of the motor, in which is produced the magnetic voltage coming from the wires. As previously stated, this part is the one producing most of the motor vibrations. A scheme of a SMPM stator is showed in figure 2.4:

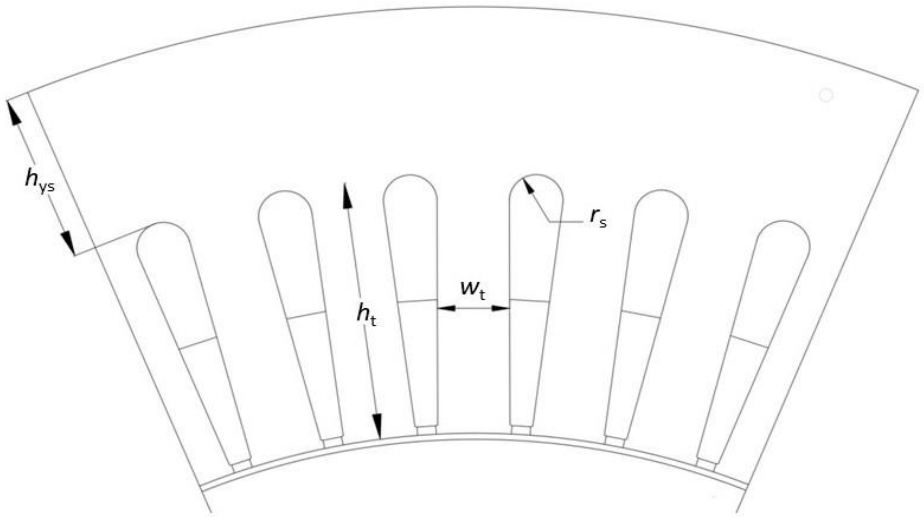

Figure 2.7 - Structure of the stator

From the figure can be distinguished four different parts:

1. Stator yoke: which is the yoke between the slot opening and the outer surface of the stator
2. Tooth face: the surface which separates two different slots
3. Tooth foot: the surface at the interface between the stator and the rotor
4. Slot: the housing of the windings

During the design phase the number of slots N_s must be set and, once decided the number of slots per pole q_f and per pole phase q can be obtained from the following expressions:

$$q_f = \frac{N_s}{p} \tag{2. 11}$$

$$q = \frac{N_s}{pm} \tag{2. 12}$$

Where p is the number of poles and m the number of phases.

There is not a rule of thumb for the selecting N_s but the number of slots and poles number should be chosen such that the Least Common Multiple (LCM) is as large as possible, obtaining in this way better cogging torque results [8]. This because the arrangement with higher LCM can guarantee a better distribution of the forces. As a result, the number of slots and poles is frequently set such that they are close to each other, pursuing the target of the highest LCM. Instead, anything can be said about the impact of the slot pole arrangement on ripple torque. In fact, in this case there are many different considerations that should be done and so it's quite hard to predict the behaviour of the motor on this side only considering the slot/pole arrangement.

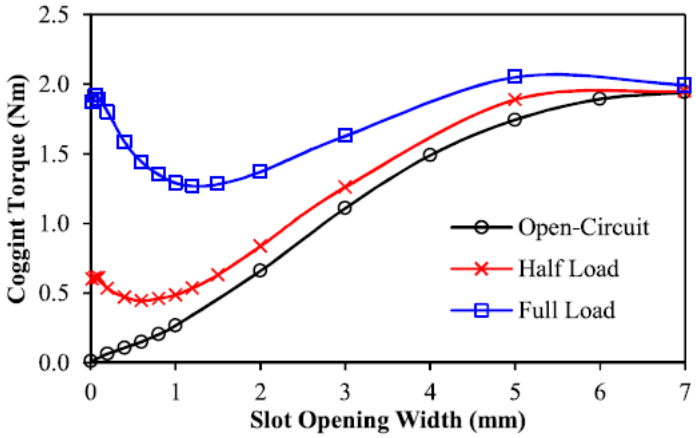

Figure 2.11 – Influence of the slot opening width on cogging torque for different loads

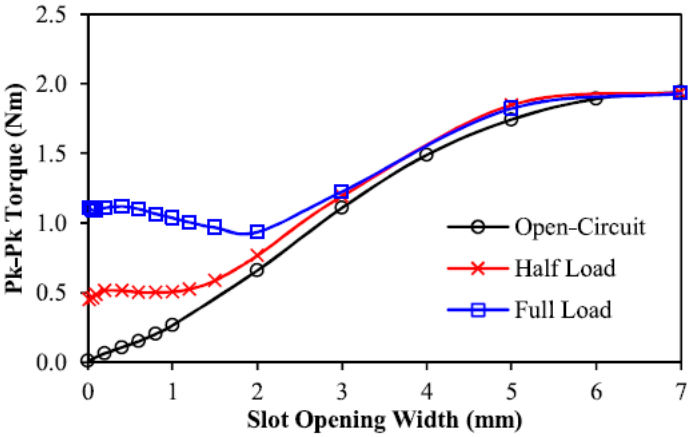

Figure 2.9 – Influence of the slot opening width on ripple torque for different loads

Another crucial aspect of the slot design that can affect cogging torque and ripple torque and hence, to some extent, noise and vibration generation is the slot opening. Considering how ripple torque and cogging torque are defined one could expect a decrease of both

when the slot opening width is reduced. [9] examined the trend of cogging torque and ripple torque against the slot opening width under three different loading condition.

From the results showed in figure 2.5 and figure 2.6 it's clear that, when a load is applied, there is an increase of both torques considered. For what concerns the cogging torque, this trend is justified by two reasons. When opening width is decreased, the tooth tip leakage flux will enhance the magnetic saturation. This will cause an increase of the airgap permeance variation leading to a higher cogging torque. At the same time, with a tighter slot opening, the slotting effect reduces, hence smoothing the variation of the airgap permeance and consequently the cogging torque. As a result of these two opposite effects, a balance is established for the minimal on-load cogging torque point. These trends also have an impact on torque ripple for different loads as shown in figure 2.6. Anyway, the trade-off point obtained for the cogging torque is not the same also for the ripple torque, in which a design trade off can be demanded to obtain for different loads conditions.

2.2.2 Windings

Windings will be fitted inside the stator slots of PM motors. They form the electrical circuit of the motors and, along with the stator tooth, generate the induced magnetic field which produce the torque of the motor.

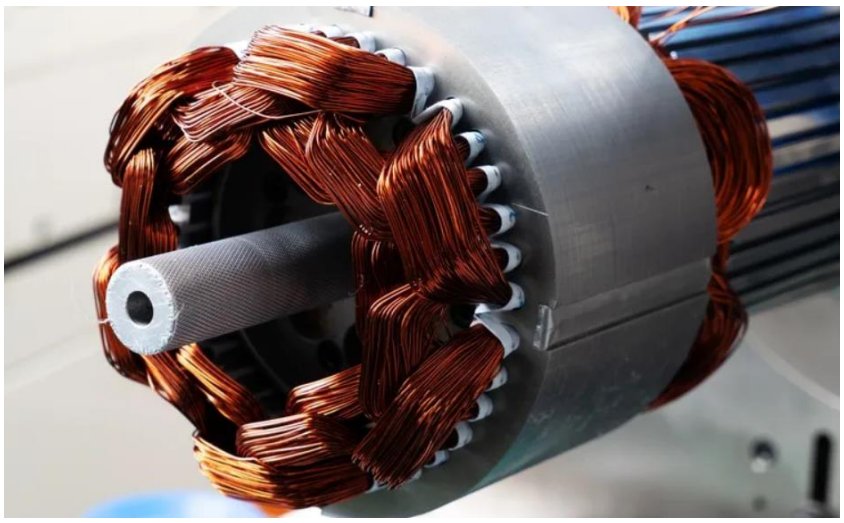

Figure 2.13 – Winding example

In principle PM motors can have any slot-pole arrangement, but only few combinations can maximise the utilisation of the stator and rotor, leading to an efficient torque

generation. Furthermore, only certain winding layouts are suitable for the chosen slot/pole combination.

One important factor to define the winding layout is the winding factor which expresses the ratio between the flux actually linked and the one that would have been linked by a single-layer full-pitch and non-skewed integer slot winding with the same number of turns and one single slot per phase [10]. Usually the winding k_w factor is expressed by:

$$k_w = k_p \cdot k_d \cdot k_s \tag{2.13}$$

Where the factor k_p is defined as the pitch factor which depends on the coil span, i.e. the circumferential width of a coil. So, for example, if a coil goes from the slot k to the slot k+2, the coil pitch is 2. To lessen the length of the end-turns their individual turns are reduced; hence the winding will not always be fully pitched.

The factor k_d instead is the distribution factor, which quantifies the number of slots in which the coils of each phase are distributed. In fact, the emf induced in different slots is not in phase, so its phasor sum will be smaller than its numerical sum.

Then the last factor k_s, defined as the skew factor, indicates the fact that sometimes the windings are angularly twisted, lowering the emf. This is true especially for the squirrel-cage induction rotor.

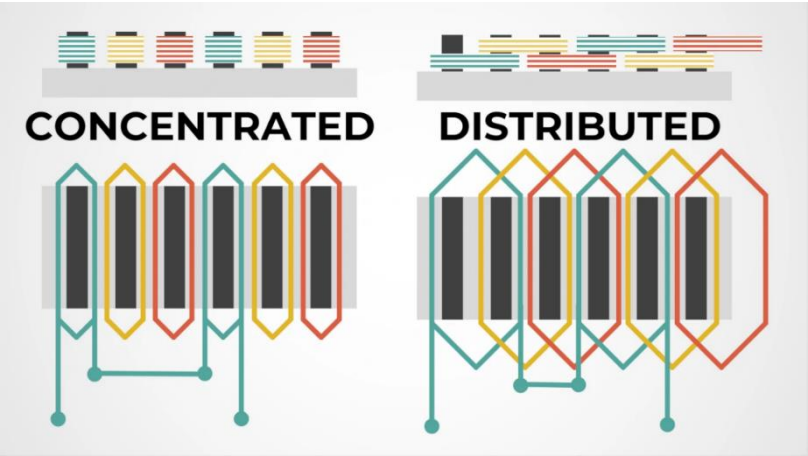

Figure 2.14 – Distributed and concentrated winding example

As a result, there are two alternative windings layout: distributed winding and concentrated winding. Distributed winding is defined as a winding that is spread over the stator's periphery and has the smallest air gap feasible. This kind of winding doesn't have

the same magnetic axis for each coil, which affects the EMF. In addition, this kind of windings are always full pitched. While in concentrated windings the coil turns are concentrated around the tooth, as the name suggests. In this kind of winding the pitch factor and the distribution factor is equal to one.

The comparison in this analysis will primarily focus on the differences in performance demonstrated by concentrated and distributed windings. Starting with the cogging torque and ripple torque, findings in [11] clearly put in evidence that the cogging torque, computed as percentage of average, is lower in CW motors.

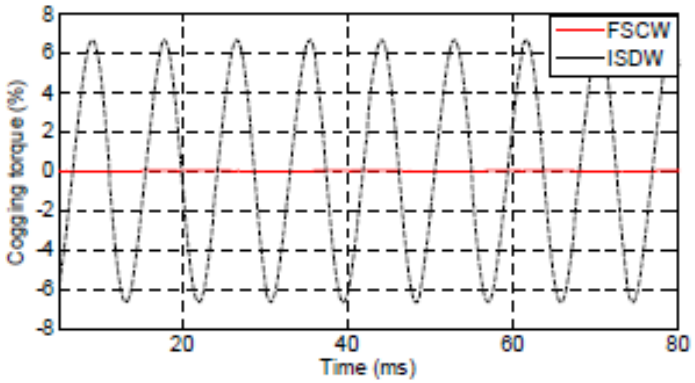

Figure 2.16 – Cogging torque as percentage of average for concentrated and distributed windings

This result is also confirmed for the ripple torque when considering different design solutions. Looking at the losses instead, DW have larger winding head size. This leads to a higher phase resistance and hence, higher DC copper losses [12]. To further evaluate the overall performances of the two designs, in terms of losses, consideration should be given to the various operating conditions. In fact looking at the engine maps calculated in [13] which compares two state-of-the-art motors with concentrated and distributed windings.

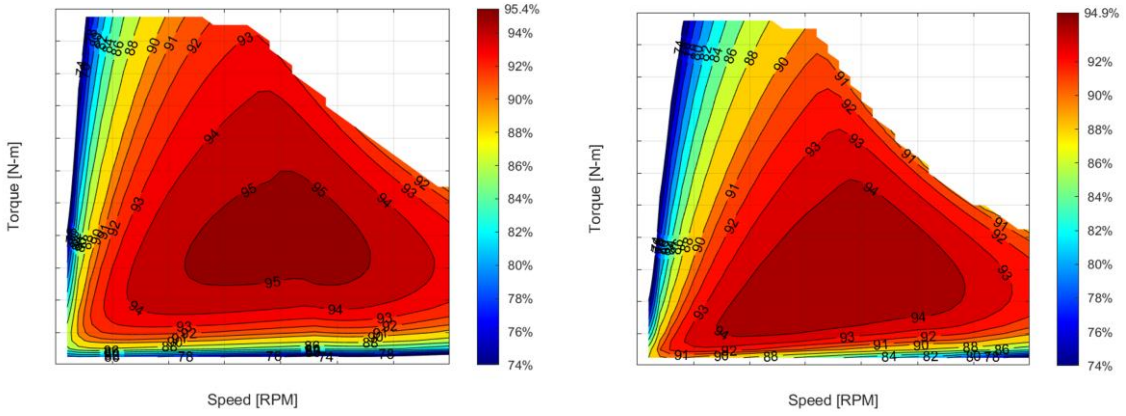

(a) CW (b) DW

Figure 2.18 – Engine maps for (a) concentrated windings (b) distributed windings

The max efficiency for the CW winding machine is higher; however, the zone in which the max efficiency may be maintained is clearly higher in DW winding machines. This because, especially in low torque regions, the core losses predominate, enhancing the DW machine efficiency. Finally, when it comes to NVH comparisons, it's difficult to make a proper comparison. This because the two different windings results in two different structures, and hence the shape mode differs between the two solutions. So nothing can be said a priori about the two different windings solutions for noise and vibration generation.

2.2.3 Rotor

The rotor constitutes the moving part of the electric machine. In PM magnet motors, it accommodates the magnets on which the magnetic field is induced. Today, several different materials are used for PM including ferritic, neodymium-iron-boron (NeFeB), samarium-cobalt. The NeFeB is the one with the best performance among them.

when comparing the behaviour of various magnets, much emphasis is paid to the magnetic hysteresis loop, which is created by the lag during the demagnetisation process displayed by the material when subjected to a transient magnetic field. In fact, considering the flux density B and the strength of the magnetic field H, in ferromagnetic materials their ratio is not constant but varies with the flux density. So, plotting the values of B against H, the magnetic hysteresis curves or B-H curve can be obtained. In figure 2.11 are plotted as example the B-h curves of air, iron, and steel.

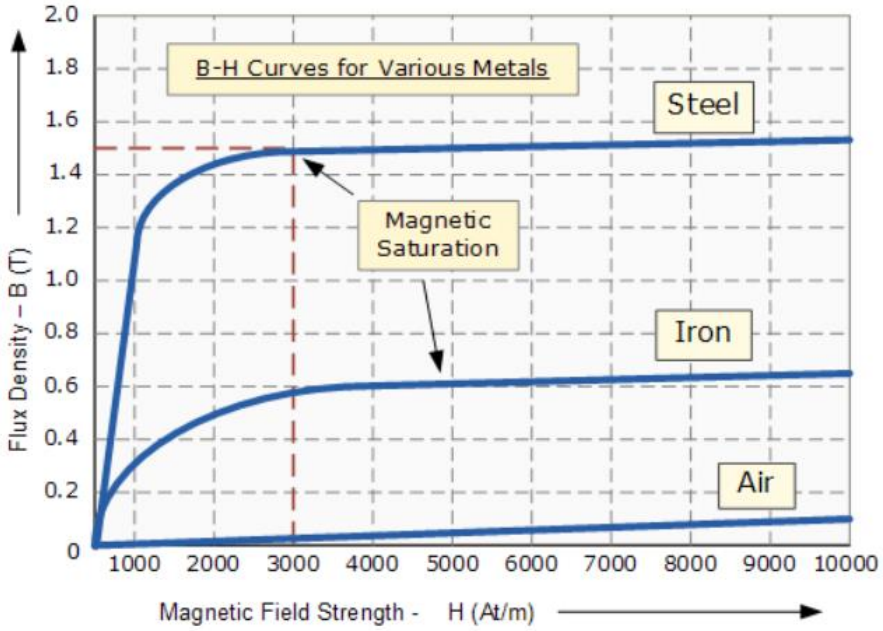

Figure 2.21 – B-H curve for Air, Iron and Steel

It can be noticed that in the first part of the curves, the flux density increases linearly with the field strength until a certain point called Magnetic Saturation. This because there is a limit to the amount of flux density that can be generated by the core, as all the domains in the iron are perfectly aligned. Depending on the application, the B-H curve is the starting point to select the proper material for the magnets.

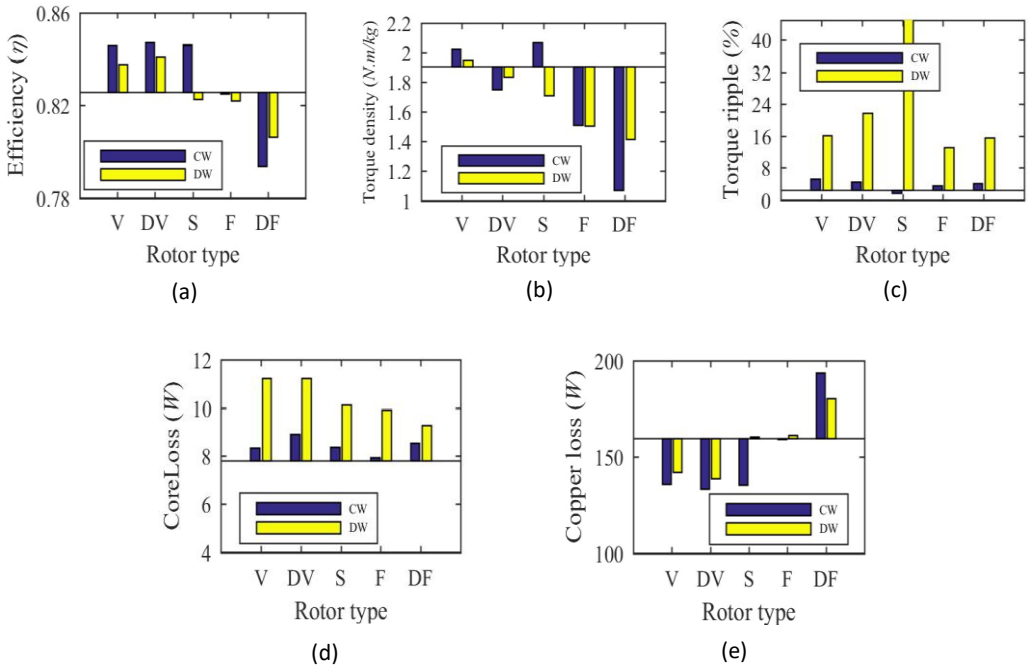

Figure 2.20 – Performance comparison for different magnet designs. (a) Efficiency, (b) Torque density, (c) Torque ripple, (d) Core losses, (e) Copper losses,

Then, another important parameter is the magnet shape. There are several conceivable forms, making a whole dissertation unfeasible. Anyway in [14] a comparison of some magnet designs is conducted. The analysis also compares a motor endowed with concentrated windings and one with distributed. As shown in the graphs in figure 2.12, the design of the magnets can affect several characteristics of the motor, thus the appropriate design is chosen based on the application.

CHAPTER III

Modelling

3.1 Electrical machine modelling

The electric machines under test will be modelled using the workflow of the tool MotorFactory, which is accessible in FluxMotor, software created by Altair®. This tool's library has a wide set of geometries for both the rotor geometry and the magnet geometry. Anyway, for this application it has been developed a new geometry both for the rotor and stator and added to the library using the macro offered in Flux2D. Once the rotor and stator geometries have been determined, the motor may be tested. It will begin with a FEM study, then will be evaluated the losses and efficiency of the various topologies, and lastly will be compared the NVH behaviour of the motors.

3.1.1 Rotor

The rotor geometry adopted for these experiments is the same for all the motors being tested. So all the machines will be equipped with a 20-poles rotor as showed in figure 3.1.

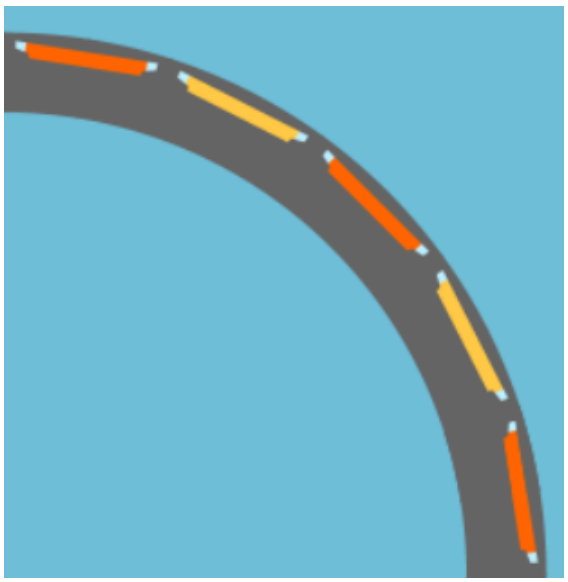

Figure 3.1 – Rotor radial view

The dimensions of the rotor are:

- Outer diameter: 210.4 mm
- Inner diameter: 181.0 mm

- Length: 50.0 mm

Moving the attention on the magnets, as above mentioned, for this task a user defined geometry that is showed in figure 3.2.

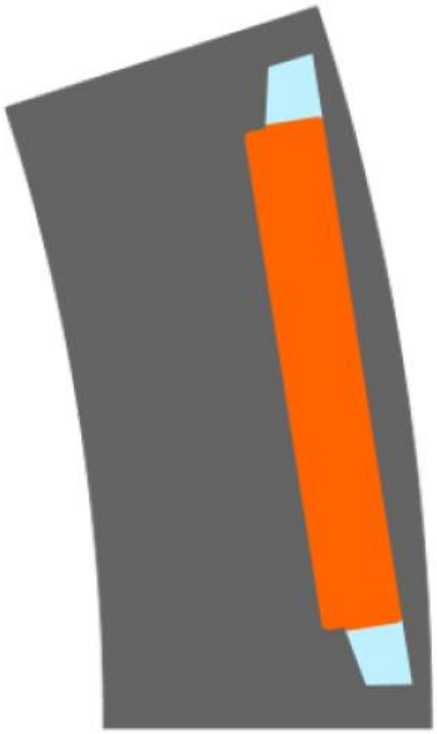

Figure 3.2 – Magnet geometry view

The magnets have a thickness of 1 mm, and the material used is NdFeB-N38UH, which has the following properties:

- Remanent induction at Tref (Br) = 1.22 T
- Relative permeability (μ_r) = 1.05
- Coercivity (Hc) = 1990000.0 A/m

3.1.2 Stator

For what concerns the stator, two different designs have been adopted: one with concentrated winding and one with distributed windings.

Anyway, the general dimensions of the stator are the same for both the designs:

- Outer diameter: 275.0 mm
- Inner diameter: 212.0 mm

- Length: 50.0 mm

In this way the air gap between the rotor and the stator for both the arrangement will be equal to 0.8 mm.

Also, the material chosen is equal for the two different machines, and it is the 20BT1500, whose properties are as follows:

- Magnetic polarization (Js) = 1.769 T
- Relative permeability (μ_s) = 5582.12

While for the winding, the material is always copper, and the Nomex 180 is for the insulation.

a. Concentred winding

The concentrated winding case is the first to be examined. In this design, the stator has 30-slots and the following dimensions as showed in figure 3.3:

- Height of the slot: 23.01 mm
- Slot width: 13.5 mm
- Tooth width: 11.3 mm
- Slot opening: 3.0 mm

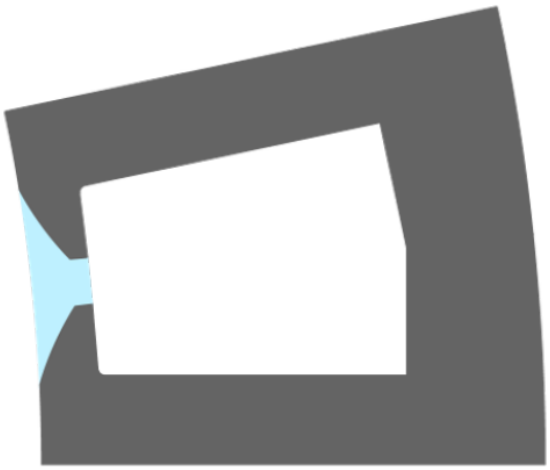

Figure 3.3 – Stator geometry for the 30s20p motor

Then, for the coils it was decided to employ rectangular windings with the following layout:

- Number of parallel paths: 1

- Coil pitch: 1
- Number of turns per coil: 18
- Number of wires in hand: 1

As a result of these settings, the slot is depicted in figure 3.4. These input data yields a net fill factor of 67.74% (gross fill factor of 59.497%). In addition, figure 3.5 depicts the winding layout.

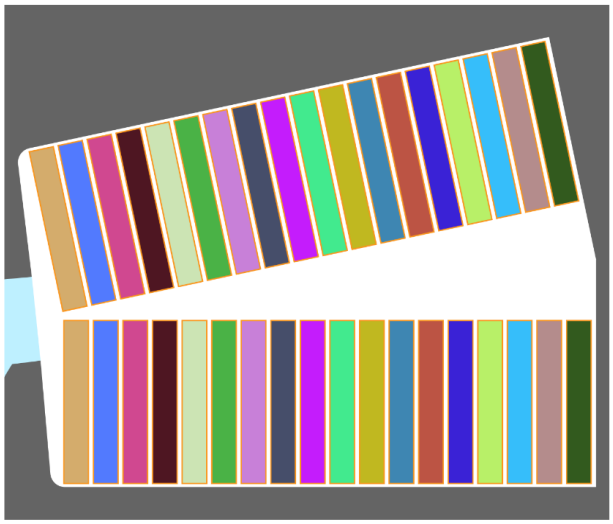

Figure 3.5 – 30s20p slot filling

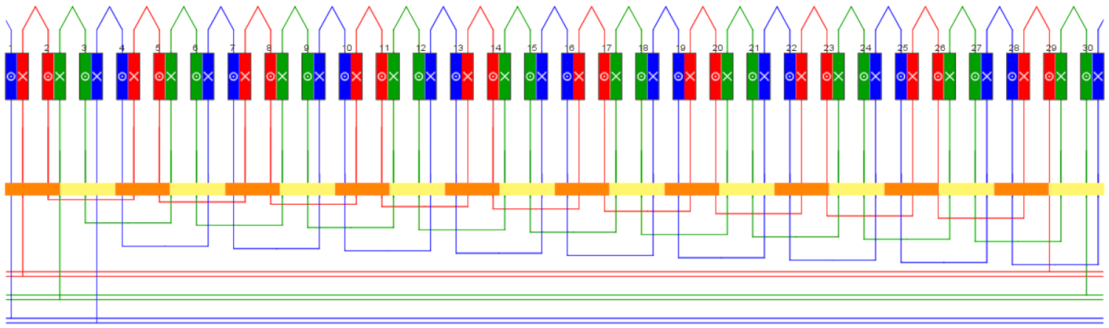

Figure 3.4 – 30s20p winding view

b. Distributed winding

For the distributed case, the rotor has 60 slots of which the dimensions are here showed, while the geometry can be seen in figure 3.6:

- Height of the slot: 23.01 mm
- Slot width: 13.5 mm
- Tooth width: 11.3 mm

- Slot opening: 3.0 mm

Figure 3.6 – Stator geometry for the 60s20p motor

The windings are again rectangular but this time the configuration is the following one:

- Number of parallel paths: 1
- Coil pitch: 3
- Number of turns per coil: 18
- Number of wires in hand: 1

In this way it has been possible to realise a fill factor of the slot comparable with respect to the concentrated winding case; in fact, the net fill factor in this case is 67.928% (the gross is equal to 59.662%). The view of the slot and the layout of the winding scheme arrangement are showed in figure 3.7 and 3.8.

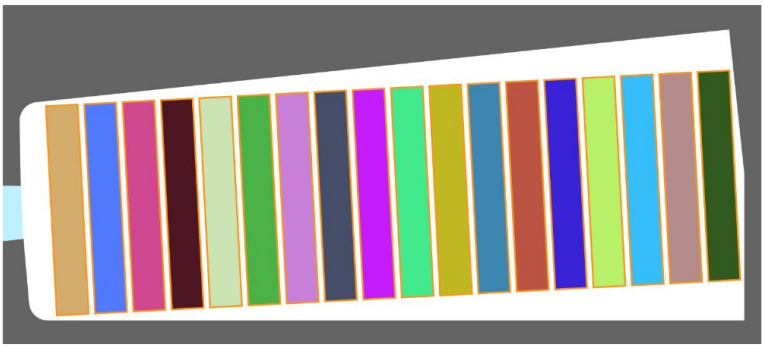

Figure 3.7 – 60s20p slot filling

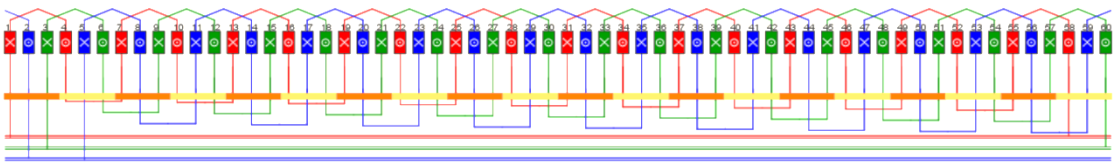

Figure 3.8 – 60s20p winding view

3.2 FEM analysis

Once defined the motor geometry, Altair FluxMotor™ dedicated test environment allow user to assess motor performances. The FEM is in charge of solving the differential equation to acquire the results in the first series of tests.

Of course, this task would be both time consuming and demanding on the computer's memory. So the software defines the boundary conditions to exploit the periodicity of the motor. In fact the calculations will be done only on one electrical period of the machine, which is equal to 6 degrees for the 30 slots 60 slots motors. Then, for FEM analysis the domain must be discretised by meshing. In FluxMotor™ can be chosen the mesh order (I^{st} order elements or II^{nd} order elements) and the airgap mesh coefficient. At this point the software calculates the size of mesh elements touching points of the geometry using the formula:

$$\text{MeshPoint} = \text{(airgap) x (airgap mesh coefficient)}$$

For this analysis will be used for all the tests a II^{nd} order mesh element and an airgap mesh coefficient equal to 0.45. So the result of this setting is showed in figure 3.9.

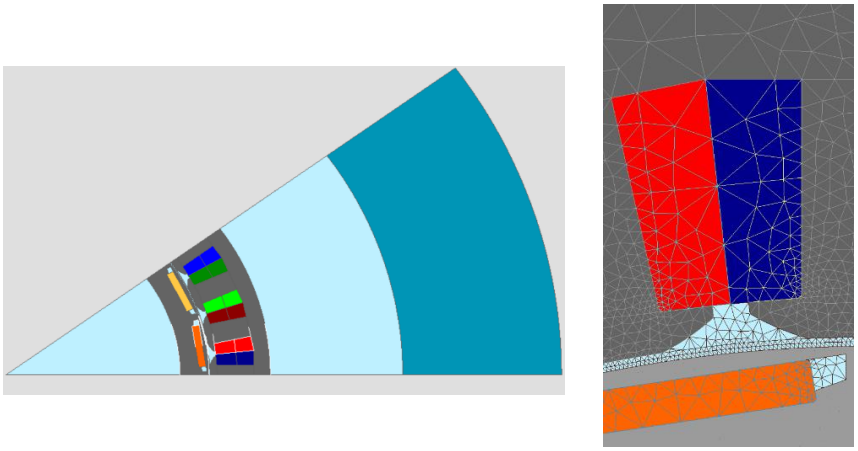

Figure 3.9 – Left: view of one electrical period of the motor. Right: example of meshing on 30s20p motor

The comparison between the different machines will be performed considering the following parameters:

- Cogging torque
- Back EMF
- Ripple torque

3.2.1 Cogging torque

The phenomenon of the cogging torque has been already examined in section 2.1.1. In other words, the cogging torque characterise the interaction between the rotor magnets and the stator teeth when there is no current. It's investigation can begin with the expression in (3.1):

$$T_{cog} = -\frac{1}{2}\phi^2 \frac{dR}{d\theta} \tag{3. 1}$$

Where ϕ is the magnetic flux that crosses the air gap while R is the reluctance through which the flux passes. As the magnets in the rotor revolve through to the stator teeth, the reluctance among the magnets fluctuates according to the slot opening in the stator teeth. So, the slot opening creates a variation of the reluctance for the magnet flux, resulting in cogging torque [15]; to further understand the causes of the cogging torque, the magnetic field lines between the edge of north and south will be showed for two rotor position in figure 3.10.

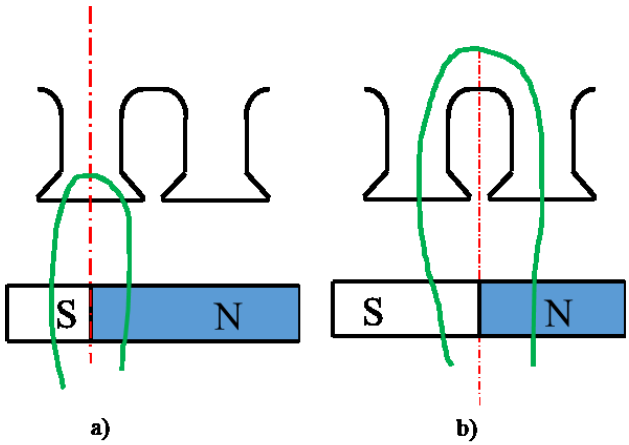

Figure 3.10 – (a) Magnetic field lines when the lines between the edge of north and south pole are aligned with the tooth (b) Magnetic field lines when the lines between the edge of north and south pole are aligned with air gap

To cogging torque test is performed on FluxMotor considering the following parameters:

- Number of computations per electric period: 45

The main output of this test will be:

- Table of the main cogging torque characteristics in terms of period of cogging torque and its peak-to-peak value

- Graph of the cogging torque versus the rotor angle position (the calculation is done for only one period

3.2.2 Back EMF

The back electromotive force refers to the voltage that occurs in electric motors when there is relative motion between the armature and the magnetic field produced by the motor's field coils or permanent magnet field, thus also acting as a generator while running as a motor. Because this voltage is in series with and opposes the initial applied voltage it is called "back-electromotive force". Then, as the motor rotates faster, with a lower overall voltage across the motor's internal resistance the current flowing into the motor decreases. Since the back-EMF is also due to inductance and Faraday's law, it can occur even when the motor current is not changing and arises from the geometric considerations of an armature spinning in a magnetic field. The amplitude of the back EMF E_b can be analytically obtained from (3.2):

$$e_b = \frac{d\lambda}{dt} = \frac{d\theta_e}{dt}\frac{d\lambda}{d\theta_e} = \omega_e \frac{d\lambda}{d\theta_e} = \frac{N_m}{2}\omega_m \frac{d\lambda}{d\theta_e} = \frac{N_m}{2}\omega_m \frac{2N\phi_g}{\pi} \tag{3.2}$$

Where:

- λ is the linkage flux
- θ is the electrical position of the rotor
- N_m is the number of magnets poles on the rotor
- ω_e and ω_m are respectively the electrical and mechanical frequency
- ϕ_g is the air gap flux
- N is the number of conductors

Then simplifying the air gap flux, the back EMF modulus can be obtained from (3.3):

$$|e_b| = E_b = \frac{N_m}{2}\omega_m \frac{2N}{\pi}\left(\frac{2\pi}{N_m} B_g L_{st} R_{ro}\right) = 2N B_g L_{st} R_{ro} \omega_m = K_e \omega_m \tag{3.3}$$

Where:

- B_g is the air gap flux density
- L_{st} is the axial length of the motor
- R_{ro} is the air gap radius at magnet surface

In the left-hand side of (3.4) appears the terms K_e, defined as the back EMF constant whose dimensions are [V/rpm].

In this work the back EMF will be analysed only in open circuit condition. Hence, the test will be conducted with the following inputs parameters:

- Speed: 1000.0 rpm
- Number of computations per electrical period: 100

In this way the results regarding the root mean square of the harmonic phase voltage can be obtained.

3.2.3 Ripple torque

Torque ripple is defined as the percentage of the difference between the maximum torque and the minimum torque compared to the average torque:

$$T_{ripple} = \frac{T_{max} - T_{\min}}{T_{avg}} \cdot 100 \tag{3.4}$$

When the motor is under load, in addition to the cogging torque, there is another component which contributes to the torque ripple. The interaction between the magneto-motive force (MMF) and the airgap flux harmonics causes torque ripple [16]. This component can be influenced by changes to the geometry of the machine design, especially the number of stator slots, the number of poles, the magnet angle, and the slot opening width. So torque ripple is a crucial parameter for this work.

Knowing the ripple torque, the torque constant k_t can be evaluated from:

$$k_t = \frac{T}{I} \tag{3.5}$$

In which is measured the ability to produce torque with respect to the current supplied.

Then, for what concerns the tests, for all machines they are carried out considering the same torque and rotating speed. In FluxMotors this test is performed in the 'working point' section, considering a sine wave drive. The following are the input parameters:

- Torque: 100.0 Nm
- Speed: 1000.0 rpm
- Number of computations per ripple period: 30

To perform the ripple torque test, the 'ripple torque analysis' request must be flagged in the input shell; then the following results are obtained:

- Ripple mechanical torque, peak to peak value
- Ripple mechanical torque magnitude versus average value
- Ripple mechanical torque versus rotor angular position graph

3.3 Loss calculation

For this analysis, the following losses will be considered:

- Winding Joule losses
- Iron losses
- Magnet losses

The first category, as the name suggests, is due to Joule effect in the wires. In fact while the current flows through the conductors, heat is generated, which dissipates some of the electrical energy produced. Considering the Joule's First Law is:

$$P = I^2R \tag{3.6}$$

Therefore, from the equation (3.6), the winding losses are proportional to the square of the induction current I, and the resistance R. The contribution of winding Joule losses will be separated into two components in this analysis: DC losses and AC losses.

Once the Joule losses are known, the so-called motor constant K_m, can be obtained calculated as follows:

$$k_m = \frac{T}{\sqrt{I^2R}} = \frac{T}{P} \tag{3. 7}$$

This parameter measures the ability of the motor to convert electrical power into mechanical power.

Then, the second form of loss to be addressed is iron losses. Because this kind of losses is the second biggest contributor to the machine losses, it has been extensively investigated by researchers throughout the years. Iron losses are induced by energy dissipation caused by hysteresis and eddy current losses that occur when ferromagnetic

materials are excited with time varying excitation. The contribution given by the eddy current losses P_e can be described by the relationship (3.8):

$$P_e = k_e h^2 f^2 B^2 \tag{3.8}$$

In which h is the material thickness, k_e is the material dependent constant, B is the magnetic field flux density and f is the frequency of the excitation. Instead the contribution due to the hysteresis P_h is given by (3.9):

$$P_h = k_h f B^n \tag{3.9}$$

Where k_h is a constant that depends on the material type and its dimensions while n is a material dependent exponent usually between 1.5 and 2.5.

According to (3.8) the power lost is proportional to the square of the frequency, hence hysteresis losses is expected to dominate at low frequencies, whereas eddy current loss are dominant at higher frequencies. In any case, since the two contributions are difficult to separate in practice, the iron losses are computed by adding them together.

The final losses evaluated are the one of the magnets. This type of losses is again related to the eddy current losses caused by flux density fluctuation in permanent magnets. This kind of losses is usually neglected, but in this application, since the employed magnets have a relatively high electrical conductivity due to their material, the eddy-current losses can be significant, leading to a critical growth in magnet temperature which can result in a partial demagnetisation of the magnets. This is a typical occurrence in machine with high electric loading, high rotational speed, or large number of poles [17]. The analysis of the magnet losses starts from (3.4) where the first contribution is split into its harmonic contribution [18]:

$$J_m = -\sigma_m j\omega A + J_c \tag{3.10}$$

In which J_c is a constraint current density selected to make the total current in the magnet cross section is equal to zero and σ_m is the electrical conductivity of the permanent magnet material. So the value of the total losses is computed summing together all the harmonics.

The test for calculating losses will always be done with the same output condition in terms of torque and speed considered for the ripple torque analysis. In any case, to do so, some

data, such as current density and control angle, will be different for each test scenario. Although the following input data will be shared by all configurations:

- Speed: 1000 rpm
- Number of computed electrical periods: 2
- Number of points per electrical period: 50

In this way the data about the losses can be obtained.

In addition to that, also a test to gather the efficiency map of the different configurations is performed. In this case the input parameters are the same for all the configurations:

- Max current density (rms): 20.0 A/mm2
- Max line-line voltage: 345.0 V
- Maximum speed: 6000 rpm

3.4 NVH analysis

The major source of noise, as described in section 2.1.1, is due to radial forces acting on the stator teeth. Anyway, the main parameter adopted in this analysis for the NVH analysis is the SPL. The procedure followed by FluxMotor for this calculation is resumed in figure 3.11. It combines the results of the analytical modal analysis, which takes the topological data of the motor as input, and the excitation computed by the FE analysis, which derives from the magnetic data of the motor and the electrical supply chosen.

The investigation looks at the behaviour of the motor when a torque of 100 Nm is applied at 1000 rpm. To do so, as already mentioned for the loss calculation, the data linked to current density and control angle relies on the test scenario. Instead for all the tests there will be 100 points for each electrical period.

In this way will be possible to obtain the data regarding the SPL and the graphs in which the radial and the tangential forces are plotted against the angular position of the rotor.

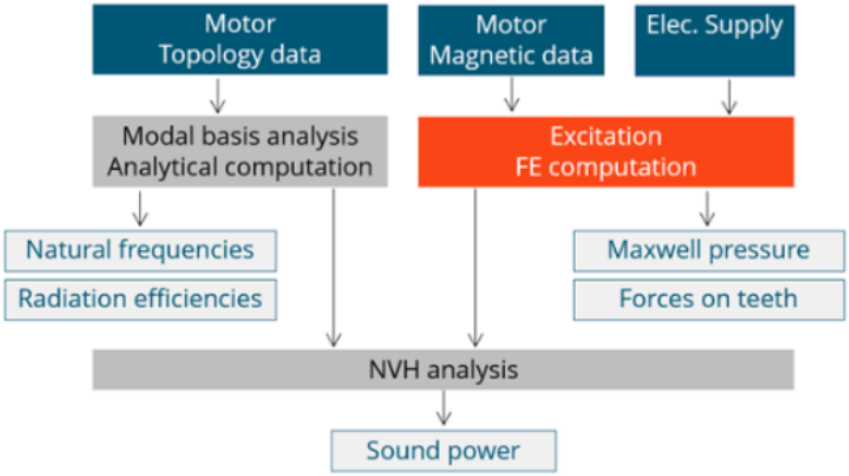

Figure 3.11 – SPL calculation workflow in FluxMotor

CHAPTER IV

Results and discussion

4.1 Test scenarios

To perform the sensitivity analysis, the following scenarios have been selected:

- *Scenario 1: concentrated and distributed winding comparison.* As already mentioned in chapter 2 the comparison will be between the 30-slots 20-poles machine with concentrated windings and the 60-slots 20-pole with distributed windings.
- *Scenario 2: influence of the slot opening.* This comparison will be carried out for both the concentrated and the distributed machine. For each, starting from a baseline opening of 3.5 mm, will be considered a slot opening reduction to 0.5mm and a slot opening expansion to 6.5 mm. The geometries for the concentrated and the distributed case are shown in figure 4.1 and figure 4.2.
- *Scenario 3: Flat tooth design.* In this case, the comparison is limited to the 30s20p machine with concentrated windings. There will also be three separate slot openings in this situation. The baseline for the slot opening is 3.5 mm and again a reduction to 0.5 mm is considered while for the enlargement an opening of 6.5 mm is considered.
- *Scenario 4: Flat tooth design with reduced height.* Here the analysis is done considering again the concentrated winding motor. The tooth again will be flat once more, but in this case the height of the tooth will be halved to 1.5 mm. To further understand the impact of this design, will be again considered three different slot opening: 3.5 mm as baseline, 0.5 mm, and 6.5 mm.

A view of the slots for each scenario is here showed.

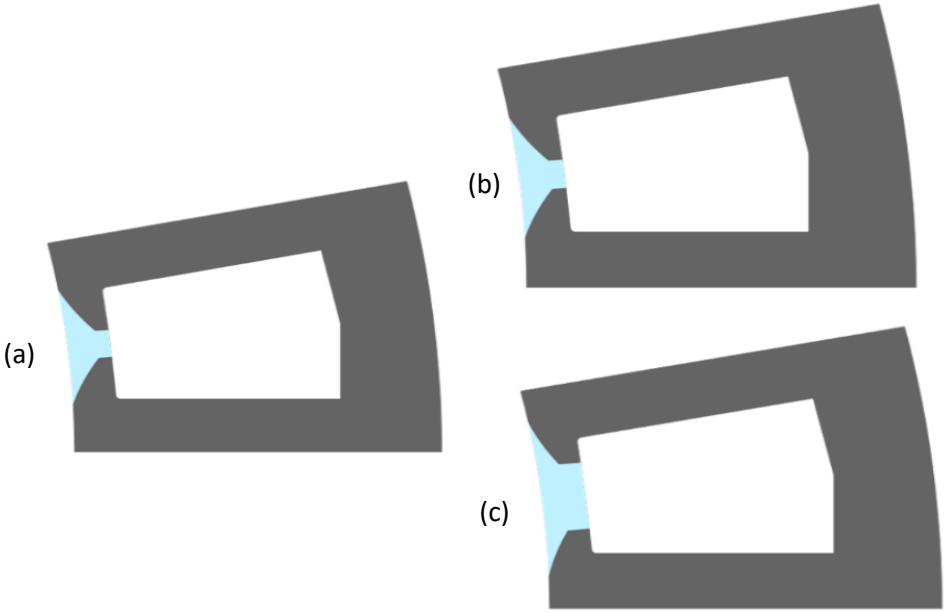

Figure 4.1 - 30s20p slot geometries for different slot opening. (a) 3.5 mm, (b) 0.5 mm, (c) 6.5 mm

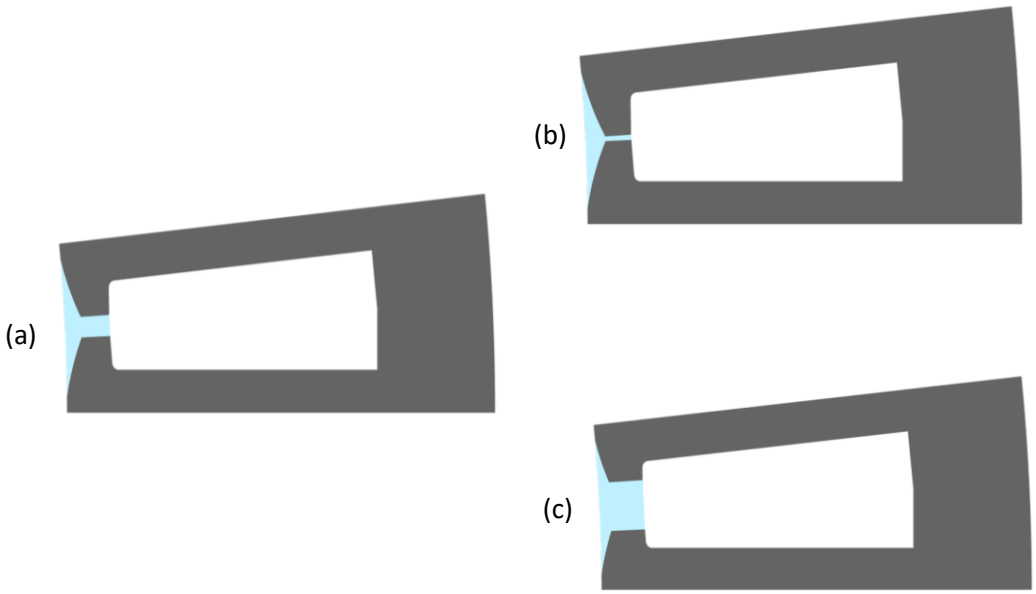

Figure 4.2 - 60s20p slot geometries for different slot opening. (a) 3.5 mm, (b) 0.5 mm, (c) 6.5 mm

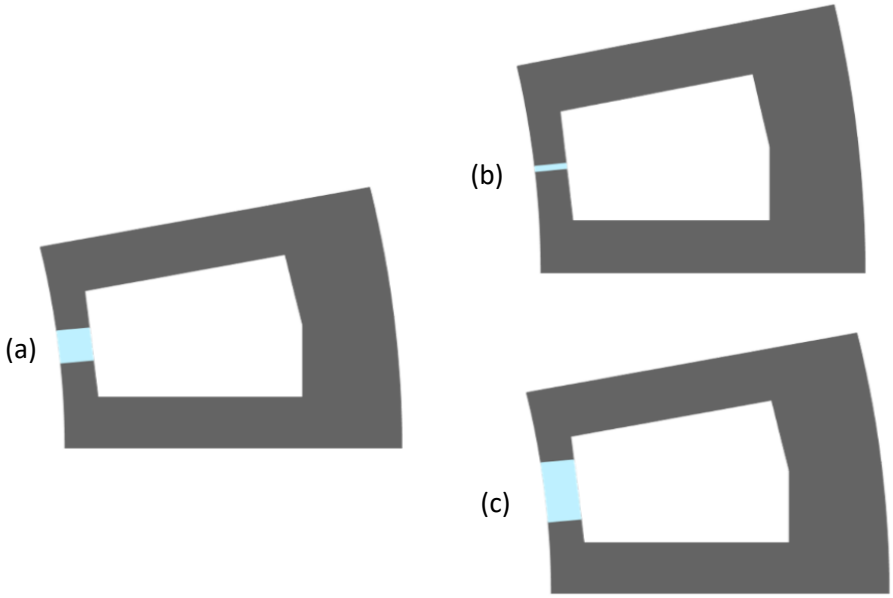

Figure 4.3 - 30s20p slot geometries with flat tooth for different slot opening. (a) 3.5 mm, (b) 0.5 mm, (c) 6.5 mm

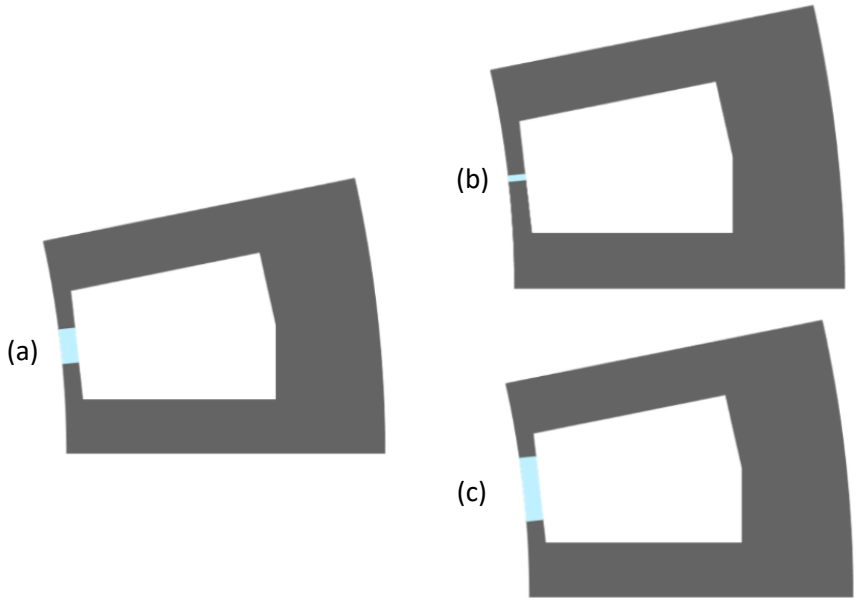

Figure 4.4 - 30s20p slot geometries with flat tooth and reduced height of the shoe of the tooth for different slot opening. (a) 3.5 mm, (b) 0.5 mm, (c) 6.5 mm

4.2 Results and discussion

Once defined the different test scenarios, following the procedure already showed in Chapter III, the results of the test are here resumed.

4.2.1 Distributed and concentrated windings comparison

Starting from the first scenario, the first family of tests that will be conducted is the open circuit test, which comprises the cogging torque test and the back EMF test. The results are showed in table 4.1, in which are highlighted the results of the cogging torque in terms of peak-to-peak value and the rms value, to better understand the harmonic content of the curve showed in figure 4.5 and 4.6. While, for what concerns the back EMF, other than the rms value is also showed the kE calculated from the (3.3).

	Coggin torque (pk-pk) [Nm]	Cogging torque (rms) [Nm]	Back EMF (rms) [V]	kE [V/rpm]
30s20p C	6.093	2.041	189.67	0.190
60s20p D	9.225	2.657	207.51	0.208

Table 4.1 - Open circuit tests results for Scenario 1

Even though the results are not so similar looking at the table 4.for the root mean square results and the curves there is not so much difference. Anyway, concentrated windings have very good results compared to the distributed case both for cogging torque and back EMF.

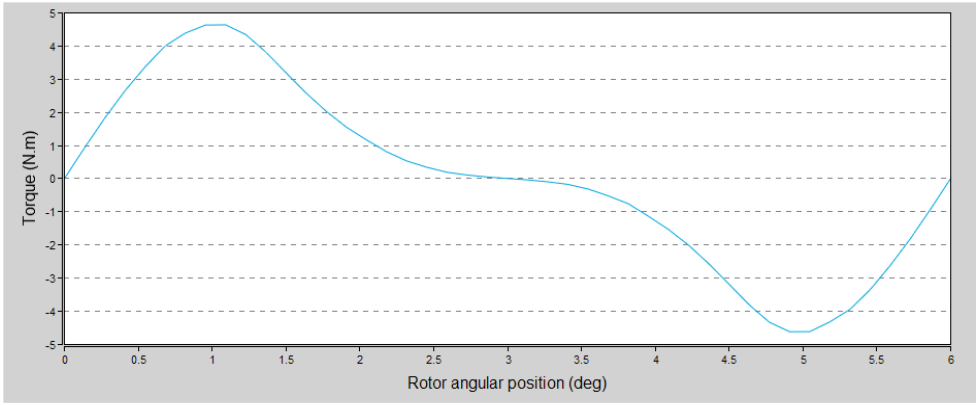

Figure 4.7 – Cogging torque curve for 30s20p C motor

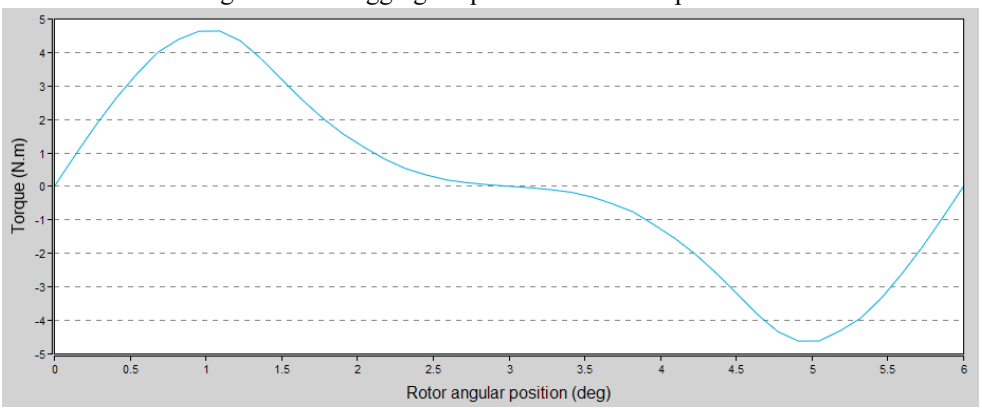

Figure 4.5 – Cogging torque curve for 60s20p D motor

The second test instead is the ripple torque test. As already mentioned in section 3.1.3 the test is performed considering an output torque of 100 Nm and a rotational speed of 1000 rpm.

In table 4.2 will be resumed the results regarding the value of the peak-to-peak torque and the standard deviation; in addition, the results related to the motor constant and the kT, calculated with (3.5) and (3.7) are showed.

	Ripple torque (pk-pk) [Nm]	Ripple torque (std deviation) [Nm]	Motor constant [Nm/√W]	kT [Nm/A]
30s20p C	5.538	1.710	5.058	2.170
60s20p D	10.339	12.455	4.444	1.436

Table 4.2 - Ripple torque test results for Scenario 1

Then, in figure 4.7 and in figure 4.8 will be plotted the trend of the ripple torque for the two motors versus the rotor angular position; in the figure there will be also the data of the current density supplied for this test and the control angle considered.

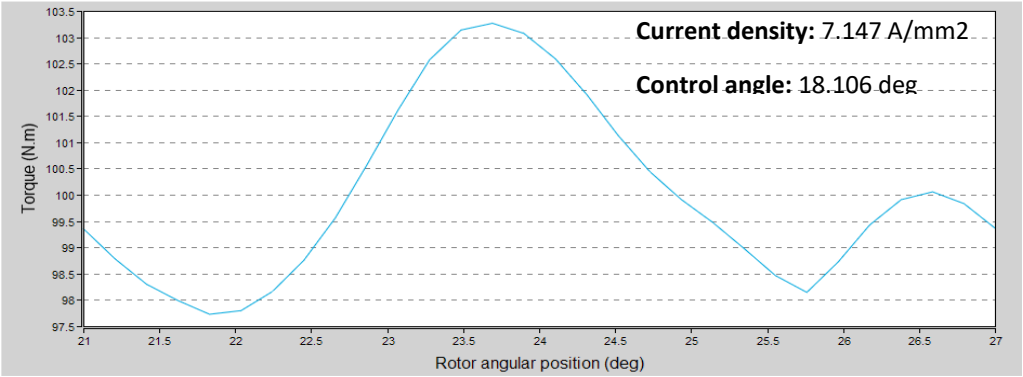

Figure 4.11 – Ripple torque curve for 30s20p C motor

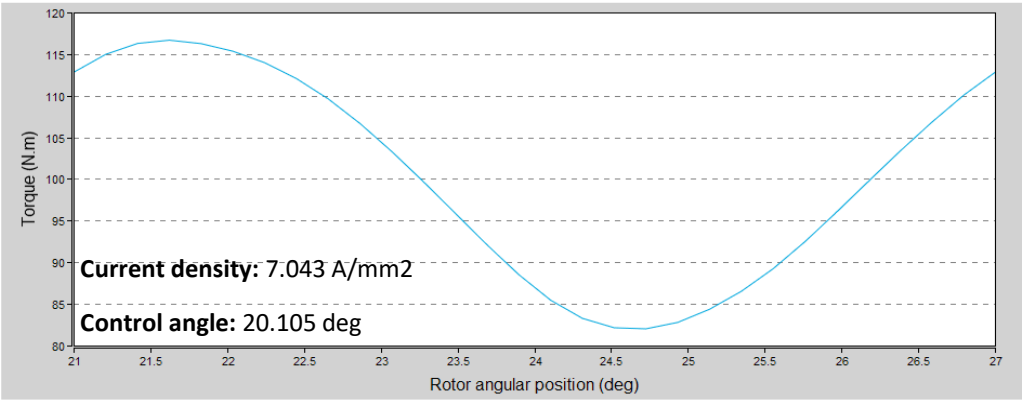

Figure 4.9 – Ripple torque curve for 60s20p D motor

From the results it is put in evidence that the concentrated windings motor have better performances in terms of ripple torque, motor constant and kT also in this case. Anyway, to reach the 100 Nm torque, it is necessary to supply it with higher current density as showed in figure 4.7 and 4.8.

Then, the analysis continues with the losses test. In table 4.3 are shown the results.

	DC Joule losses [W]	AC Joule losses [W]	Total Joule losses [W]	Magnet losses [W]	Iron losses [W]	Total losses [W]
30s20p C	368.627	23.092	391.719	80.133	85.393	557.245
60s20p D	382.338	5.707	388.045	2.126	90.53	480.701

Table 4.3 - Losses test results for Scenario 1

In this case the best performances are shown from the distributed winding motor. In particular, it shows very good results for the AC Joule losses and the magnet losses, while it has a worse behaviour for what concerns the iron losses. Anyway this difference is not very significant and in fact the 60s20p machine shows lower total losses.

Another important result to show is the efficiency map of both the motors. In this way the two machines can be compared on a broad range of performances. So the two maps are showed in figure 4.9 and figure 4.10 and on each map are also reported the base point speed results in terms of torque, speed, and efficiency; then is added also the result to show the maximum efficiency.

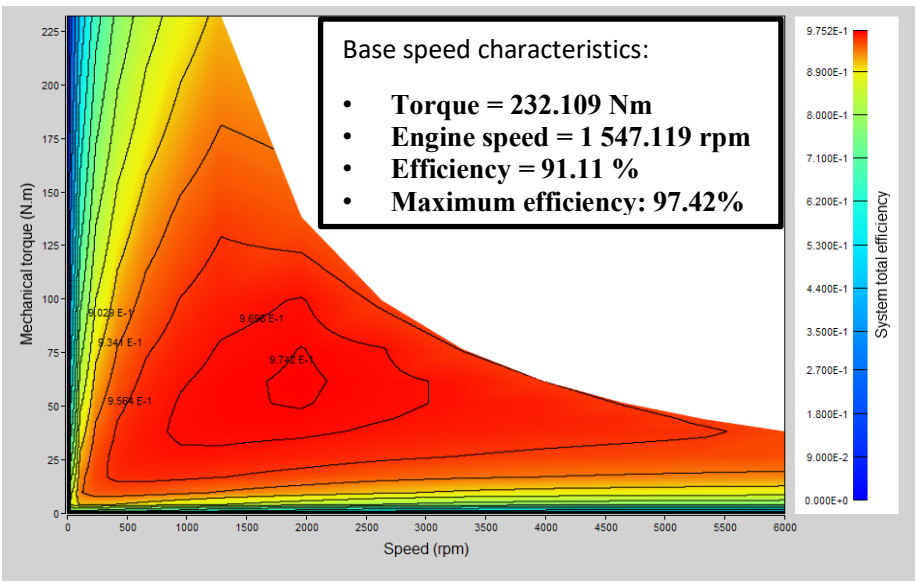

Figure 4.13 – Engine map e base speed performance for 30s20p C motor

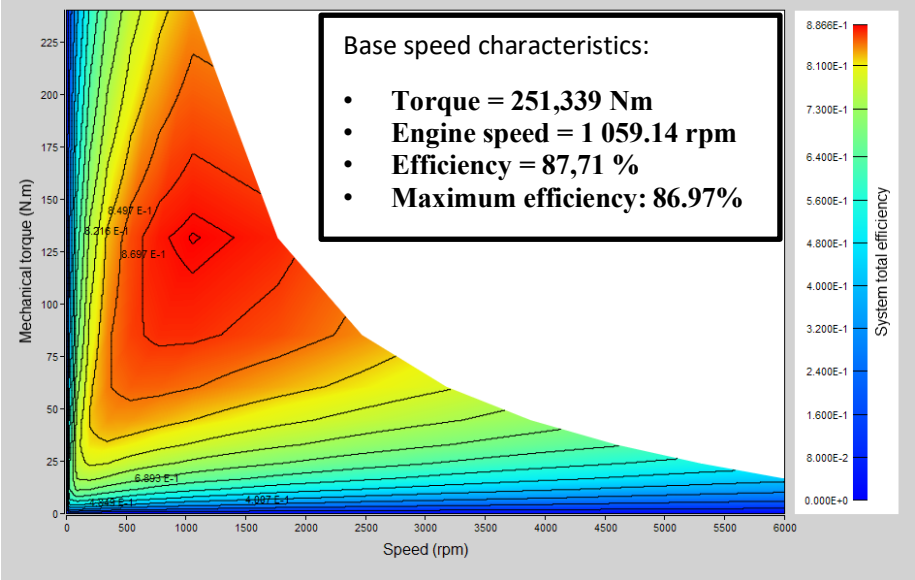

Figure 4.14 – Engine map and base speed performance for 60s20p motor

Comparing the performances of the two motors at the base speed point the two graph shows that the 30s20p machine can reach higher maximum rotational speed and higher efficiencies at lower torque, confirming also the results related to the kT. Also for what concerns the maximum efficiency the 30s20p configuration is better.

Then to conclude the analysis of this scenario the NVH test is performed. First the results of the SPL are shown in table 4.4. To obtain these results the motor is fed with the same current seen for the ripple torque test and the same control angle is considered.

	Overall sound power level [dB]
30s20p C	63.236
60s20p D	51.580

Table 4.4 – SPL results for Scenario 1

Even if the results regarding the ripple torque are worse, the machine with distributed windings has better performance for what concerns the SPL. This confirms the results coming from literature showed in the Chapter II. In fact looking at the trend of the radial forces showed in figure 4.11, the concentrated winding configuration has a lower amplitude of the excitation.

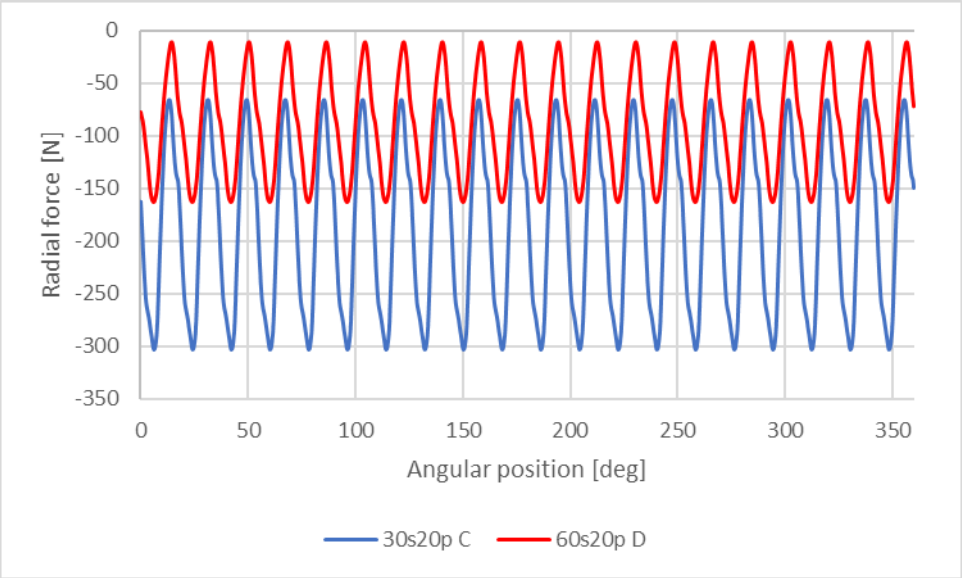

Figure 4.16 – Radial forces comparison for Scenario 1

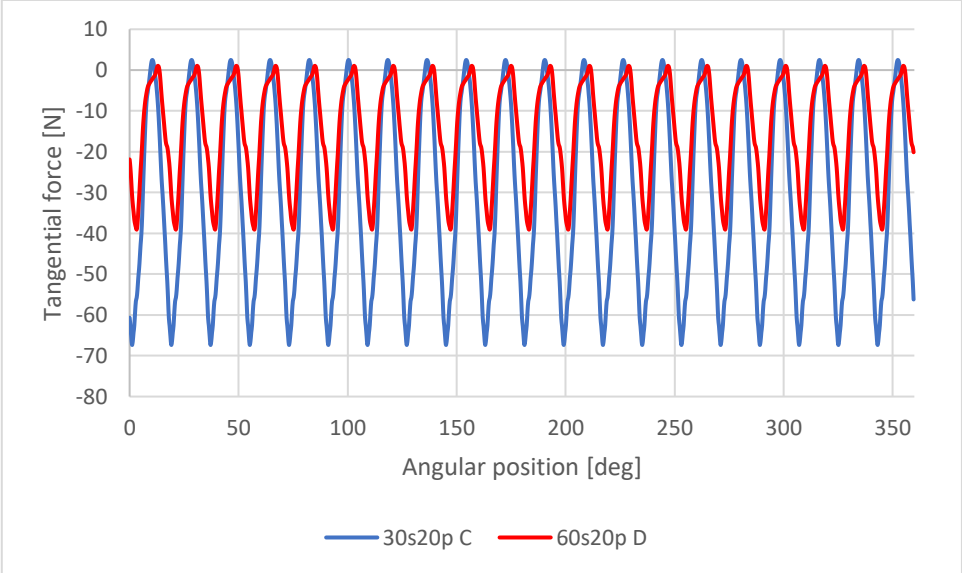

Figure 4.18 – Tangential forces comparison for Scenario 1

4.2.2 Influence of the slot opening

For the Scenario 2, the same procedure seen in the previous section will be followed.

The first case to be analysed is the concentrated winding layout. So, the analysis starts from the cogging torque and back EMF. Again the results are plotted first in table 4.5 and then the trends of the cogging torque against the rotor angular position are showed in figure 4.13, figure 4.14 and figure 4.15 respectively for the baseline slot opening, the 0.5 mm slot opening and the 6.5 mm slot opening.

	Coggin torque (pk-pk) [Nm]	Cogging torque (rms) [Nm]	Back EMF (rms) [V]	kE [V/rpm]
3.5 mm (baseline)	6.093	2.041	189.67	0.1094
0.5 mm	6.913	2.174	190.26	0.1097
6.5 mm	5.671	1.841	181.39	0.1045

Table 4.5 – Cogging torque results for Scenario 2 for concentrated winding motors

In this case there is not a big discrepancy between the results. Anyway the 6.5 mm opening solution has best results for all the parameters under analysis. While considering the trends of the cogging torque they confirm that there is not a high difference between the three solutions.

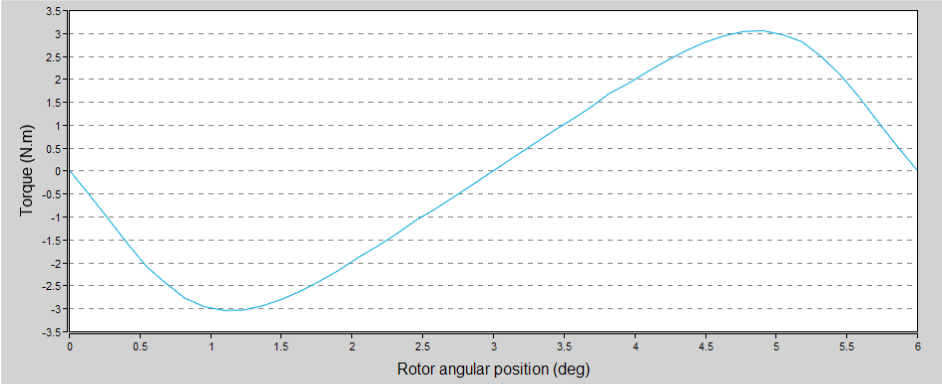

Figure 4.20 – Cogging torque curve for concentrated winding motor with 3.5 mm slot opening

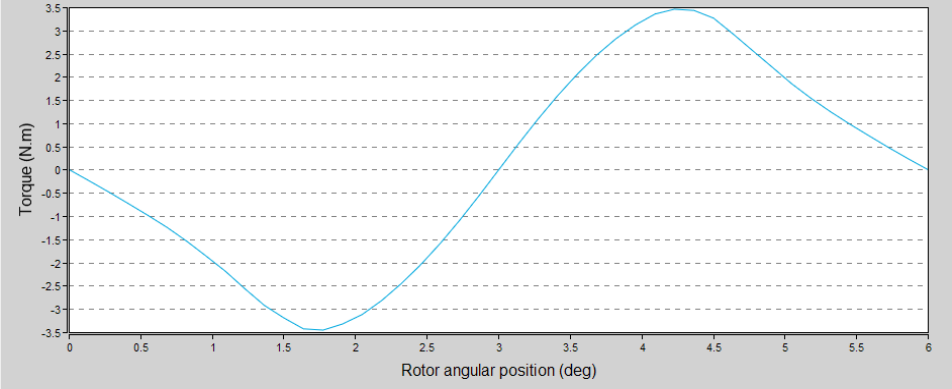

Figure 4.19 – Cogging torque curve for concentrated winding motor with 0.5 mm slot opening

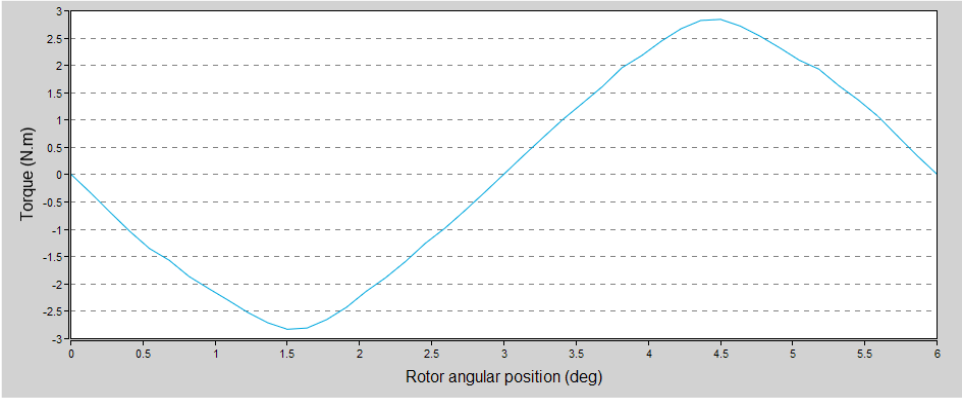

Figure 4.21 – Cogging torque curve for concentrated winding motor with 6.5 mm slot opening

Then the ripple torque analysis is conducted. From the table 4.6, as showed in the previous section, the 3.5 mm case has good performance, also for what concerns the standard deviation.

	Ripple torque (pk-pk) [Nm]	Ripple torque (std deviation) [Nm]	Motor constant [Nm/√W]	kT [Nm/A]
3.5 mm (baseline)	5.538	1.710	5.058	2.170
0.5 mm	10.339	7.385	4.444	1.436
6.5 mm	7.873	2.379	4.808	1.654

Table 4.6 – Ripple torque results for Scenario 2 for concentrated winding motors

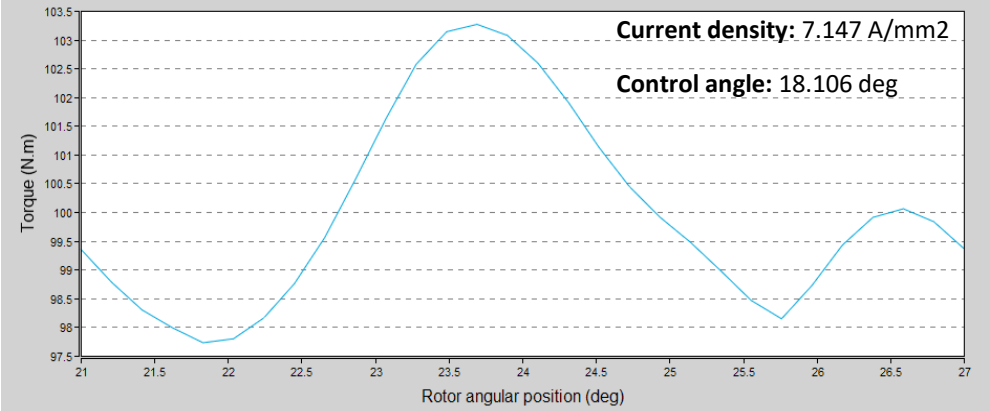

Figure 4.23 – Ripple torque curve for concentrated winding motor with 3.5 mm slot opening

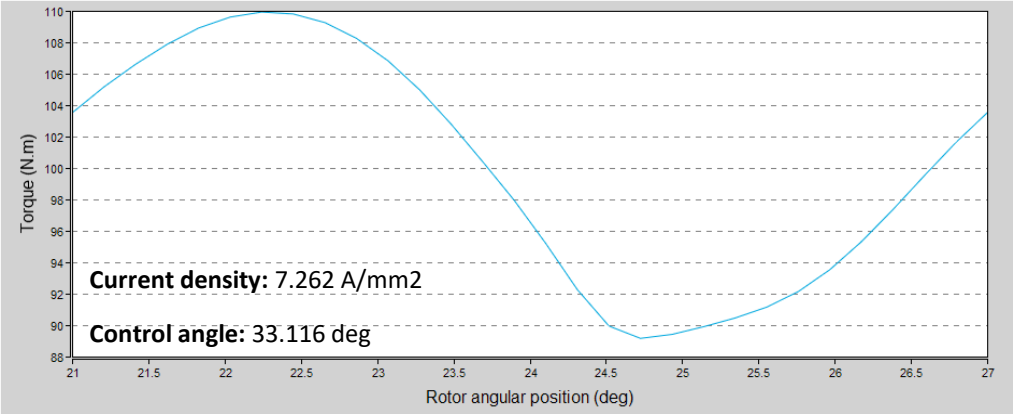

Figure 4.26 – Ripple torque curve for concentrated winding motor with 0.5 mm slot opening

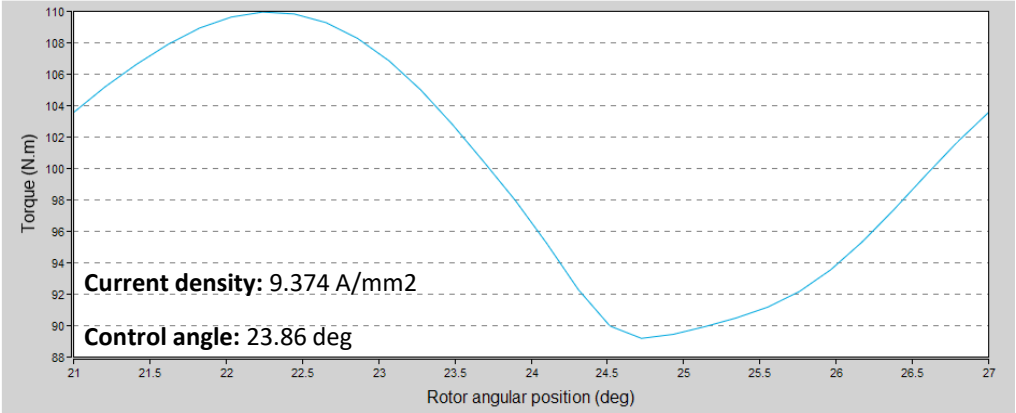

Figure 4.24 – Ripple torque curve for concentrated winding motor with 6.5 mm slot opening

Also in this case the baseline solution is the one fed with the lowest current density as also shown from the kT result.

After that, the analysis focuses on the losses. In table 4.7. the results regarding the losses in the three different configurations are resumed.

	DC Joule losses [W]	AC Joule losses [W]	Total Joule losses [W]	Magnet losses [W]	Iron losses [W]	Total losses [W]
3.5 mm (baseline)	368.627	23.092	391.719	80.133	85.393	557.245
0.5 mm	469.165	42.194	511.359	55.224	87.99	654.573
6.5 mm	463.049	13.545	476.594	87.201	70.956	634.751

Table 4.7 – Losses results for Scenario 2 for concentrated winding motors

Even if the result of the AC losses and of the iron losses are not the best of the three, for what concerns the Joule losses, the iron losses and the total losses, the 3.5 mm solution with the lower values. One thing to mention is the good result of the 0.5 mm case with the magnet losses and the iron losses obtained for the iron losses by the 6.5 mm solution.

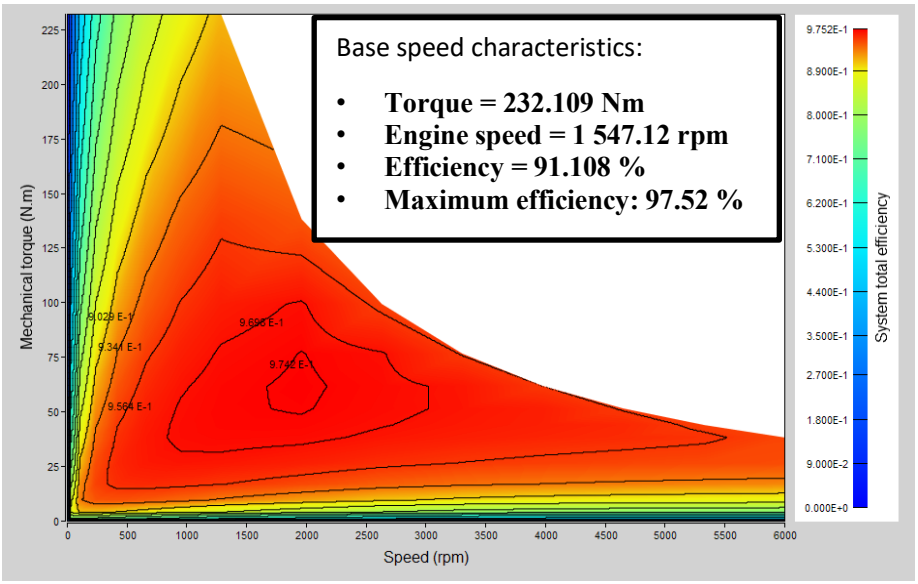

Figure 4.30 – Engine map and base speed performance for concentrated winding motor with 3.5 mm slot opening

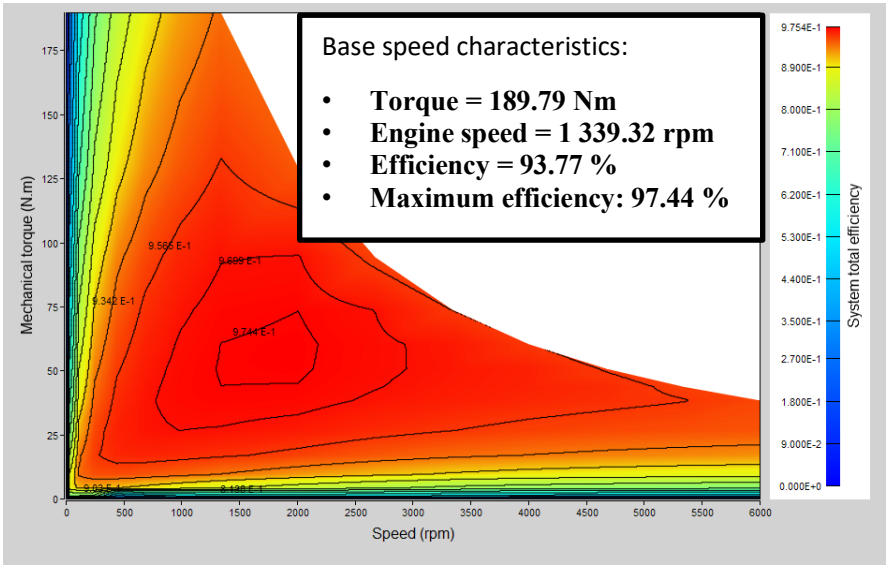

Figure 4.28 - Engine map and base speed performance for concentrated winding motor with 3.5 mm slot opening

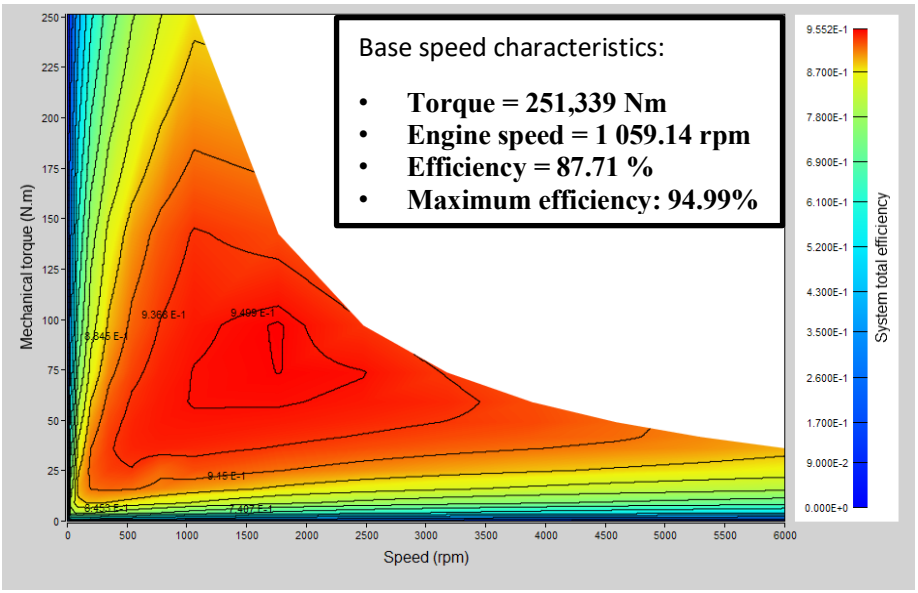

Figure 4.32 - Engine map and base speed performance for concentrated winding motor with 3.5 mm slot opening

Results related to losses confirms that the 3.5 mm configuration is the best one of this comparison.

Then the first part of the analysis of this scenario concludes with the NVH analysis. The comparison starts from the analysis of the SPL.

	Overall sound power level [dB]
3.5 mm (baseline)	63.236
0.5 mm	52.834
6.5 mm	45.281

Table 4.8 – SPL results for Scenario 2 for concentrated winding motors

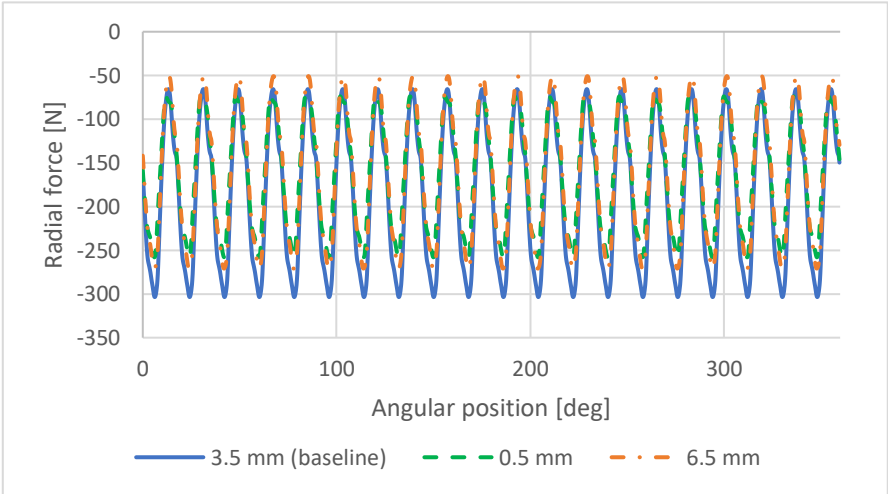

Figure 4.34 – Radial force comparison for Scenario 1 for concentrated windings motors

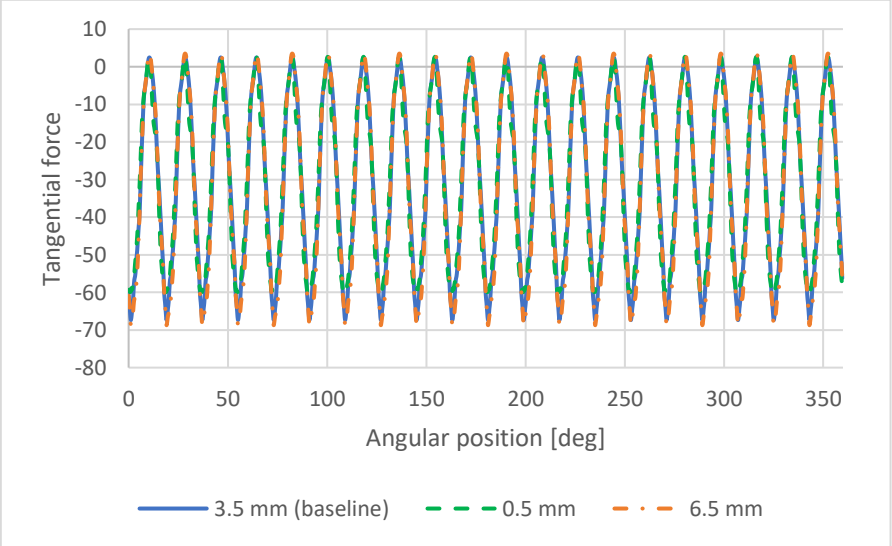

Figure 4.35 – Tangential force comparison for Scenario 1 for concentrated winding motors

In this case there is a significative reduction of SPL in the 6.5 mm machine. This is again confirmed looking at the results related to the radial force comparison; in fact, from figure 4.22 it's shown a small reduction of the amplitude of the curves, both for the 0.5 mm and the 6.5 mm case.

Concluded the part related to the 30s20p machine, the same procedure is followed for the 60s20p case with distributed windings for the same three slot openings.

Starting from the open circuit test, the results in table 4.9 shows that the 0.5 mm slot opening is the configuration that minimises the cogging torque and the back EMF. Whereas for what concerns the kE, the results are almost the same. The same can be told for the cogging torque against the rotor angular positions trends.

	Coggin torque (pk-pk) [Nm]	**Cogging torque (rms) [Nm]**	**Back EMF (rms) [V]**	**kE [V/rpm]**
3.5 mm (baseline)	9.255	2.657	207.514	0.122
0.5 mm	8.991	2.583	204.980	0.120
6.5 mm	11.14	3.077	207.237	0.122

Table 4.9 – Cogging torque results for Scenario 2 for distributed winding motors

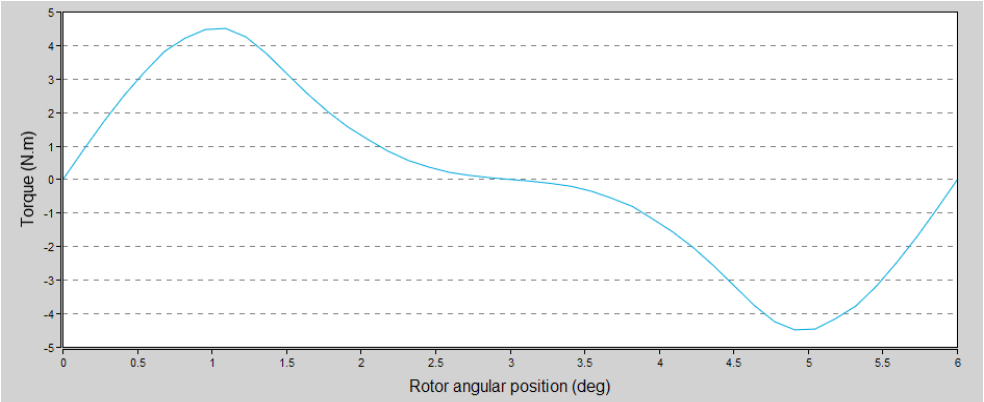

Figure 4.37 – Cogging torque curve for distributed winding motor with 3.5 mm slot opening

Figure 4.41 – Cogging torque curve for distributed winding motor with 0.5 mm slot opening

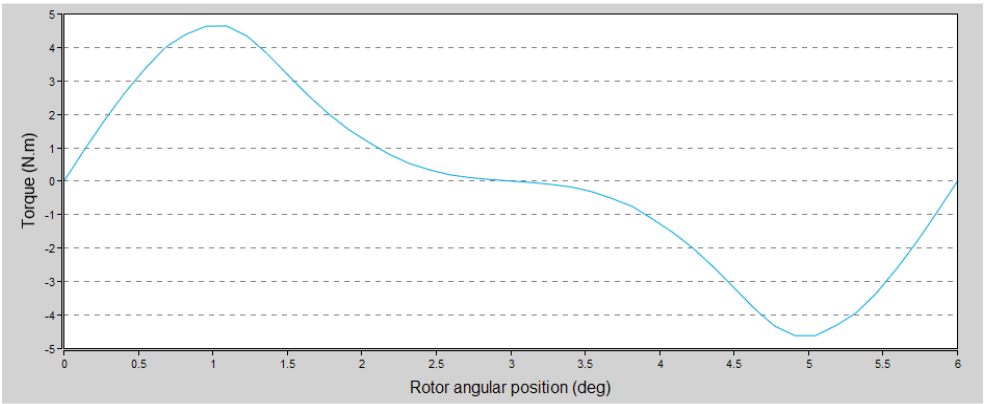

Figure 4.39 – Cogging torque curve for distributed winding motor with 6.5 mm slot opening

Then, there are the results related to the ripple torque. 3.5 mm and 6.5 mm have results quite comparable in this case, with a little better result for the baseline, while the 0.5 mm as expected has worse performances. This is not true instead for the kT analysis in which the 0.5 mm solution appears to be the best one. Anyway the 6.5 mm case can

reach the target of 100 Nm of torque with the lowest current supply as showed in figure 4.29.

	Ripple torque (pk-pk) [Nm]	Ripple torque (std deviation) [Nm]	Motor constant [Nm/√W]	kT [Nm/A]
3.5 mm (baseline)	34.660	12.455	5.178	2.202
0.5 mm	41.207	14.822	4.786	2.135
6.5 mm	35.339	12.531	5.243	2.250

Table 4.10 – Ripple torque results for Scenario 2 for distributed winding motors

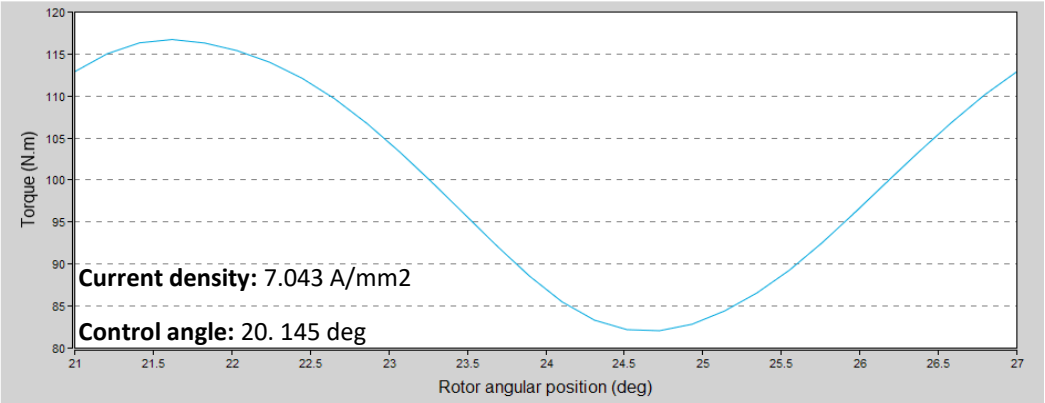

Figure 4.45 - Ripple torque curve for distributed winding motor with 3.5 mm slot opening

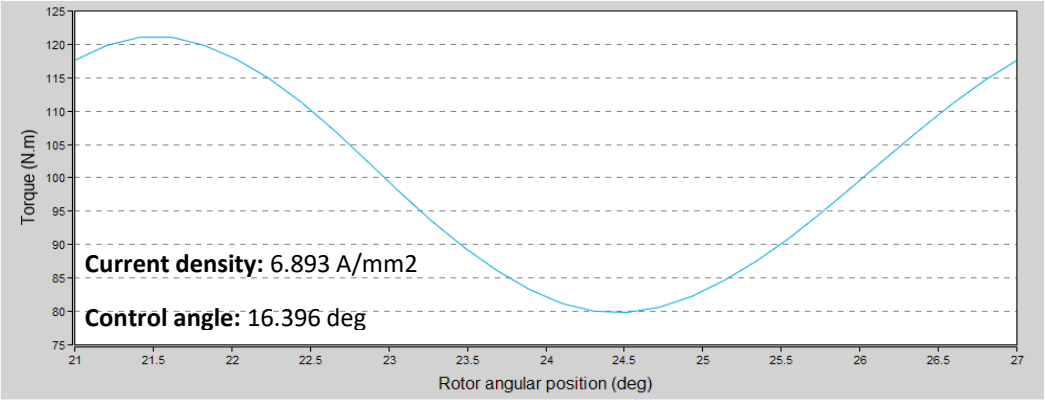

Figure 4.43 - Ripple torque curve for distributed winding motor with 0.5 mm slot opening

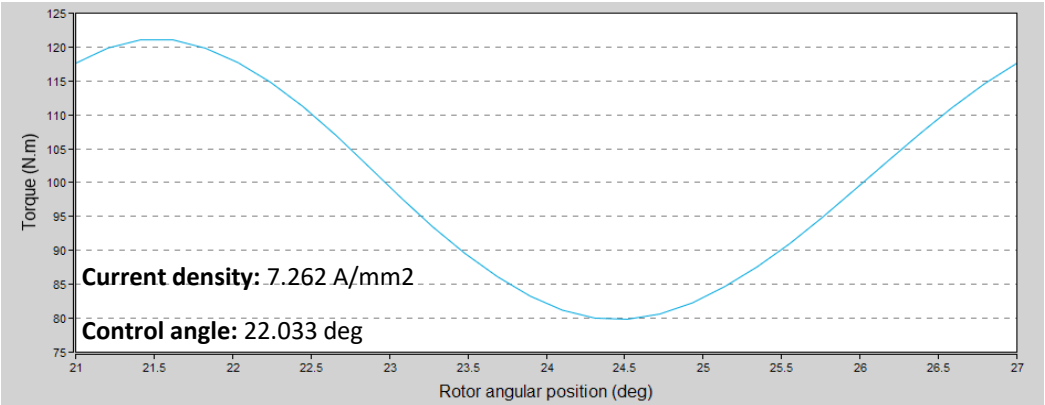

Figure 4.47 - Ripple torque curve for distributed winding motor with 6.5 mm slot opening

While for what concerns the results regarding the losses, they are resumed in table 4.11.

	DC Joule losses [W]	AC Joule losses [W]	Total Joule losses [W]	Magnet losses [W]	Iron losses [W]	Total losses [W]
3.5mm (baseline)	382.338	5.707	388.045	2.126	90.53	480.701
0.5 mm	452.159	11.038	463.197	2.387	106.36	571.944
6.5 mm	366.188	4.318	370.506	2.810	86.654	459.970

Table 4.11 – Losses results for Scenario 2 for distributed winding motors

Looking at the table the 3.5 mm configuration has very good results, also looking at the 0.5 mm case. In particular, this configuration is very effective to reduce the Joule losses. Then the three engine maps are plotted below.

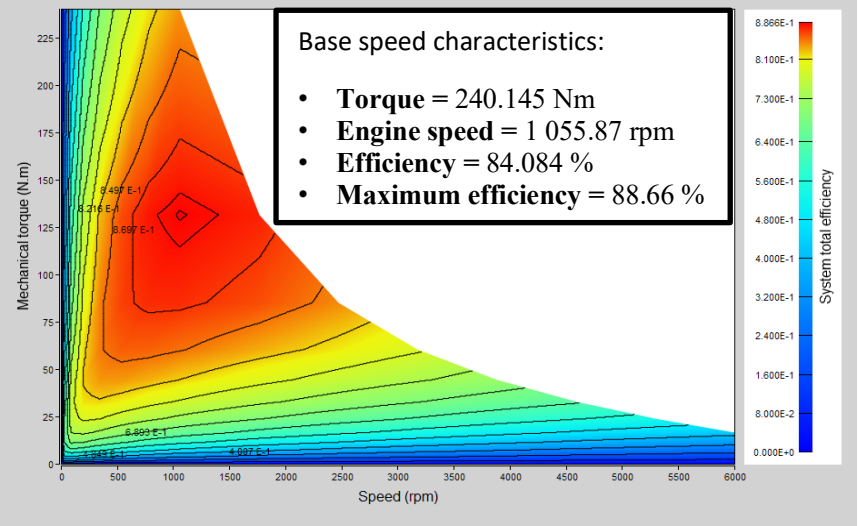

Figure 4.51 - Engine map and base speed performance for distributed winding motor with 3.5 mm slot opening

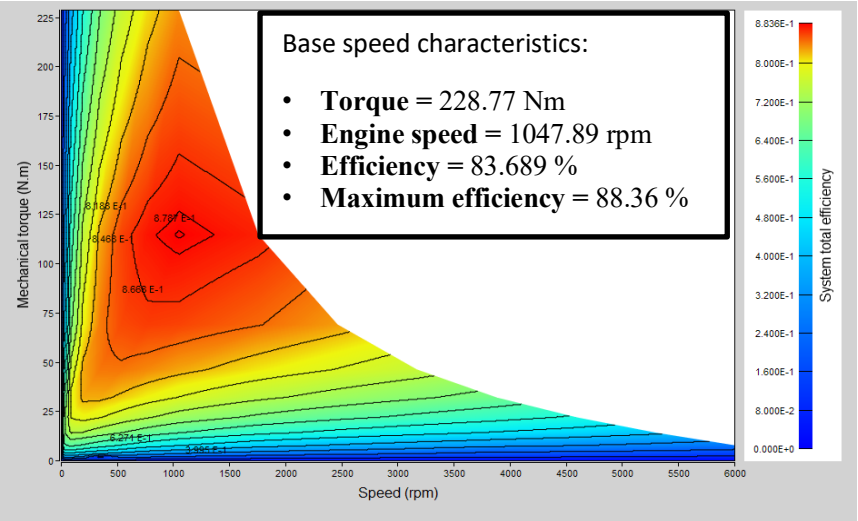

Figure 4.49 - Engine map and base speed performance for distributed winding motor with 0.5 mm slot opening

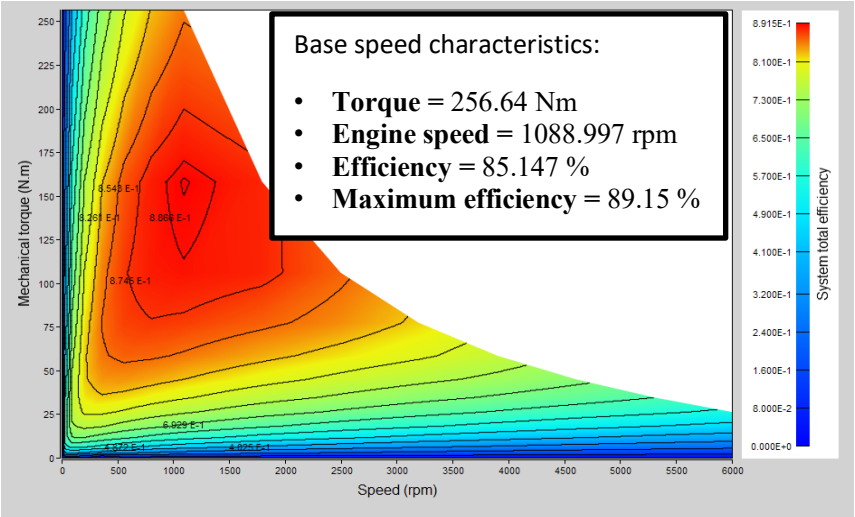

Figure 4.53 - Engine map and base speed performance for distributed winding motor with 6.5 mm slot opening

With respect to the concentrated winding case these machines work at maximum efficiency in a narrow range of torque and speed. Anyway, the configuration that has the best performances is the 6.5 mm slot opening.

	Overall sound pressure level [dB]
3.5 mm (baseline)	51.580
0.5 mm	48.304
6.5 mm	51.617

Table 4.12 – SPL results for Scenario 2 for distributed winding motors

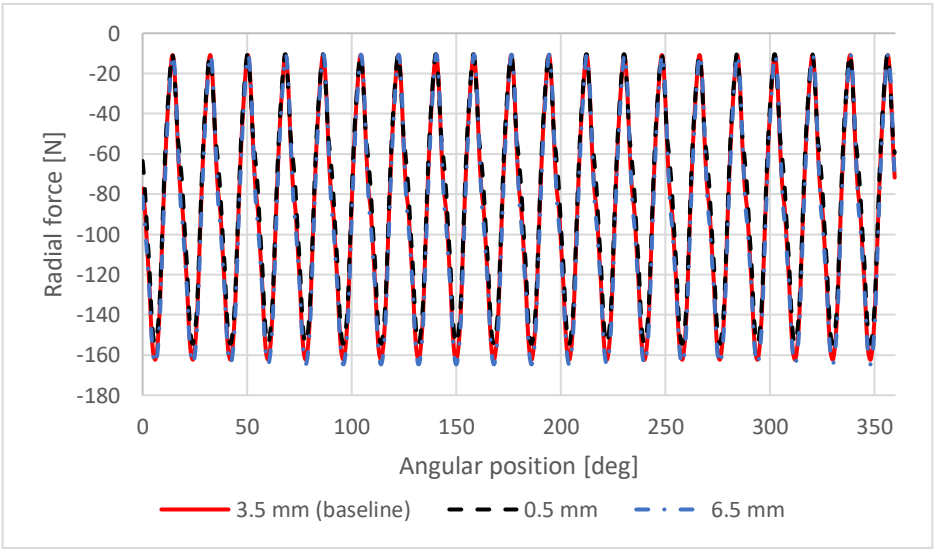

Figure 4.55 - Radial force comparison for Scenario 2 for distributed windings motors

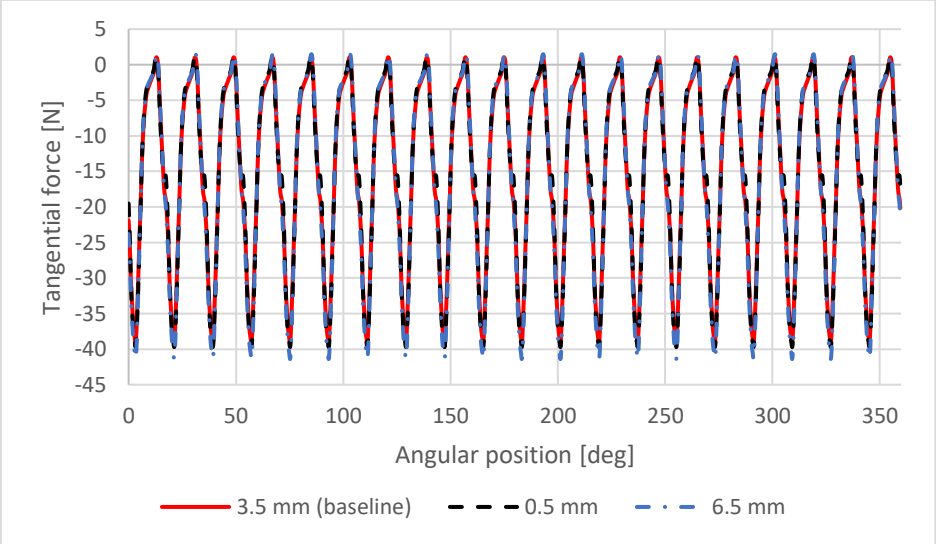

Figure 4.57 - Tangential force comparison for Scenario 2 for distributed windings motors

Then to conclude this analysis the NVH test results are showed here. In this case the 0.5 mm solution is the one which shows the best behaviour between the three configurations. Anyway the reduction of the noise is not so significant, and this can be clearly seen from the figure 4.33 in which are plotted the radial forces and the trends are almost overlapped.

At this point it's useful to compare again the concentrated and the distributed winding for the different slot opening. The results for all the section previously seen will be resumed in histograms to better understand the difference between the two configurations.

Starting from the two graphs related to the cogging torque; in this case the performance offered by the distributed winding motor are worse both in terms of peak-to-peak values and rms values.

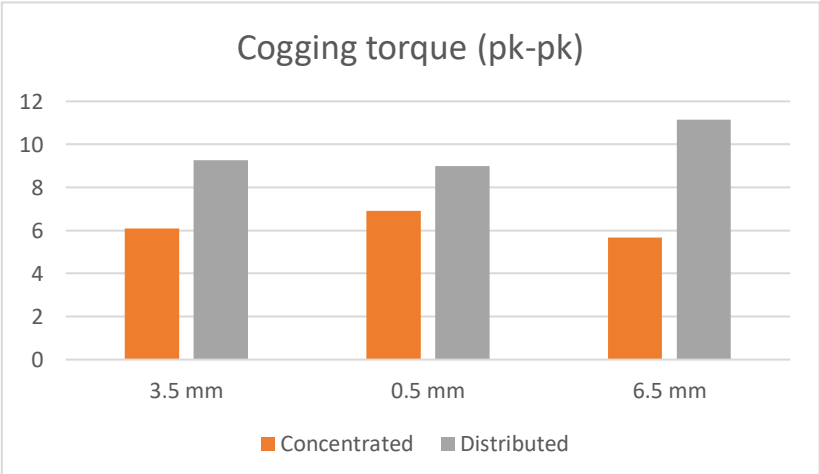

Figure 4.59 – Peak-to-peak cogging torque comparison for Scenario 2

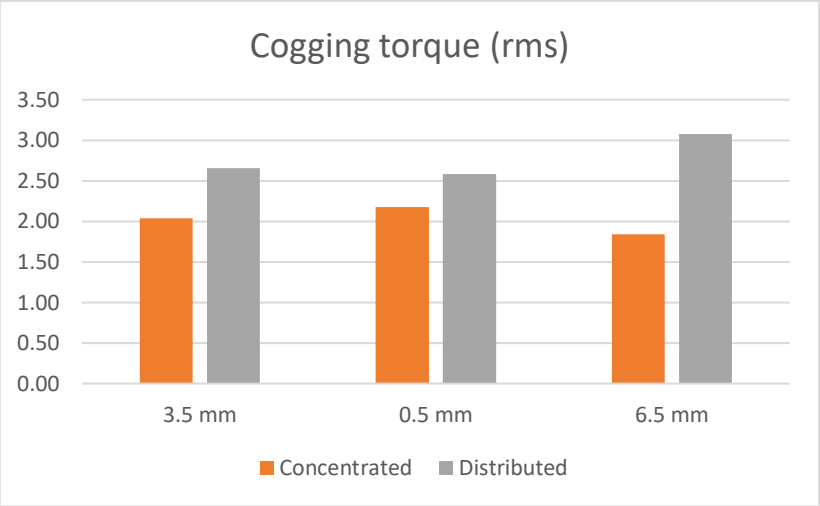

Figure 4.61 - Rms cogging torque comparison for Scenario 2

This result is also confirmed for the back EMF and the kE with a high discrepancy mainly in for the 6.5 mm configuration.

The benefits of the concentrated winding layout are confirmed also looking at the back EMF performances and the kE. In particular, the best solution in this case is the concentrated winding layout with 6.5 mm slot opening.

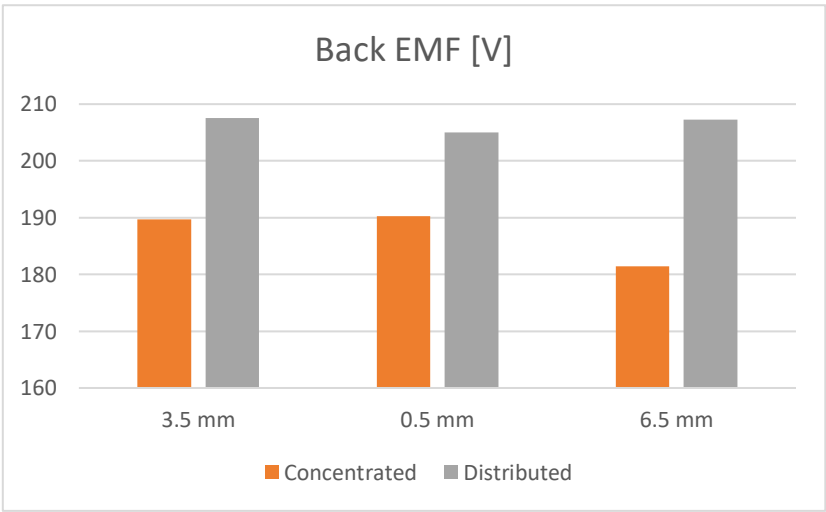

Figure 4.63 – Back EMF comparison for Scenario 2

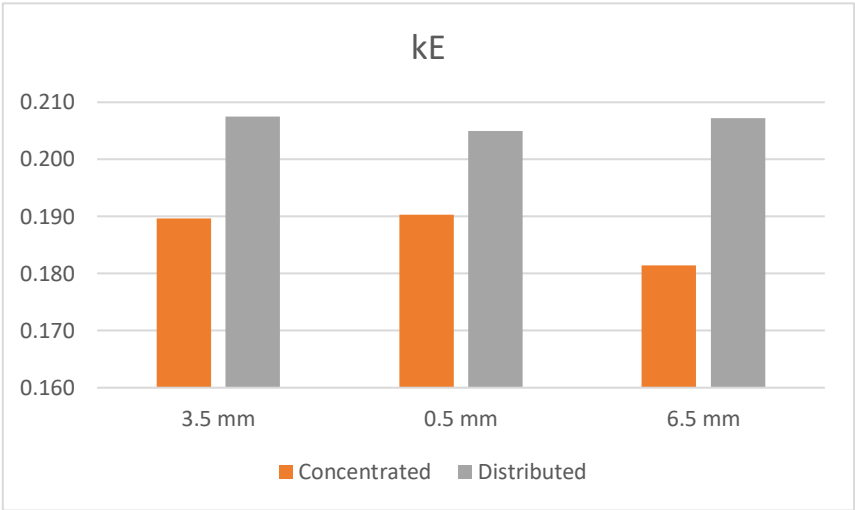

Figure 4.68 – kE comparison for Scenario 2

The concentrated winding layout is also beneficial to reduce the ripple torque as showed in figure 4.39 and 4.40.

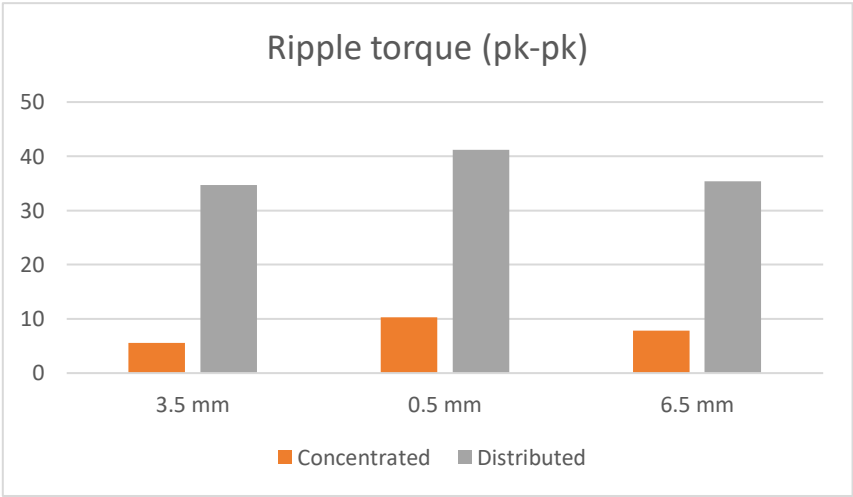

Figure 4.64 – Peak to peak ripple torque comparison for Scenario 2

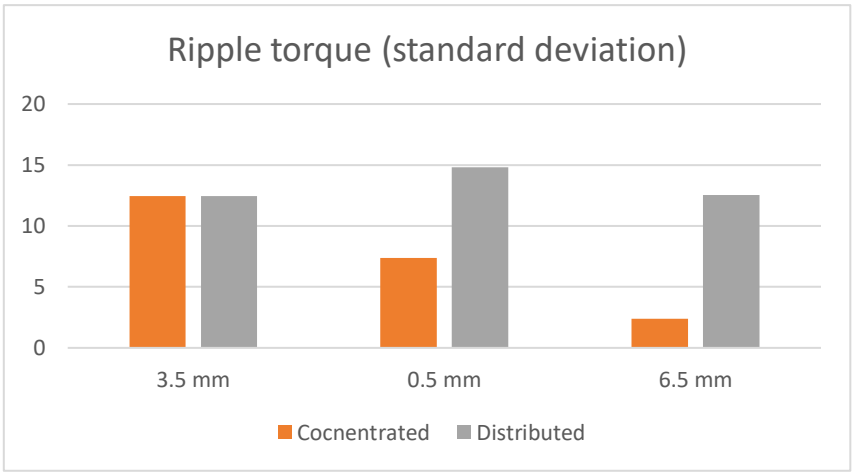

Figure 4.66 – Ripple torque standard deviation comparison for Scenario 2

Because the spread winding motors perform poorly for ripple torque, the motor constant and the kT comparison shows that the concentrated winding works better for all slot openings studied as shown in figure 4.41 and 4.42.

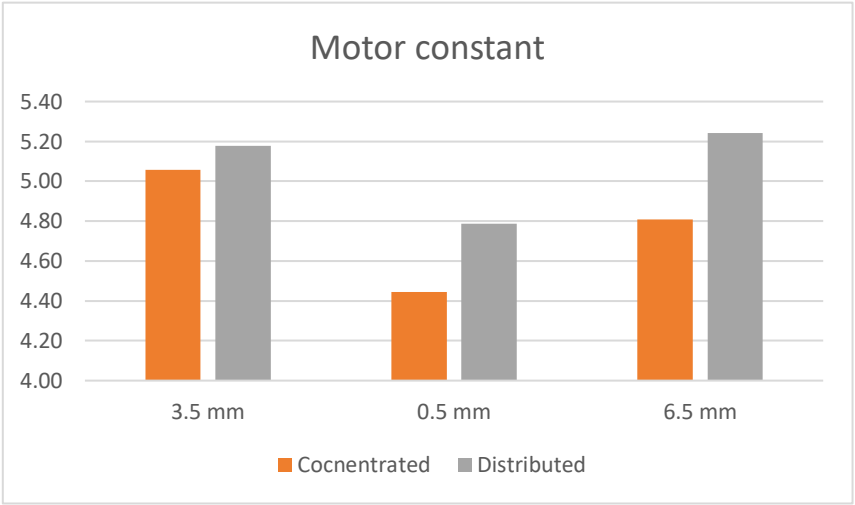

Figure 4.72 – Motor constant comparison for Scenario 2

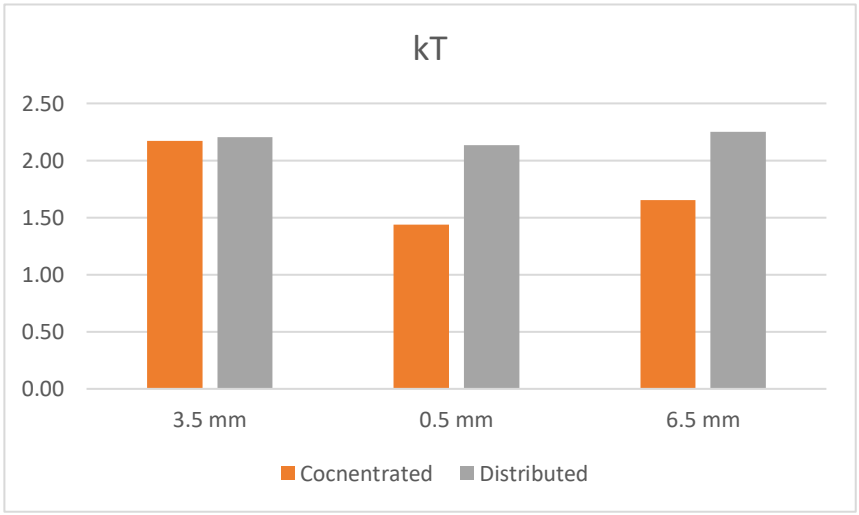

Figure 4.70 – kT comparison for Scenario 2

Then there is the comparison for the losses. First will be considered the Joule losses, considering the contribution of the DC losses and AC losses. In the first two configurations the DC losses are quite comparable, while in the 6.5 mm case there is a significant reduction of the losses in the distributed case. Instead looking at the AC losses for the concentrated winding case they always double the distributed windings AC losses.

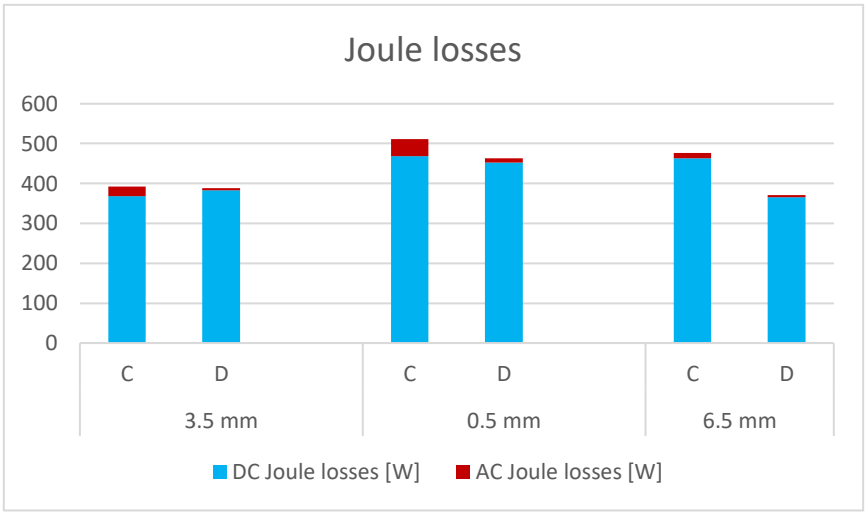

Figure 4.75 – Joule losses comparison for Scenario 2

For the total losses it can be seen the great difference between the two configurations for what concerns the magnet losses which are minimal for the distributed case. More in general anyway, again the losses in the concentrated winding case exceed the ones in the distributed winding motor due to the Joule losses as seen in figure 4.43.

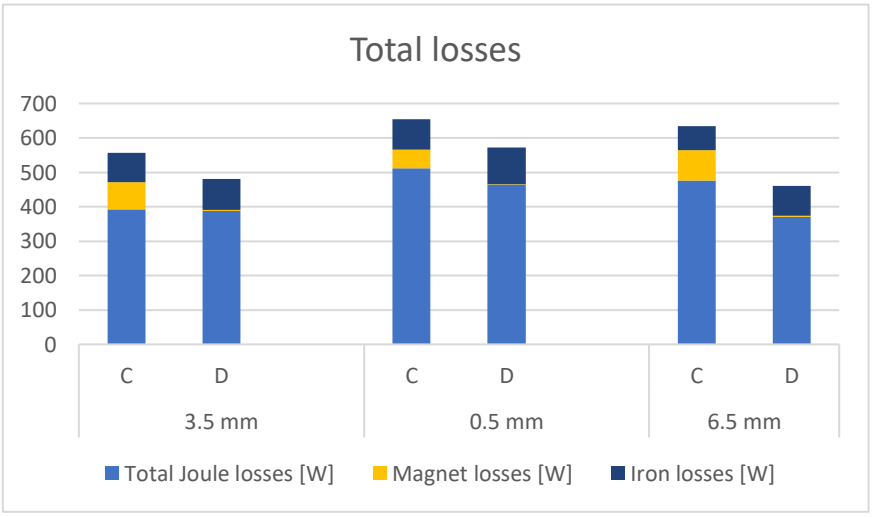

Figure 4.73 – Total losses comparison for Scenario 2

Then to conclude this section, the SPL results are compared. Again, despite the worse results seen for both the cogging torque and the ripple torque, distributed winding case can reduce the noise generated in the baseline conditions and in the 0.5 mm. Instead the 6.5 mm case shows better performances for the concentrated case.

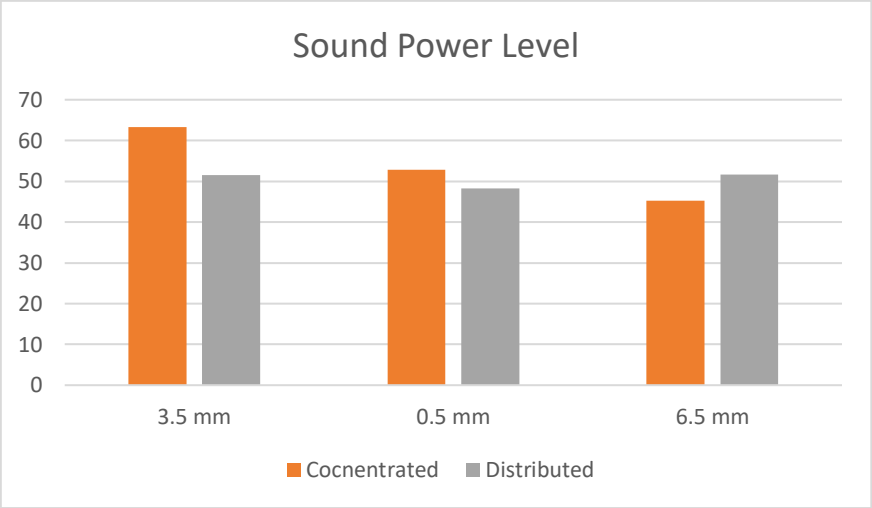

Figure 4.77 – SPL comparison for Scenario 2

4.2.3 Flat tooth design

The following analysis, as mentioned in section 4.1, only considers the concentrated winding case. So, starting from the results related to the cogging torque and the back EMF.

	Coggin torque (pk-pk) [Nm]	Cogging torque (rms) [Nm]	Back EMF (rms) [V]	kE [V/rpm]
3.5 mm (baseline)	5.179	1.626	195.104	0.113
0.5 mm	1.735	0.616	188.783	0.109
6.5 mm	9.778	2.909	196.104	0.113

Table 4.13 – Cogging torque results for Scenario 3

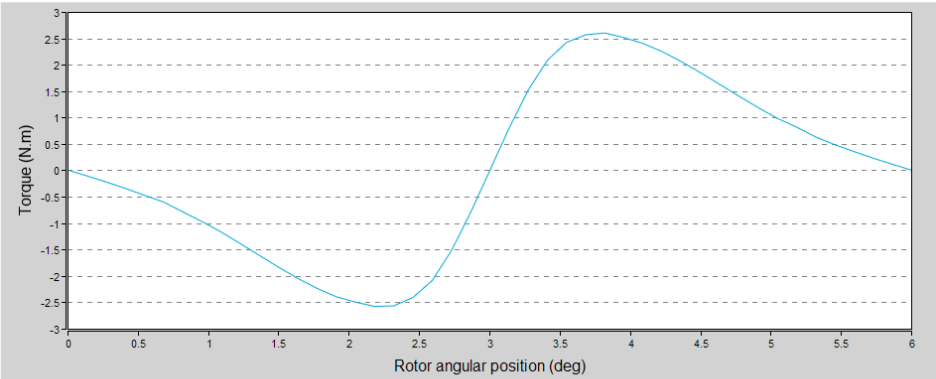

Figure 4.78 - Cogging torque curve for flat tooth design motor with 3.5 mm slot opening

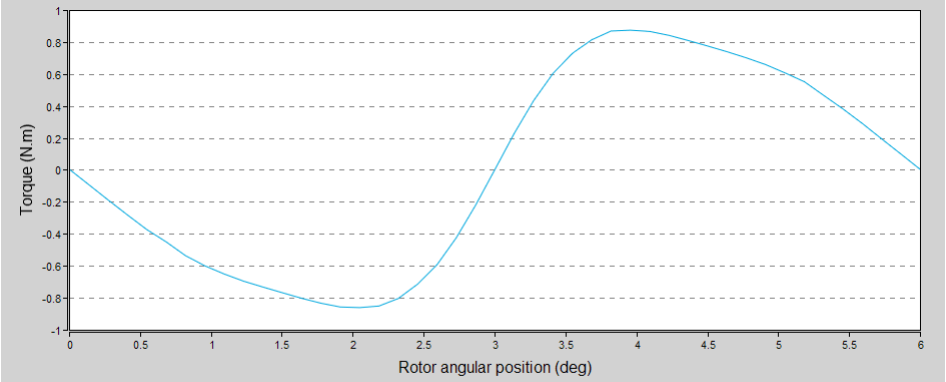

Figure 4.80 - Cogging torque curve for distributed winding motor with 0.5 mm slot opening

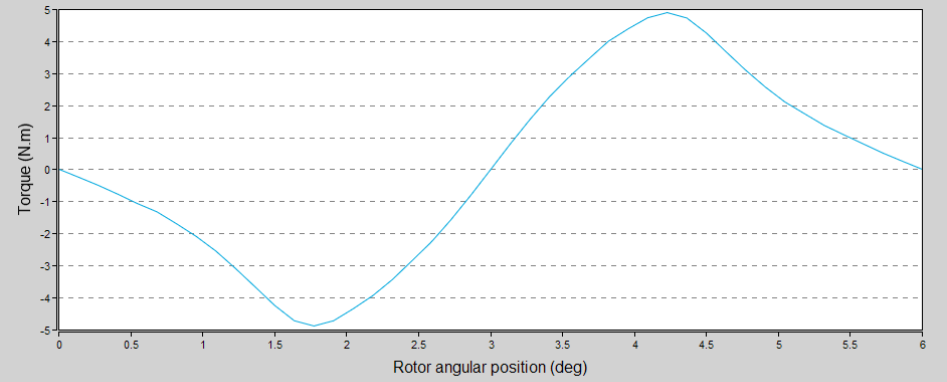

Figure 4.82 - Cogging torque curve for distributed winding motor with 6.5 mm slot opening

In this case very good results are archived with the 0.5 mm layout both for the cogging torque and the back EMF. The results regarding the root mean square of the cogging torque can be better understood looking at the figures of the cogging torque against the angular position of the motor. Then, the higher harmonic content related to the cogging torque in the 6.5 mm is justified by the curve in figure 4.48.

	Ripple torque (pk-pk) [Nm]	Ripple torque (std deviation) [Nm]	Motor constant [Nm/√W]	kT [Nm/A]
3.5 mm (baseline)	12.774	3.886	5.178	2.297
0.5 mm	22.56	6.989	4.478	2.091
6.5 mm	14.205	4.798	5.332	2.31

Table 4.14 – Ripple torque results for Scenario 3

Considering the ripple torque analysis, the first results showed are resumed in table 4.14. Despite a good result for what concerns the cogging torque, in this case the 0.5 mm solutions appears to be the worst in terms of ripple torque. This result is also confirmed in the analysis of the other two parameters. Instead, the baseline has the best results in terms of ripple torque, whereas for what concerns the motor constant and the kT, the best

solution is the 6.5 mm one. Then the curves for alle the three cases are showed. The trends for the 0.5 mm and the baseline are quite similar despite a higher standard deviation for the 0.5 mm configuration. Instead the trend showed in the 6.5 mm is quite different, despite the result showed in table 4.14.

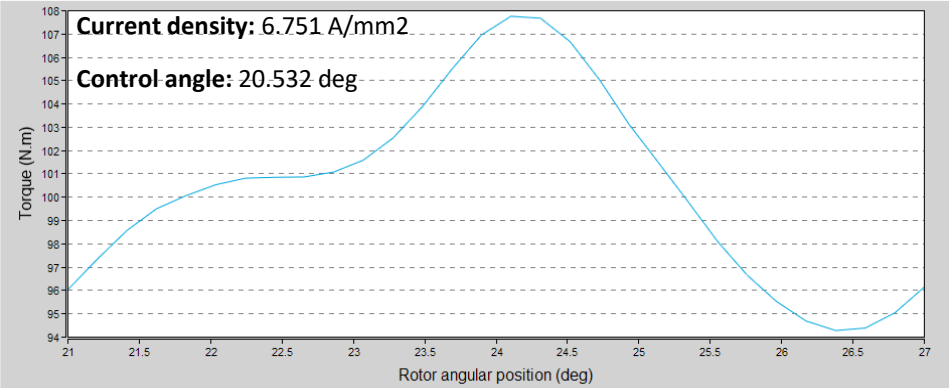

Figure 4.88 - Ripple torque curve for flat tooth design motor with 3.5 mm slot opening

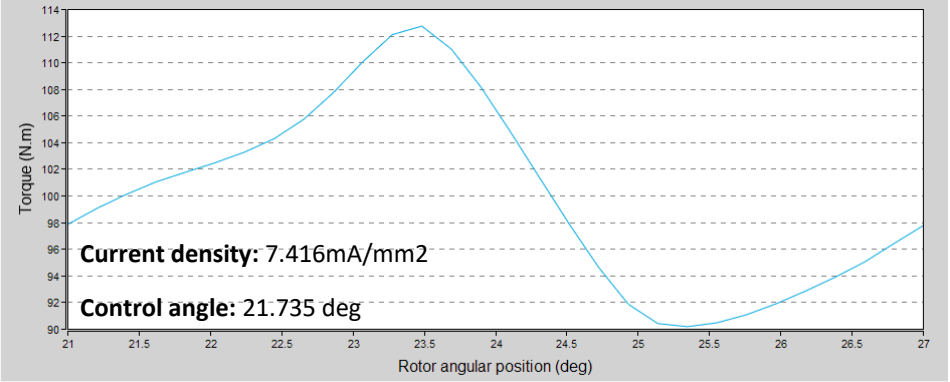

Figure 4.84 - Ripple torque curve for flat tooth design motor with 0.5 mm slot opening

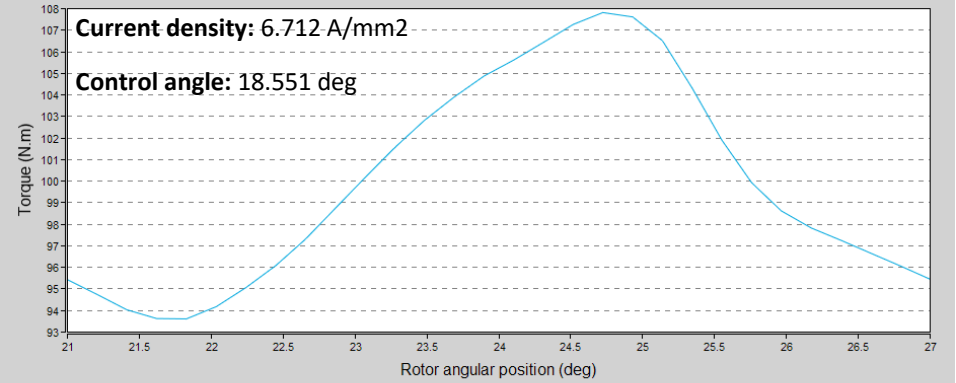

Figure 4.86 - Ripple torque curve for flat tooth design motor with 6.5 mm slot opening

Looking at the currents in the figures, the kT results are justified. In fact the baseline configuration and the 6.5 mm case are the ones that need less current to be supplied to deploy the same torque.

Then the results regarding the losses are showed in table 4.15.

	DC Joule losses [W]	AC Joule losses [W]	Total Joule losses [W]	Magnet losses [W]	Iron losses [W]	Total losses [W]
3.5 mm (baseline)	333.700	32.093	365.793	41.690	85.635	493.118
0.5 mm	404.206	63.851	468.057	41.366	92.494	601.917
6.5 mm	329.842	15.762	345.604	71.095	83.757	500.456

Table 4.15 – Losses results for Scenario 3

For what concerns the Joule losses, the best result is achieved by the 6.5 mm opening solution. This is mainly due to the good results showed by the machine with the AC losses; in fact there is not so much difference between the baseline and the 6.5 mm case for what concerns the DC losses, while the 3.5 mm losses in AC doubles the ones in the 6.5 mm machine. Anyway looking at the overall losses the results achieved by the baseline are the best, this is mainly due to the low magnet losses, in which the machine with the wider opening has worse result.

Then the engine maps of the three motors are showed in the figures below. The best results are the one obtained in the 6.5 mm configuration which can obtain higher values for the torque, the speed and the efficiency at the base point. For what concerns the maximum efficiency there is not so much discrepancy.

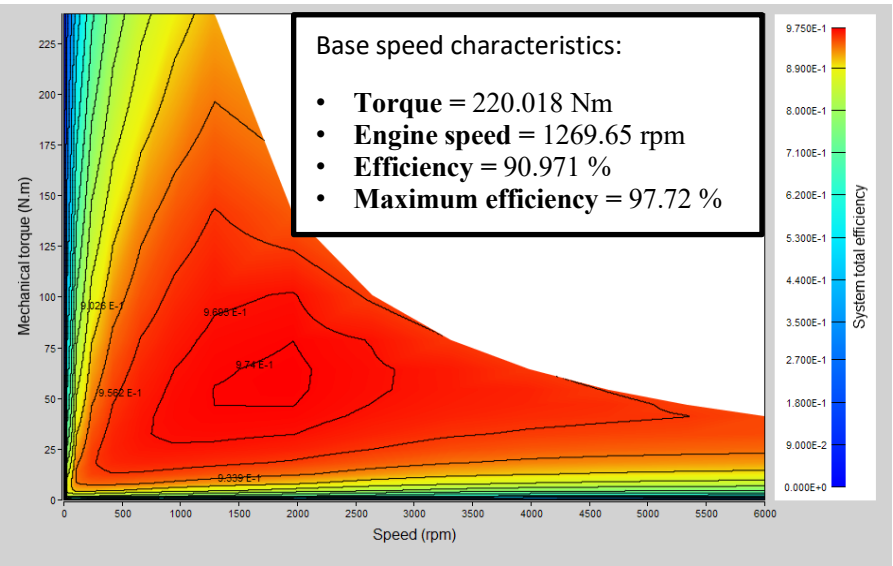

Figure 4.90 - Engine map and base speed performance for flat tooth design motor with 3.5 mm slot opening

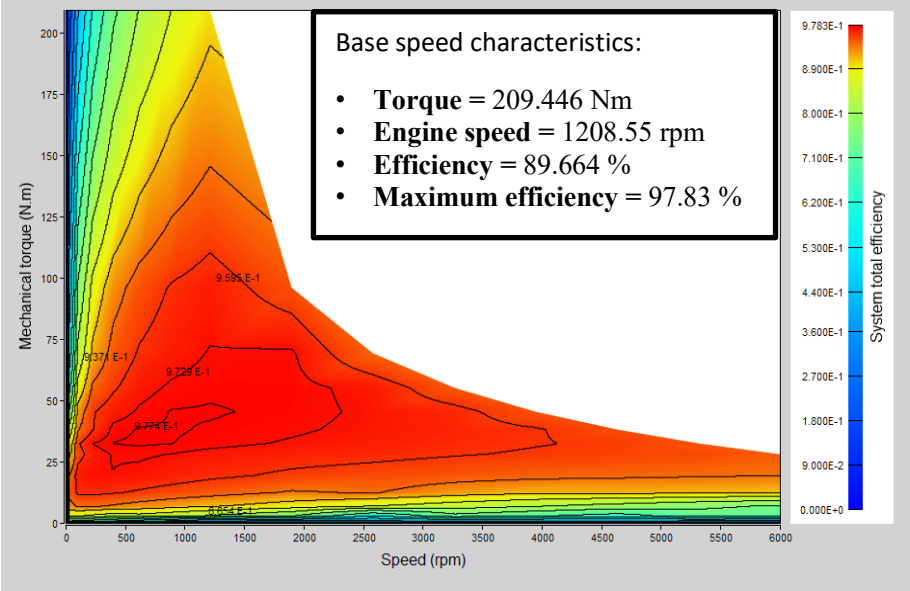

Figure 4.94 - Engine map and base speed performance for flat tooth design motor with 0.5 mm slot opening

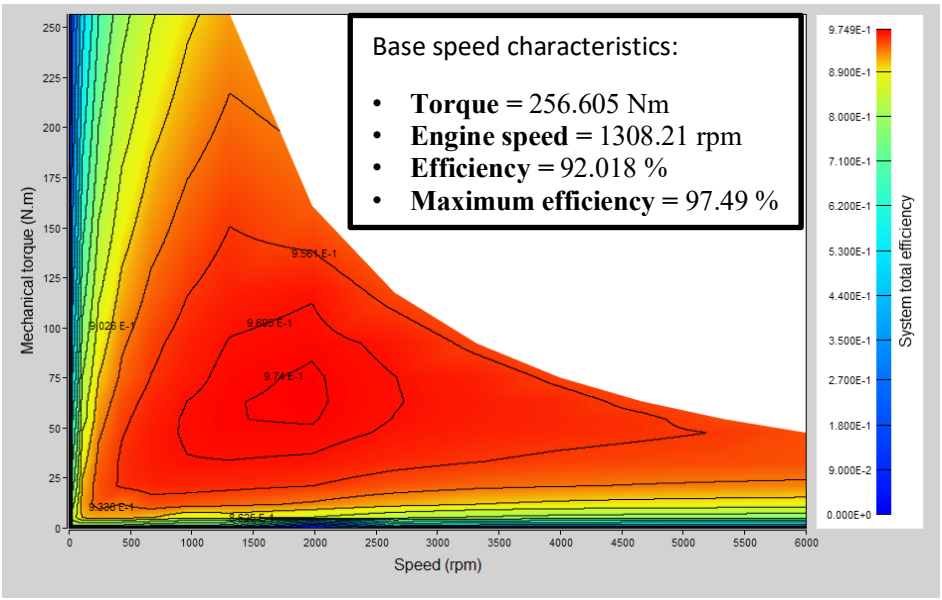

Figure 4.92 - Engine map and base speed performance for flat tooth design motor with 6.5 mm slot opening

Then the analysis concludes with the NVH results. The SPL results are showed in table 4.14.

	Overall sound pressure level [dB]
3.5 mm (baseline)	69.947
0.5 mm	67.459
6.5 mm	66.969

Table 4.16 – SPL results for Scenario 3

The results in this case are quite comparable, since there's not a clear reduction of the SPL in one of the three motors; anyway the best performance are achieved for the 6.5 mm case that shows the lowest results in this analysis.

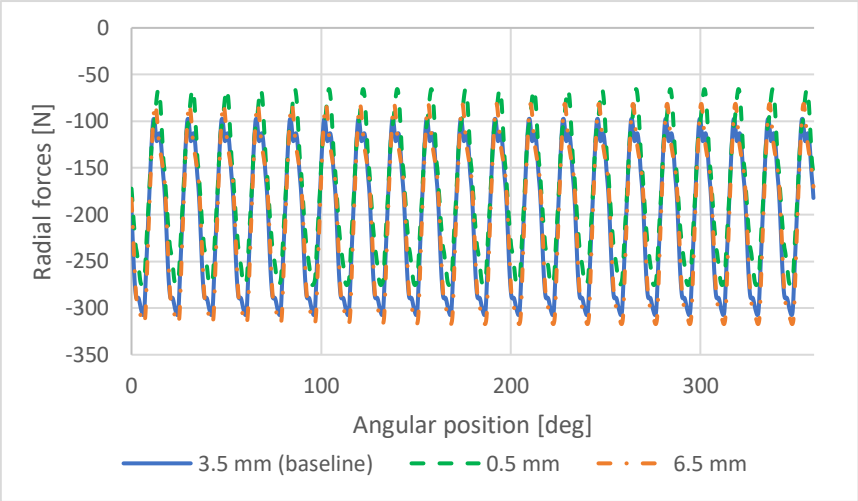

Figure 4.98 – Radial force comparison for Scenario 3

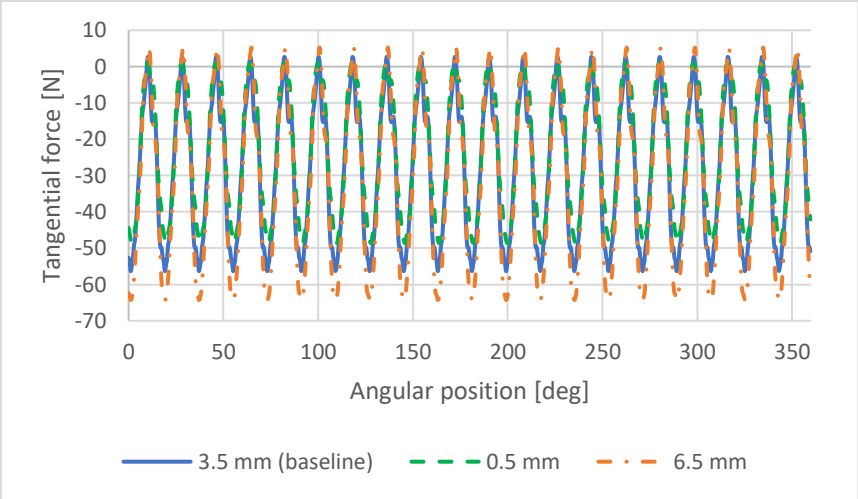

Figure 4.96 – Tangential force comparison for Scenario 3

Then in figures 4.55 and 4.56 are showed the plot of the radial force and tangential forces against the angular position of the rotor. Also from the graph it's clear there is not so much difference between the three configurations.

4.2.4 Flat tooth design with reduced height of the shoe

The last scenario to be analysed is the one with flat tooth with reduced height of the tooth shoe. The results of the open circuit tests are showed in table 4.17.

	Coggin torque (pk-pk) [Nm]	Cogging torque (rms) [Nm]	Back EMF (rms) [V]	kE [V/rpm]
3.5 mm (baseline)	9.945	2.897	191.449	0.111
0.5 mm	4.744	1.524	185.429	0.108
6.5 mm	11.498	3.485	193.677	0.112

Table 4.17 – Cogging torque results for Scenario 4

The results are again in line with the other scenarios, confirming the good results of the 0.5 mm layout for what concerns both the cogging torque and the back EMF. The results of the cogging torque rms are also confirmed by the graph in the figures 4.57, 4,58 and 4.59. In fact even if they are quite different one from each other, as confirmed by the results in the table, the 0.5 mm layout has the most regular trend.

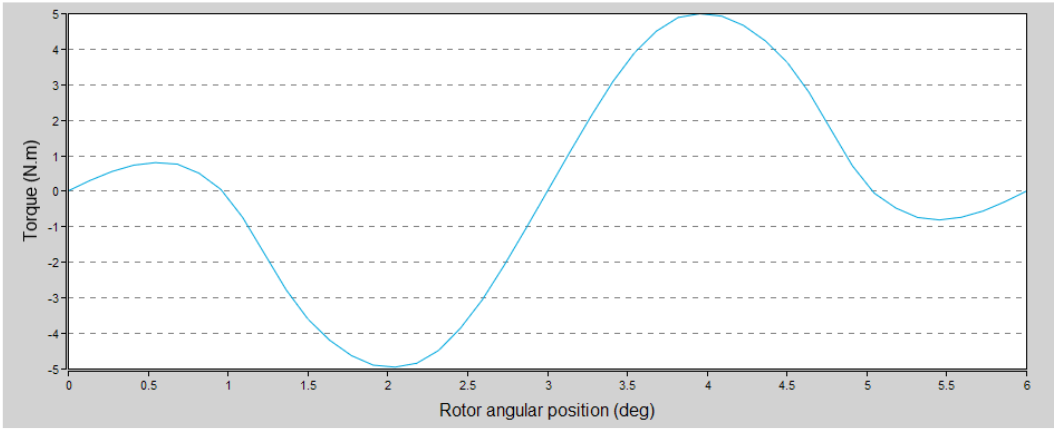

Figure 4.102 - Cogging torque curve for flat tooth design with reduced height of the shoe motor with 3.5 mm slot opening

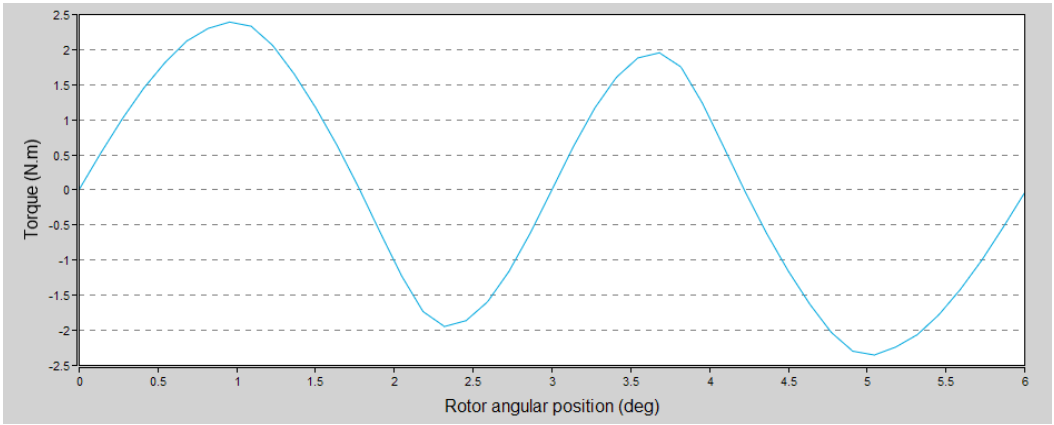

Figure 4.100 - Cogging torque curve for flat tooth design with reduced height of the shoe motor with 0.5 mm slot opening

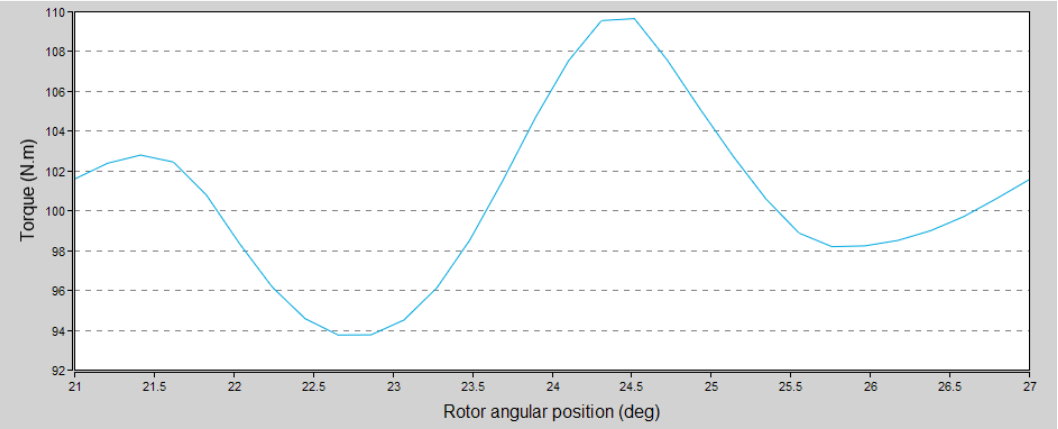

Figure 4.103 - Cogging torque curve for flat tooth design with reduced height of the shoe motor with 6.5 mm slot opening

Then, in the table 4.18 are resumed the table regarding the ripple torque performances of the three motors. The results show good performance for the ripple torque for the 0.5 mm layout again; anyway considering the motor constant and the kT this layout is not the best. In fact even if there is not a big gap between the three configurations, the best results are achieved by the 6.5 mm for what concerns the motor constant whereas is the 3.5 mm for the kT case.

	Ripple torque (pk-pk) [Nm]	Ripple torque (std deviation) [Nm]	Motor constant [Nm/√W]	kT [Nm/A]
3.5 mm (baseline)	15.338	4.208	5.032	2.334
0.5 mm	11.155	3.346	4.773	2.299
6.5 mm	14.916	4.821	5.087	2.323

Table 4.18 – Ripple torque results for Scenario 4

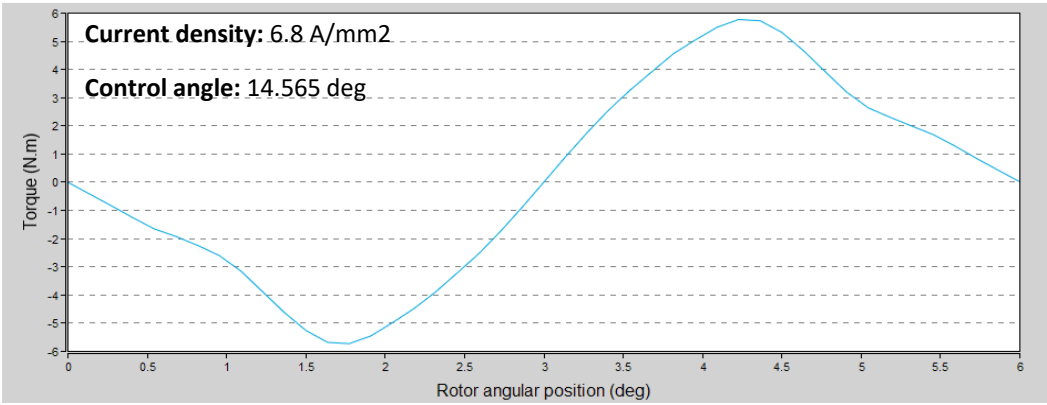

Figure 4.105 - Ripple torque curve for flat tooth with reduced height of the shoe motor with 3.5 mm slot opening

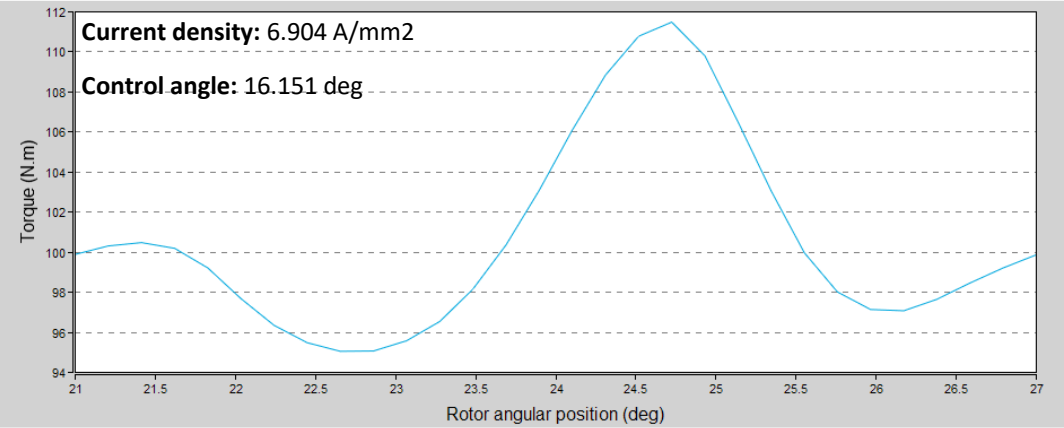

Figure 4.109 - Ripple torque curve for flat tooth with reduced height of the shoe motor with 0.5 mm slot opening

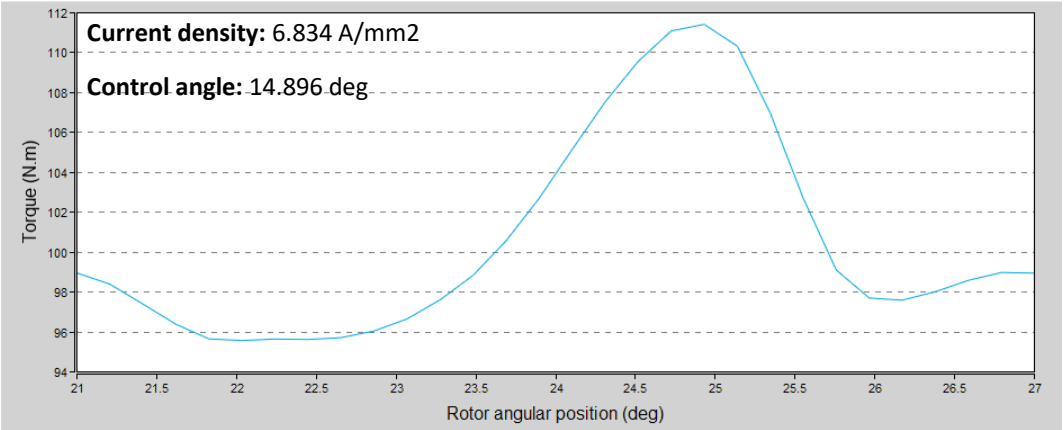

Figure 4.107 - Ripple torque curve for flat tooth with reduced height of the shoe motor with 6.5 mm slot opening

For what concerns the trends of the ripple torque, the three curves are not so much different one for each other except for the baseline case. The result regarding the current density reflects the ones related to the kT in which there's not so much difference between the various configurations.

Then considering the losses the following results are obtained.

	DC Joule losses [W]	AC Joule losses [W]	Total Joule losses [W]	Magnet losses [W]	Iron Losses [W]	Total Losses [W]
3.5 mm (baseline)	330.238	49.759	379.997	48.982	79.347	508.326
0.5 mm	340.482	68.291	408.773	48.434	79.977	537.184
6.5 mm	333.538	37.444	370.982	68.811	78.147	517.940

Table 4.19 – Losses results for Scenario 4

Also for this scenario the best results are obtained for the 6.5 mm case in the Joule losses, mainly due to the good performances with the AC losses. But also this time the magnet

losses are quite worse in this layout, and this makes the 3.5 mm machine the best for what concerns the overall losses. Then the engine maps are plotted.

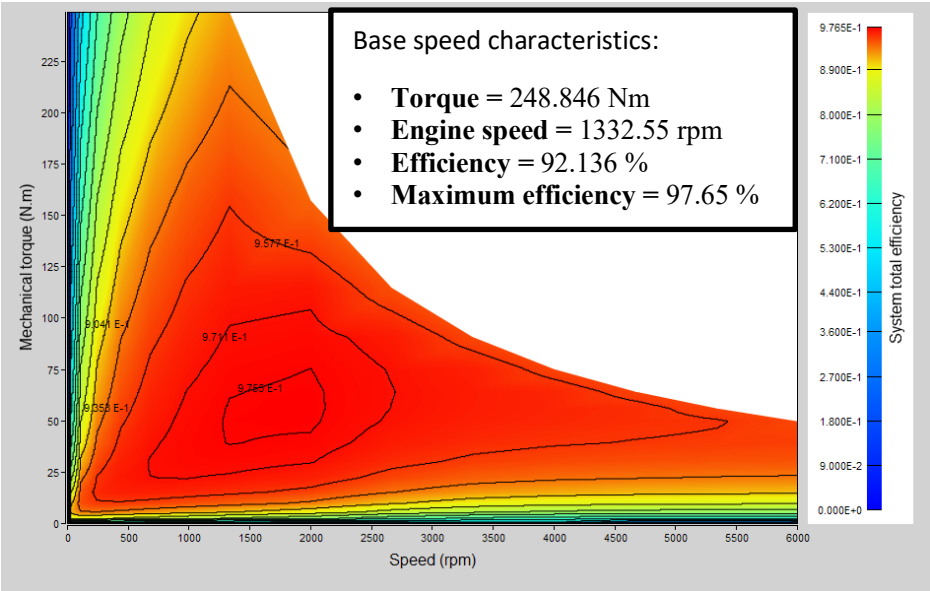

Figure 4.112 - Engine map and base speed performance for flat tooth with reduced height of the shoe motor with 3.5 mm slot opening

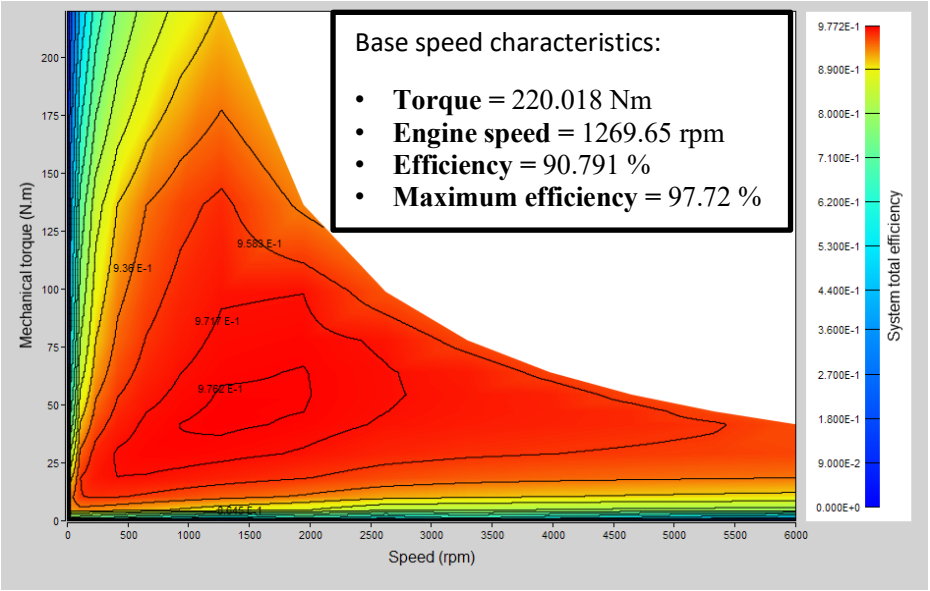

Figure 4.111 - Engine map and base speed performance for flat tooth with reduced height of the shoe motor with 0.5 mm slot opening

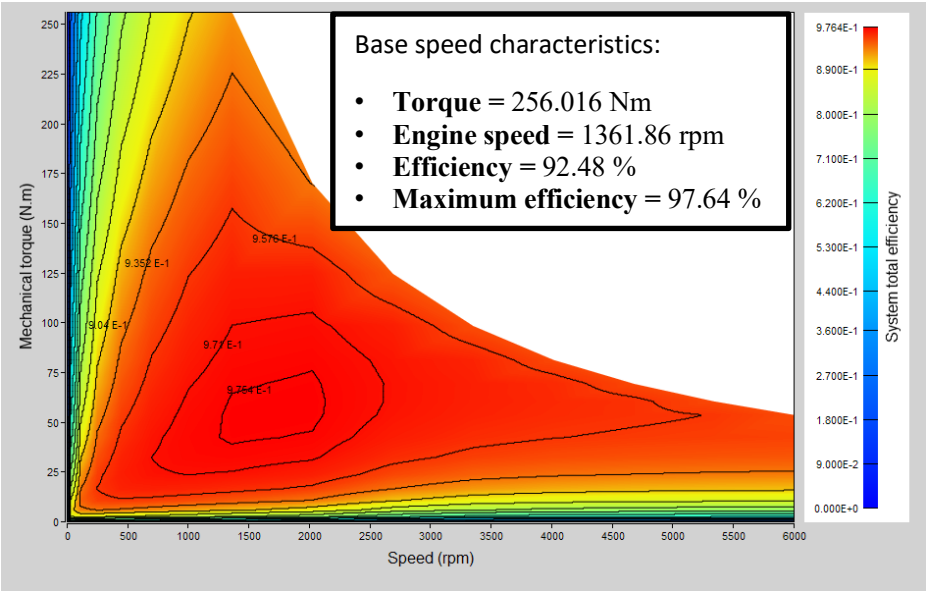

Figure 4.113 - Engine map and base speed performance for flat tooth with reduced height of the shoe motor with 6.5 mm slot opening

Also in this scenario the 6.5 mm configuration shows the best results for torque, speed and efficiency at the base point.

Then to conclude the analysis the NVH performances are compared. The first parameter to be showed is the SPL.

	Overall sound power level [dB]
3.5 mm (baseline)	65.9
0.5 mm	63.325
6.5 mm	67.6

Table 4.20 – SPL results for Scenario 4

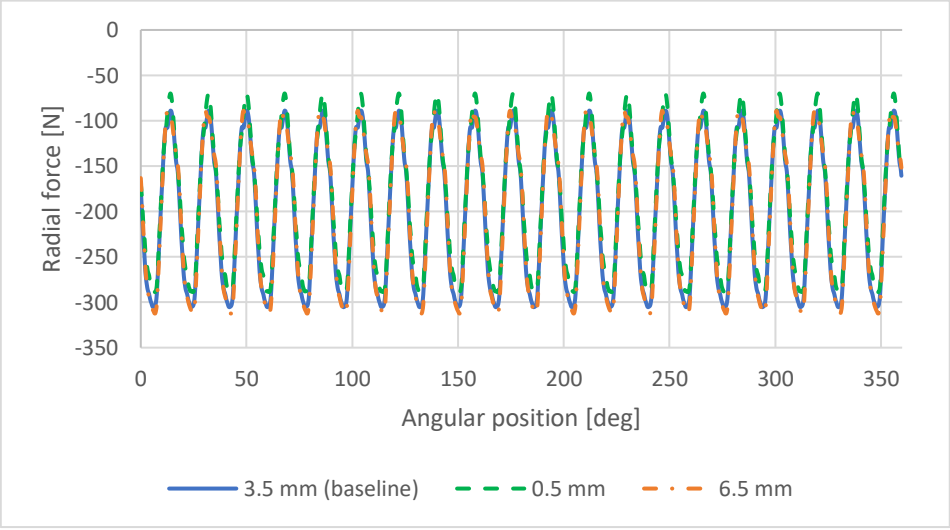

Figure 4.115 – Radial force comparison for Scenario 4

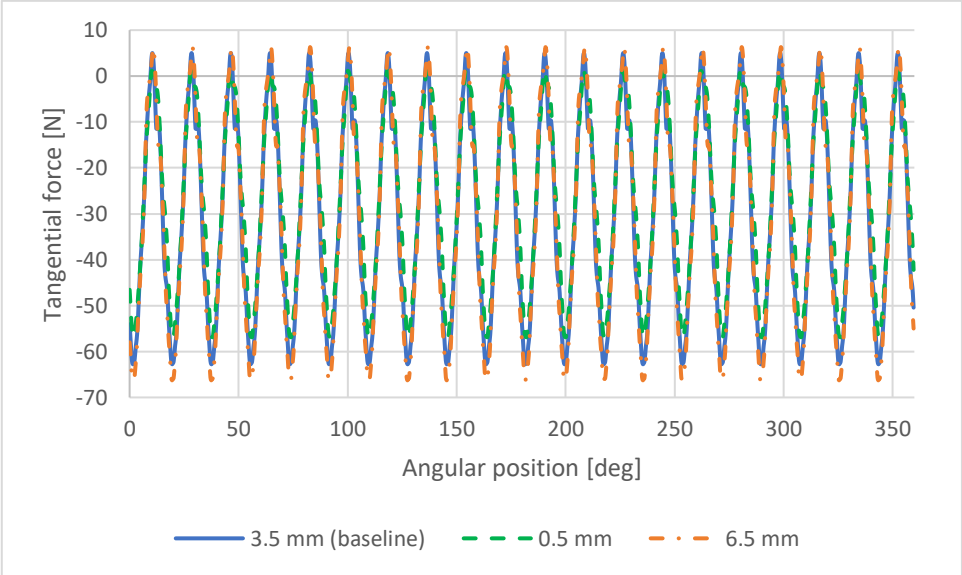

Figure 4.117 – Tangential force comparison for Scenario 4

For the noise and vibration performance there is not a real reduction of the SPL, anyway the best results are the one obtained from the 0.5 mm layout. Then the graphs of the radial and tangential forces conclude this analysis; also in this scenario the discrepancy between the curves is not so high, reflecting the results of the SPL.

4.2.5 Final comparison

To give a general idea of the impact of all these parameters on the results of the motors, in this section will be compared the 30s20p configurations for the slot with the fillet, the flat tooth and the flat tooth with reduced height of the shoe. The procedure will be the same seen also in the sections 4.2.2.

Starting from the cogging torque, the results are showed in figure 4.68 and 4.69.

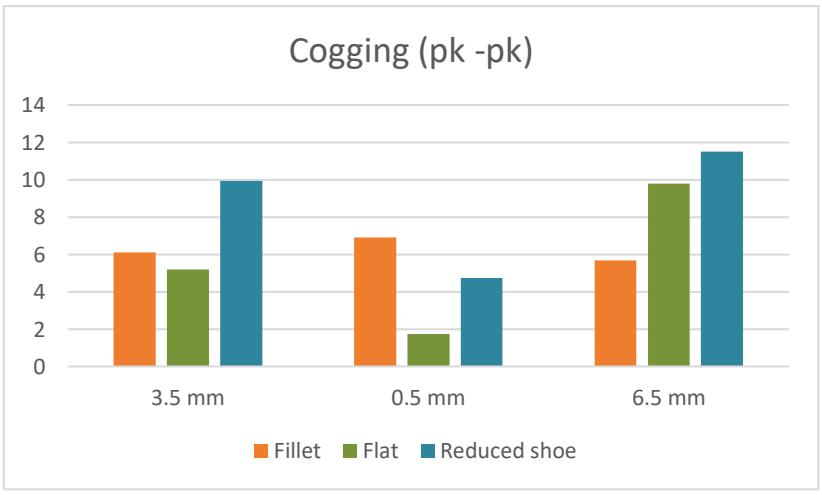

Figure 4.119 – Peak-to-peak cogging torque final comparison for concentrated motor layouts

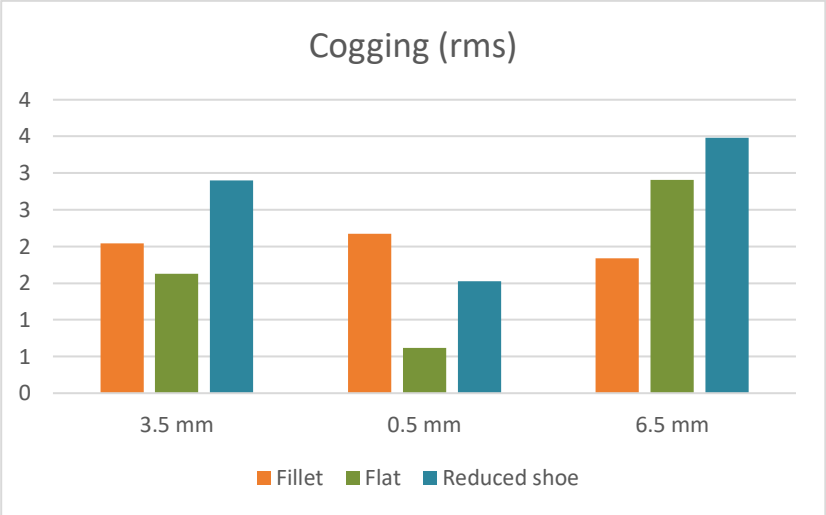

Figure 4.121 – Cogging torque rms final comparison for concentrated winding motor layouts

The results are not homogeneous, in fact looking at the figure 4.68, the flat solution has the best results for both the 3.5 mm and the 6.5 mm configurations, but it worsen with the wider opening. Instead, looking at the figure 4.69, the trend follows what has been seen for the peak-to-peak values.

For the back EMF also for this case, depending on the configuration, there is a solution that is better in one case while it worsen in another case.

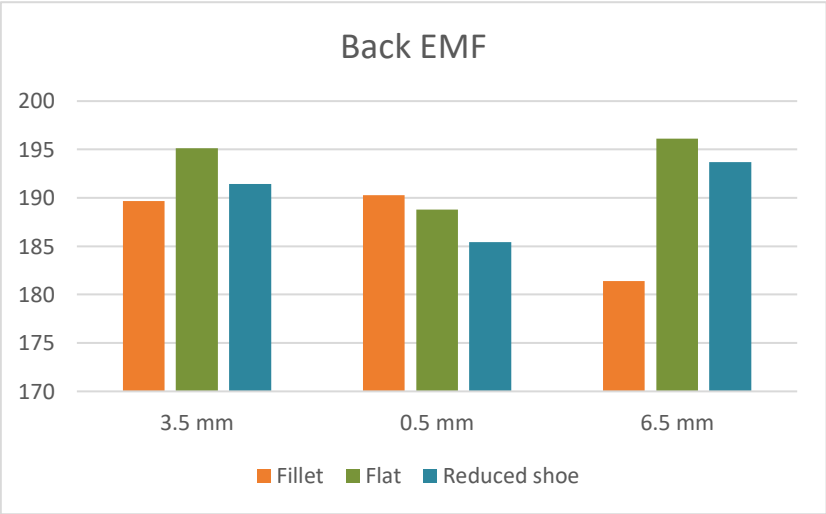

Figure 4.123 – Back EMF final comparison for concentrated winding motor layouts

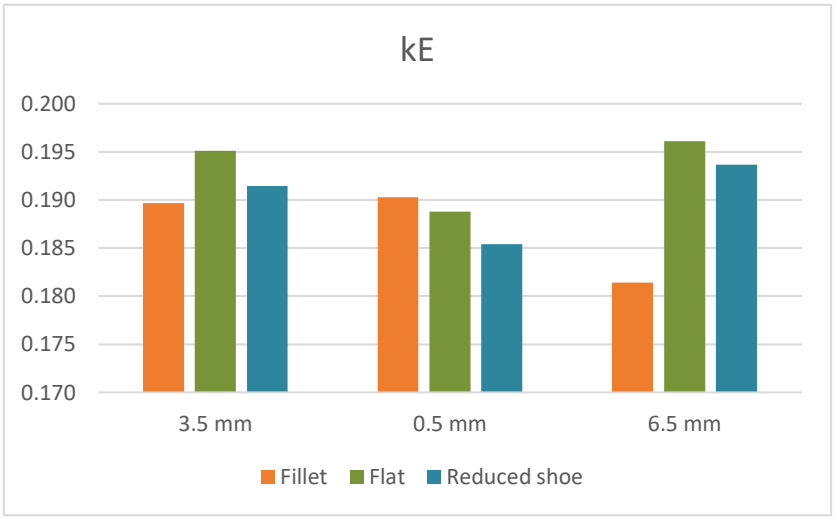

Figure 4.126 – kE final comparison for concentrated winding motor layouts

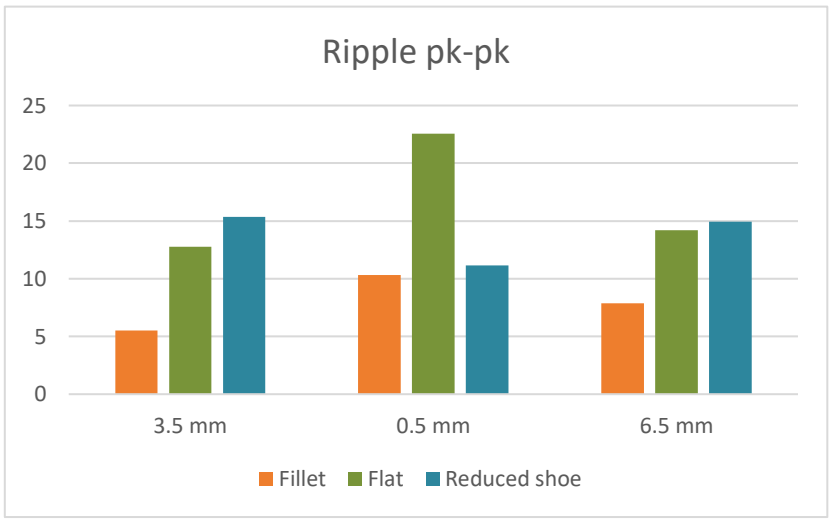

Figure 4.125 – Ripple torque peak-to-peak final comparison for concentrated winding motor layouts

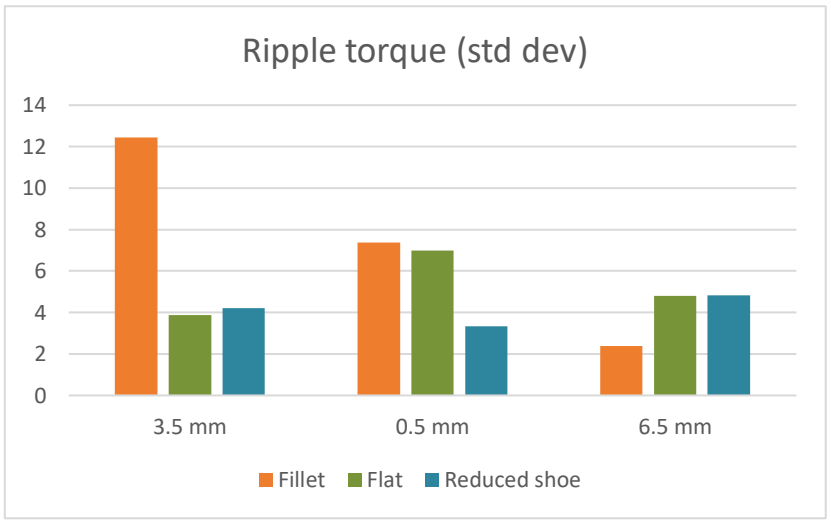

Figure 4.124 – Ripple torque standard deviation final comparison for concentrated winding motor layouts

Then there are the results related to the ripple torque. In this case the configuration with the fillet is the one with the best results in all the three cases. Particular attention should be paid at the ripple torque in case of flat tooth. In fact looking at the figure 4.72, in the 3.5 mm case, there is a significant increase of the ripple torque. Considering instead the standard deviation, the fillet configuration has good performance only in the 6.5 mm case, while looking at the figure 4.73, the standard deviation showed by the reduced heigh of the flat tooth is the one which has very good performances in all the cases.

These results are also confirmed looking at the motor constant and the kT results. The baseline solution has good results both for the parameters considered

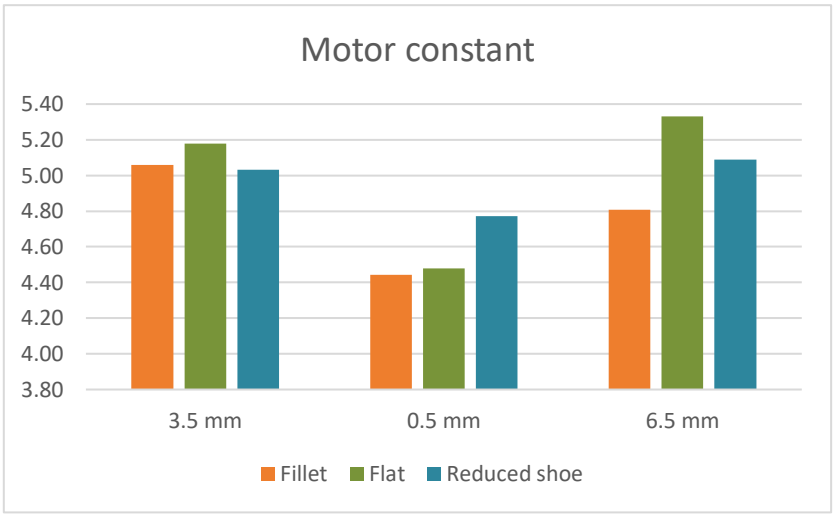

Figure 4.129 – Motor constant final comparison for concentrated winding motor layouts

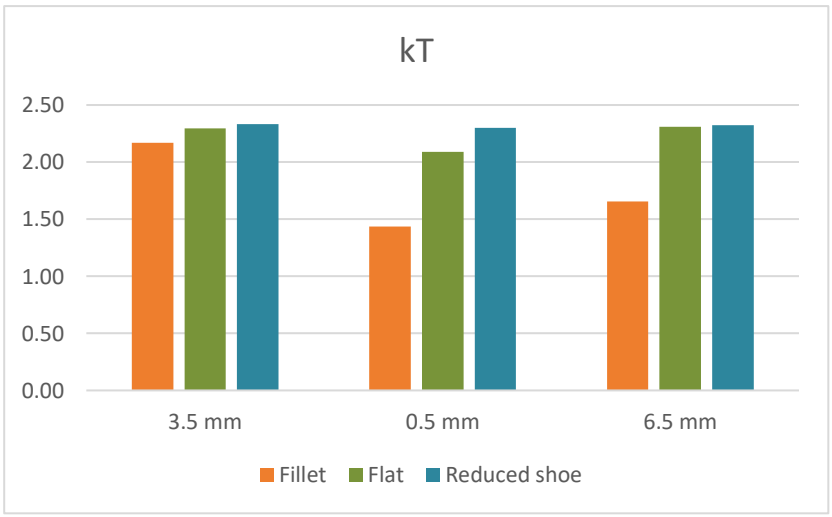

Figure 4.127 – kT final comparison for concentrated winding motor layouts

For what concerns the losses, first the results related to the Joule losses are shown. In general there is not a different best solution depending on the slot opening considered,

anyway the flat solution shows good performances in the 3.5 mm case and very good performances for the largest opening considered. Another thing to point out is the fact that, enlarging the slot opening, for all the configurations there is a decrease of the AC Joule losses.

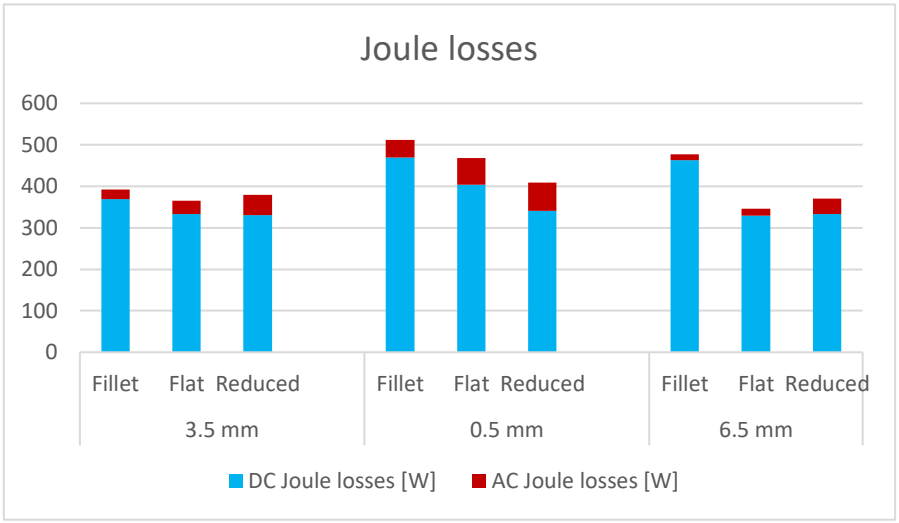

Figure 4.133 – Joule losses final comparison for concentrated winding motor layouts

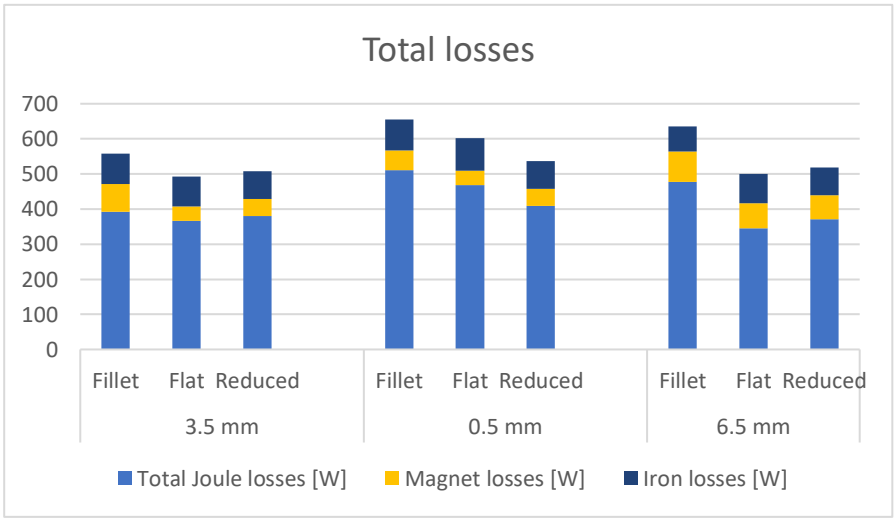

Figure 4.131 – Total losses comparison for concentrated winding motor layouts

Then the analysis moves towards the comparison of the total losses. As expected, the best solution changes for the different opening.

Then to conclude the analysis the SPL of the different configurations is considered. The fillet solution is the one able to reach the lowest value of SPL in all the configuration, in particular with the 6.5 mm solution.

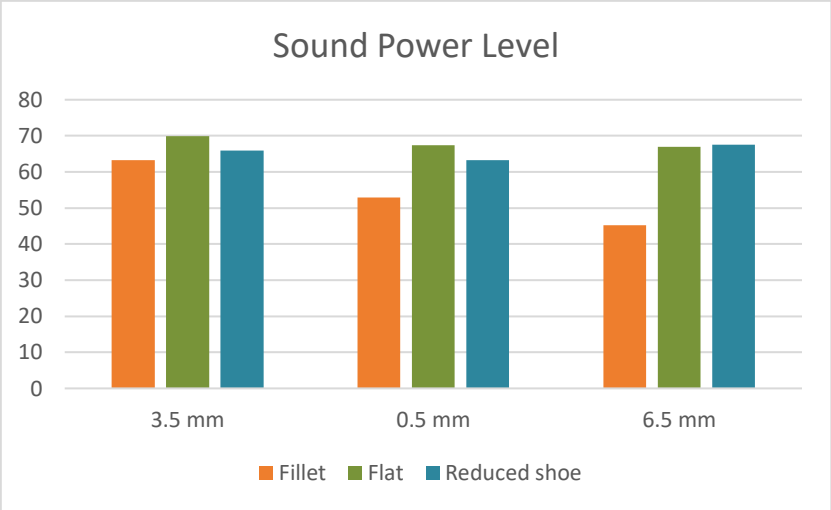

Figure 4.135 – SPL final comparison for concentrated winding motor layouts

CHAPTER V

Conclusion and future works

In this thesis work, the impact of different parameters impacting on the noise and vibration generation and, more in general, on the performances of the motor is showed. For this purpose, a sensitivity analysis is conducted considering different scenarios such as: concentrated windings versus distributed windings, influence of the slot opening, flat tooth design and flat tooth with reduced height of the shoe. The parameter considered for to evaluate the best combinations are cogging torque and ripple torque, back EMF, losses and efficiency, SPL and the forces acting on the stator tooth, which are obtained using the Altair software FluxMotor

The results do not show a configuration that is able to obtain the best results for all the parameters under test. In fact, considering the comparison between concentrated and distributed analysis, it has showed that the distributed windings configuration is able to reduce the overall Sound Power Level, and has very good performances for what concerns the loss reduction (particularly for the magnet losses). Anyway for what concerns the cogging torque and the ripple torque this configuration is not so good compared with the concentrated windings solution. This situation comes again considering the flat tooth configuration and the one with reduced height of the shoe of the tooth in which there is a high sensitivity to the slot opening of the stator slot. In fact considering for example the losses of the two motors, it has showed that the flat tooth design is able to reduce the total losses with respect to the configuration with the reduced height of the shoe in the 3.5 mm and in the 6.5 mm case, whereas this is not true for the 0.5 mm case. So what can be concluded is that, depending on the application and on the parameters to optimise there is a different solution able to pursue this objective.

Anyway, some future works can improve and extend this thesis work. The first thing that could be done is to validate all these tests done in this work on a real application, even considering that this kind of activity is expensive and time consuming. Anyway, even if this analysis is conducted on an IPM technology, it can be of interest to further extend this methodology to other types of motor available on the market.

Finally, since this thesis contributes to the research for electric and hybrid powertrain at LIM (Laboratorio Interdisciplinare di Meccatronica), this thesis can be used by other students to further develop the work on this field.

Bibliography and webliography

[1] Arora, A., Niese, N., Dreyer, E., Waas, A., & Xie, A. (2020). Why Electric Cars Can't Come Fast Enough. *BCG. https://www.bcg.com/it-it/publications/2021/why-evs-need-to-accelerate-their-market-penetration.*

[2] Arora, A., Niese, N., Dreyer, E., Waas, A., & Xie, A. (2020). Electric Cars Are Finding Their Next Gear. *BCG. https://www.bcg.com/it-it/publications/2022/electric-cars-finding-next-gear.*

[3] Regulation of the European Parliament and of the council amending Regulation (EU) 2019/631 as regards strengthening the CO2 emission performance standards for new passenger cars and new light commercial vehicles in line with the Union's increased climate ambition.

[4] Huynh, T. A., & Hsieh, M. F. (2017). Comparative Study of PM-Assisted SynRM and IPMSM on Constant Power Speed Range for EV Applications. *IEEE Transactions on Magnetics*, *53*(11).

[5] Remus, N., Toulabi, M. S., Mukundan, S., Dhulipati, H., Li, W., Novak, C., & Kar, N. C. (2020). Electromagnetic Noise and Vibration in PMSM and Their Sources: An Overview. *Canadian Conference on Electrical and Computer Engineering*, *2020-August*. https://doi.org/10.1109/CCECE47787.2020.9255787

[6] Remus, N. (2020). Parametric Investigation of the Core Geometry of an IPMSM to Reduce Vibrations.

[7] Islam, M. S., Islam, R., & Sebastian, T. (2014). Noise and vibration characteristics of permanent-magnet synchronous motors using electromagnetic and structural analyses. *IEEE Transactions on Industry Applications*, *50*(5), 3214–3222. https://doi.org/10.1109/TIA.2014.2305767

[8] Libert, F., & Soulard, J. Investigation on Pole-Slot Combinations for Permanent-Magnet Machines with Concentrated Windings.

[9] Wu, D., & Zhu, Z. (2015, July 14). Design trade-off between cogging torque and torque ripple in fractional slot surface-mounted permanent magnet machines. *2015 IEEE International Magnetics Conference, INTERMAG 2015*. https://doi.org/10.1109/INTMAG.2015.7157400

[10] *Emetor - Glossary - Winding factor*

[11] Islam, J., Svechkarenko, D., Chin, R., Szucs, A., Mantere, J., & Sakki, R. (2012). Cogging torque and vibration analysis of a direct-driven PM wind generator with concentrated and distributed windings. In *2012 15th International Conference on Electrical Machines and Systems (ICEMS)*.

[12] Halwas, M., Hausmann, L., Wirth, F., Fleischer, J., Jux, B., & Doppelbauer, M. (2020). Influences of design and manufacturing on the performance of electric traction drives. *Proceedings - 2020 International Conference on Electrical Machines, ICEM 2020*, 488–494.

[13] Husain, T., Ma, C., Taran, N., & Wan, Z. (2021). A Comprehensive Comparison of Concentrated Winding and Distributed Continuous Winding Machine Topologies for Hybrid Electric Vehicles. *2021 IEEE Energy Conversion Congress and Exposition, ECCE 2021 - Proceedings*, 3683–3689. https://doi.org/10.1109/ECCE47101.2021.9595089

[14] Alireza, P., Rukmi, D., & Rahman, M. F. Preliminary Study on Differences in the Performance Characteristics of Concentrated and Distributed Winding IPM Machines with Different Rotor Topologies. https://doi.org/10.1109/ICEM49940.2020.9270899

[15] Hanselman, D. (2006). *Brushless Permanent Magnet Motor Design Second Edition*.

[16] *https://www.emetor.com/glossary/torque-ripple/*.

[17] Ishak, D., Zhu, Z. Q., & Howe, D. (2005). Eddy-current loss in the rotor magnets of permanent-magnet brushless machines having a fractional number of slots per pole. *IEEE Transactions on Magnetics*, *41*(9), 2462–2469. https://doi.org/10.1109/TMAG.2005.854337 https://doi.org/10.1109/TMAG.2017.2707125

[18] Meeker, D., (2017). *Rotating Losses in a Surface Mount Permanent Magnet Motor*. https://www.femm.info/wiki/SPMLoss